AD-A182 771 FLOW AND FAILURE OF ROCKS CONCRETE AND OTHER GEOMATERIALS(U) CALIFORNIA UNIV SAN DIEGO LA JOLLA DEPT OF APPLIED MECHANICS A S NEMAT-NASSER NOV 86 1/2

UNCLASSIFIED AFOSR-TR-87-0890 AFOSR-86-0035 F/G 8/7 NL

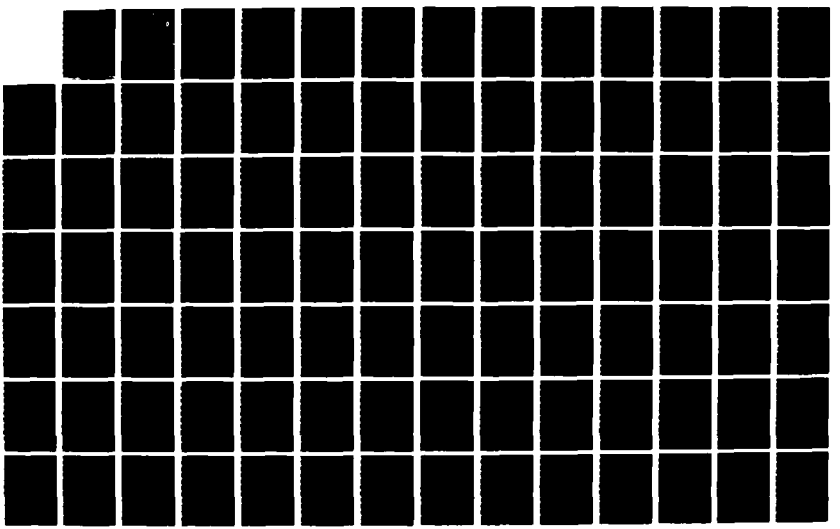

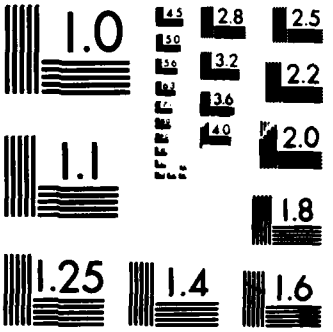

MICROCOPY RESOLUTION TEST CHART
NATIONAL BUREAU OF STANDARDS 1963-A

AFOSR-TR- 87-0890

FINAL SCIENTIFIC REPORT

for the period

1 October 1985 to 30 September 1986

on

FLOW AND FAILURE OF ROCKS, CONCRETE AND OTHER GEOMATERIALS

Grant No. AFOSR 86-0035

S. Nemat-Nasser, Principal Investigator
University of California, San Diego, La Jolla, California 92093

November 1986

ADA182771

Unclassified

SECURITY CLASSIFICATION OF THIS PAGE

REPORT DOCUMENTATION PAGE

1a. REPORT SECURITY CLASSIFICATION: Unclassified	1b. RESTRICTIVE MARKINGS
2a. SECURITY CLASSIFICATION AUTHORITY	3. DISTRIBUTION/AVAILABILITY OF REPORT: Approved for public release; distribution unlimited
2b. DECLASSIFICATION/DOWNGRADING SCHEDULE	
4. PERFORMING ORGANIZATION REPORT NUMBER(S)	5. MONITORING ORGANIZATION REPORT NUMBER(S): AFOSR-TR- 87-0890
6a. NAME OF PERFORMING ORGANIZATION: Department of AMES, University of California, San Diego; 6b. OFFICE SYMBOL (If applicable)	7a. NAME OF MONITORING ORGANIZATION: Air Force Office of Scientific Research/NA
6c. ADDRESS (City, State and ZIP Code): La Jolla, California 92093	7b. ADDRESS (City, State and ZIP Code): BLDG 410 Bolling Air Force Base, D.C. 20332
8a. NAME OF FUNDING/SPONSORING ORGANIZATION: AFOSR/NA; 8b. OFFICE SYMBOL (If applicable): AFOSR/NA	9. PROCUREMENT INSTRUMENT IDENTIFICATION NUMBER: Grant AFOSR 86-0035
8c. ADDRESS (City, State and ZIP Code): AFOSR/NA, BLDG 410 Bolling AFB, DC 20332	10. SOURCE OF FUNDING NOS. — PROGRAM ELEMENT NO.: 61102F; PROJECT NO.: 2302/B2; TASK NO.: C2; WORK UNIT NO.:
11. TITLE (Include Security Classification): "Flow and Failure of Rocks, Concrete and Other Geomaterials (Unclassified)	
12. PERSONAL AUTHOR(S): S. Nemat-Nasser	
13a. TYPE OF REPORT: Final Report; 13b. TIME COVERED: FROM 10-1-85 TO 9-30-86	14. DATE OF REPORT (Yr., Mo., Day): November 1986; 15. PAGE COUNT: 191
16. SUPPLEMENTARY NOTATION	

17. COSATI CODES		
FIELD	GROUP	SUB. GR.

18. SUBJECT TERMS (Continue on reverse if necessary and identify by block number): Micro-mechanics of flow and failure of rocks, concrete, and other geomaterials; macroscopic nonlinear constitutive models; macroscopic nonlinear and anisotropic responses.

19. ABSTRACT (Continue on reverse if necessary and identify by block number)

The research completed under this AFOSR award was the continuation of efforts already initiated under Grant AFOSR-84-0004 at Northwestern University. The research aims at experimental and theoretical investigation of the micromechanics of flow and failure of rocks, concrete, and other related geo-materials at moderate to very high pressures and temperatures. As a result of this work, certain macroscopic nonlinear constitutive models have been developed, which reflect realistically the micromechanical events that produce observed macroscopic nonlinear and anisotropic responses of materials of this kind.

The theoretical work followed the principal investigator's recent effort in the micromechanical modeling of nonlinear material response. It included calculations of

(continued on reverse)

20. DISTRIBUTION/AVAILABILITY OF ABSTRACT: UNCLASSIFIED/UNLIMITED ☐ SAME AS RPT. ☒ DTIC USERS ☒	21. ABSTRACT SECURITY CLASSIFICATION: Unclassified
22a. NAME OF RESPONSIBLE INDIVIDUAL: Dr. Spencer T. Wu	22b. TELEPHONE NUMBER (Include Area Code): (202) 767-4935; 22c. OFFICE SYMBOL: AFOSR/NA

DD FORM 1473, 83 APR EDITION OF 1 JAN 73 IS OBSOLETE.

Unclassified

SECURITY CLASSIFICATION OF THIS PAGE

Section 19. ABSTRACT (Continued)

microcrack initiation under overall compression, interaction between cracks, development of plastic zones and their interaction with cracks, and the final failure mode of, say, rocks. In particular, attention was focused on the influence of the pressure and temperature on the failure mode and on the transition from brittle to ductile response. The modeling of observed axial splitting and faulting at moderate pressures and low temperatures was completed, and through some theoretical and model experiments, a basic understanding has been gained for the phenomenon of brittle-ductile transition at elevated pressures.

The experimental effort was carefully coordinated with the theoretical one. It consisted of two parts: (1) qualitative model studies in order to identify and understand the involved micromechanics; and (2) quantitative model tests.

FINAL SCIENTIFIC REPORT

for the period

1 October 1985 to 30 September 1986

on

FLOW AND FAILURE OF ROCKS, CONCRETE AND OTHER GEOMATERIALS

Grant No. AFOSR-86-0035

S. Nemat-Nasser, Principal Investigator
University of California, San Diego, La Jolla, California 92093

Table of Contents

November 1986

RESEARCH OBJECTIVES

The research completed under this AFOSR award was the continuation of efforts already initiated under Grant AFOSR-84-0004 at Northwestern University. The research aims at experimental and theoretical investigation of the micromechanics of flow and failure of rocks, concrete, and other related geo-materials at moderate to very high pressures and temperatures. As a result of this work, certain macroscopic nonlinear constitutive models have been developed, which reflect realistically the micromechanical events that produce observed macroscopic nonlinear and anisotropic responses of materials of this kind.

The theoretical work followed the principal investigator's recent effort in the micromechanical modeling of nonlinear material response. It included calculations of microcrack initiation under overall compression, interaction between cracks, development of plastic zones and their interaction with cracks, and the final failure mode of, say, rocks. In particular, attention was focused on the influence of the pressure and temperature on the failure mode and on the transition from brittle to ductile response. Under the AFOSR-84-0004, the modeling of observed axial splitting and faulting at moderate pressures and low temperatures was completed, and through some theoretical and model experiments, a basic understanding has been gained for the phenomenon of brittle-ductile transition at elevated pressures.

The experimental effort was carefully coordinated with the theoretical one. It consisted of two parts: (1) qualitative model studies in order to identify and understand the involved micromechanics; and (2) quantitative model tests.

ORGANIZATION OF THIS REPORT

This report is organized in the following manner.

In Chapter I, we list the papers that have been completed and provide a brief abstract of each paper. At the end of Chapter I, a list of scientific articles completed under this project is given. In Chapter I, we also give the list of participants and related information. Chapters II - IV each presents a complete research effort which, although finished, has not yet been published. Since Grant AFOSR-86-0035 actually constitutes the final year support for a three-year research effort which was started at Northwestern University under Grant AFOSR-84-0004, this report also includes a discussion of work completed under Grant AFOSR-84-0004.

CHAPTER I

Table of Contents

Table of Contents (Continued)

CHAPTER I

RESEARCH ACCOMPLISHMENTS

1. INTRODUCTION

The description of the mechanical response of rocks, concrete, and other related geo-materials under moderate to very high pressures and temperatures is of fundamental importance to current and future technological efforts. Many large-scale computer codes require accurate and realistic constitutive modeling of materials of this kind. At the same time, to be useful and effective, these models must be simple. Therefore, it is of paramount importance first to develop an in-depth understanding of the essential features responsible for the behavior of this kind of material in various loading and temperature regimes, and then to seek to formulate macroscopic constitutive models that embody the most essential micromechanical features. In this manner, one will have a good chance of arriving at realistic models of required simplicity.

One main feature of materials at focus here is that they naturally contain many microdefects and inhomogeneities. These defects and inhomogeneities serve as stress and strain concentrators, resulting in local stresses which are, in general, truly three-dimensional and very large, even when the overall applied load is one-dimensional (uni-axial) and relatively small. The overall behavior, therefore, is greatly influenced by the microstructure, and changes as the microstructure is changed in response to the applied loads.

The pressure affects the changes of the microstructure to a great extent. At low confining pressures, the existing cracks may open under tension or may undergo frictional sliding when under overall compression, with shear stress acting across the plane of the crack. In either case, tension cracks develop at the tips of the pre-existing flaws, and grow in the direction parallel to the maximum compression. At higher pressures, the growth of such tension cracks is soon arrested, but under overall applied loads, smaller flaws and inhomogeneities that are closely spaced begin to interact. This leads to a different microscopic response and, therefore, macroscopic failure. When the pressures are very high, local plastic flow is the major micromechanics of deformation, and the overall response, though highly nonlinear and still pressure-sensitive, becomes plastic.

The temperature has a similar effect. At low temperatures the response is more brittle, whereas at high temperatures it is more ductile.

Therefore, macroscopic constitutive modeling must take into account such varied microscopic behavior patterns. The aim of the research completed under this grant has been to develop theoretical micromechanical models, to verify these by quantitative and qualitative model experiments, and then to seek to develop appropriate macroscopic constitutive relations which embody the essential microfeatures.

2. PROGRESS

Under Grant AFOSR-84-0004, effort has been concentrated on completing the microscopic modeling: (1) analyzing the phenomenon of faulting under moderate confining presures; and (2) understanding the transition from brittle to ductile failure, under suitably high confining pressures, of brittle solids containing microdefects such as pre-existing cracks. This

work was continued under Grant AFOSR-86-0035 at the University of California, San Diego. Microcracking from voids in an elastic solid was formulated and solved. In addition, nonlinear constitutive relations associated with microcracking and damage have been developed. In the sequel, papers completed and published under both grants, AFOSR-84-0004 and AFOSR-86-0035, are listed together with their abstracts. In addition, wherever appropriate, comments are made to point out the significance of the obtained results.

2.1 Papers Published Under Grant AFOSR-84-0004:

2.1.1 H. Horii and S. Nemat-Nasser, "Elastic Fields of Interacting Inhomogeneities," *Int. J. Solids Structures, 21* (1985) 731-745.

In this paper a rather effective method has been developed, by which the interaction between two or among several defects in an elastic solid can be computed on the basis of the solution of a single defect in an infinitely extended homogeneous solid. The results are fundamental and allow us to estimate the failure mechanism in the presence of large confining pressures where the interaction among neighboring flaws leads to faulting. The abstract of this paper is as follows.

A rather general technique -- called the "method of pseudotractions" -- is presented for the calculation of the stress and strain fields in a linearly elastic homogeneous solid which contains any number of defects of arbitrary shape. The method is introduced and illustrated in terms of the problems of elastic solids containing two or several circular holes and solids containing two or several cracks, including the cases of rows of holes or cracks. It is shown that the solution of these and similar problems can be obtained to any desired degree of accuracy. Furthermore, if only estimates are needed, then the method is capable of yeilding closed-form analytic expressions for many interesting cases, e.g. the stress intensity factors at the crack tips.

2.1.2 H. Horii and S. Nemat-Nasser, "Brittle Failure in Compression: Splitting, Faulting, and Brittle-Ductile Transition," *Philosophical Transactions of the Royal Society of London 319,* No. 1549 (1986) 337-374.

This is a comprehensive paper which we hope will have a lasting effect on the understanding of the mechanics of brittle failure in compression and the mechanism of brittle-ductile transition at elevated pressures. Considerable effort has been required in preparing and publishing this paper.

The micromechanics of brittle failure in compression and the transition from brittle to ductile failure, observed under increasing confining pressures, are examined in the light of existing experimental results and model studies. First, the micromechanics of axial splitting and faulting is briefly reviewed, certain mathematical models recently developed for analysing these failure modes are outlined, and some new, simple closed-form analytic solutions of crack growth in compression and some new quantitative model experimental results are presented. Then, a simple two-dimensional mathematical model is proposed for the analysis of the brittle-ductile transition process, the corresponding elasticity boundary-value problem is formulated in terms of singular integral equations, the solution method is given, and numerical results are obtained and their physical implications are discussed. In addition, a simple closed-form analytic solution is presented and, by comparing its results with those of the exact formulation, it is shown that the analytic estimates are reasonably accurate in the range of the brittle response of the material. Finally, the results of some laboratory model experiments are reported in an effort to support the mathematical models.

In addition, the following papers have been published:

2.1.3 S. Nemat-Nasser and H. Horii, "Micro-mechanics of Fracture and Failure of Geo-materials in Compression," Proceedings of the ICF 6th Int. Conf. on Fracture, New Delhi, India, December 4-10, 1984; Pergamon Press, 1984, Vol. 1-R, pp. 515-524.

Recent analytical results on non-coplanar crack growth in elastic solids under far-field compressive stresses, are used to examine the micromechanics of brittle failure in compression. The three distinct failure modes -- axial splitting, faulting, and the transition from brittle to ductile response -- observed under axial compression for different confining pressures, are discussed in terms of simple plausible micro-mechanical models. The failure strength and the orientation of failure planes, as well as the stress ratio which marks the birttle-ductile transition, are estimated and compared with published data on various rocks, arriving at good correlations. In addition, certain model experiments which seem to support the analytical models, are examined.

2.1.4 S. Nemat-Nasser and H. Horii, "Rock Failure in Compression," *Int. J. Engng. Sci., Letters in Appl. and Engrg. Sciences*, 1984, Vol. 22, No. 8-10, pp. 999-1011.

Mechanisms of rock failure in compression -- axial splitting and shear failure -- are studied, based on a microscopic consideration. Analytical models are constructed and model experiments on plates of a brittle polymer are performed. It is shown that unstable growth of tension cracks which propagate from the tips of pre-existing cracks and curve towards the maximum compressive direction, is the fundamental mechanism that produces axial splitting of a uniaxially compressed rock specimen, whereas shear failure of a triaxially compressed specimen is a result of sudden growth of tension cracks at tips of a suitably arranged interacting set of microcracks. The

simultaneous out-of-plane unstable growth of a suitably oriented row of cracks is analyzed and, on the basis of this model, the variations of the "ultimate strength" and the orientation of the overall fault plane with the confining pressure are estimated. The brittle-ductile transition is discussed with the aid of a model which includes both tension crack extension and plastic zone development from the pre-existing cracks.

2.1.5 H. Horii and S. Nemat-Nasser, "Compression-Induced Microcrack Growth in Brittle Solids: Axial Splitting and Shear Failure," *J. Geophys. Res.*, 1985, Vol. 90, No. B4, pp. 3105-3125.

Micromechanisms of rock failure (axial splitting and shear failure) are examined in light of simple mathematical models motivated by microscopic observations. The elasticity boundary value problem associated with cracks growing from the tips of a model flaw is solved. It is shown that under axial compression, tension cracks nucleate at the tips of the preexisting model flaw, grow with increasing compression, and become parallel to the direction of the maximum far-field compression. When a lateral compression also exists, the crack growth is stable and stops at some finite crack length. With a small lateral tension, on the other hand, the crack growth becomes unstable after a certain crack length is attained. This is considered to be the fundamental mechanism of axial splitting observed in uniaxially compressed rock specimens. To model the mechanism of shear failure, a row of suitably oriented model flaws is considered and the elasticity boundary value problem associated with the out-of-plane crack growth from the tips of the flaws is solved. It is shown that for a certain overall orientation of the flaws the growth of the out-of-plane cracks may become unstable, leading to possible macroscopic faulting. On the basis of this model the variations of the "ultimate strength" and the orientation of the overall fault plane with confining pressure are estimated, and the results are compared with published experimental data. In addition, the results of a set of model experiments on plates of Columbia resin CR39 containing preexisting flaws are reported. These experiments are specifically designed in order to show the effect of confining pressure on the crack growth regime. The experiments seem to support qualitatively the analytical results.

2.1.6 S. Nemat-Nasser and H. Horii, "Mechanics of Brittle Failure in Compression," *Computers & Structures*, 1985, Vol. 20, No. 1-3, pp. 235-237.

The mechanics of brittle failure in compression is reviewed in light of experimental observations and some recent results from micromechanical modeling. The axial splitting, faulting and the transition from brittle to ductile response are discussed. It is concluded that the descending portion of the stress-strain curve (i.e. the strain-softening), often observed for materials of this kind, does not represent a continuum response: therefore, many numerical calculations in the strain-softening range should be viewed with caution.

2.2 Work Completed Under Grant AFOSR-86-0035

Three major papers and a short note were completed, submitted for publication, and since have been accepted. Two of these papers, items 2.2.1 and 2.2.2, relate to the failure of porous solids in compression. The results apply to porous rocks and to ice where bubbles and cavities are responsible for initiating microcracking under compressive loads. The third paper, item 2.2.3, is a major contribution in obtaining overall nonlinear constitutive relations for brittle solids in compression. The effects of microflaws are formulated and the corresponding overall response is computed. The short note is an interesting illustration of the complex overall material response in the presence of microcracks.

2.2.1 "A Unified Analysis of Various Problems Relating to Circular Holes with Edge Cracks" Engineering Fracture Mechanics, in press.

A unified method of analysis is developed for various problems relating to elastic plates containing circular holes with edge cracks. The method is based on the analysis of a unit rectangular region containing a circular hole with edge cracks, where the boundary conditions of the outer edges are suitably adjusted in order to treat various problems including periodic arrays of holes with edge cracks. The method is applied to five problems, and accurate values of the stress intensity factors are obtained. These analytical values of the stress intensity factors are fitted by polynomials which are convenient for practical applications.

2.2.2 "On Mechanics of Crack Growth and Its Effects on the Overall Response of Brittle Porous Solids," Acta Metallurgica, in press.

This paper is concerned with crack growth in brittle porous solids under compression and its effects on the overall response of the material. As a mathematical model, we consider an elastic solid containing a zig-zag array of circular holes with a pair of edge cracks (two-dimensional problem), and solve this problem by using a theory which gives numerical results as accurate as desired. Based on the analytical results, we discuss the crack growth process and estimate the effective Young's moduli as well as the stress-strain relation for porous solids. Our computations show that the cracks emanating from the poles of the circular holes extend in the axial direction and grow -- in most cases in a stable manner, but for certain cases in an unstable manner during an intermediate loading state -- as the overall applied uniaxial compression increases, reaching a certain limiting maximum length. This maximum crack length strongly depends on the ratio of the hole radius to the hole spacing in the loading direction. The effective Young's modulus in the direction of the crack growth is basically determined by the initial porosity, and is little affected by the crack length or its growth regime, i.e., whether stable or unstable. We find that the overall axial stress-strain curve remains monotonic, exhibiting no peak stress or strain softening, as cracks extend in the axial direction and reach their limiting length with increasing axial stress.

2.2.3 "A Microcrack Model of Dilatancy in Brittle Materials," Journal of Applied Mechanics, in press.

For a solid containing preexisting flaws, overall nonlinear constitutive relations are developed on the basis of a model which endows a preexisting flaw with frictional and cohesive resistance, and which includes nucleation and growth of tension cracks at the preexisting flaw, as it deforms under the action of an overall compressive load. The preexisting flaws may be randomly distributed or may have an initial preferential distribution. They may be of varying sizes and orientations. Even when the flaws are randomly distributed, their preferential activation, and the nucleation and growth of tension cracks at preferential flaws, render the overall response of the solid highly anisotropic. As a first step toward a more complete constitutive micromechanical modeling, a dilute distribution of preexisting flaws is assumed, rate constitutive relations are developed for loading and unloading, which include hysteresis, dilatancy, and other characteristics observed experimentally in rocks, ceramics, concrete, and similar brittle materials. A number of illustrative examples are worked out, and the results are compared to relevant experimental observations.

The following papers were revised as required during the review process, considerably improved and expanded, and the final manuscripts were submitted for publication:

B. Rowshandel and S. Nemat-Nasser, "Finite Strain Rock Plasticity: Stress Triaxiality, Pressure, and Temperature Effects," Soil Dynamics and Earthquake Engineering, in press.

B. Rowshandel and S. Nemat-Nasser, "A Mechanical Model for Deformation and Earthquake on Strike-Slip Faults," Pure and Applied Geophysics 124, No. 3 (1986) 532-566.

3. LIST OF PUBLICATIONS COMPLETED

H. Horii and S. Nemat-Nasser, "Elastic Fields of Inhomogeneities," Int. J. Solids Structures, 21 (1985) 731-745.

H. Horii and S. Nemat-Nasser, "Brittle Failure in Compression: Splitting, Faulting, and Brittle-Ductile Transition," Philosophical Transactions of the Royal Society of London 319, No. 1549 (1986) 337-374. (Considerable effort has been devoted to completing this manuscript, which is a rather comprehensive account of our work supported by AFOSR).

S. Nemat-Nasser and H. Horii, "Micromechanics of Fracture and Failure of Geomaterials in Compression," Proceedings of the ICF 6th Int. Conf. on Fracture, New Delhi, India, December 4-10, 1984: Pergamon Press, 1984, Vol. 1-R, pp. 515-524.

S. Nemat-Nasser and H. Horii, "Rock Failure in Compression," Int. J. Engrg. Sci., Letters in Appl. and Engrg. Sciences, 1984, Vol. 22, No. 8-10, pp. 999-1011.

H. Horii and S. Nemat-Nasser, "Compression-Induced Micro-Crack Growth in Brittle Solids: Axial Splitting and Shear Failure," J. Geophys. Res., 1985, Vol. 90, No. B4, pp. 3105-3125.

S. Nemat-Nasser and H. Horii, "Mechanics of Brittle Failure in Compression," Computers & Structures, 1985, Vol. 20, No. 1-3, pp. 235-237.

M. Isida and S. Nemat-Nasser, "A Unified Analysis of Various Problems Relating to Circular Holes with Edge Cracks," Engineering Fracture Mechanics, in press.

M. Isida and S. Nemat-Nasser, "On Mechanics of Crack Growth and Its Effects on the Overall Response of Brittle Porous Solids," Acta Metallurgica, in press.

S. Nemat Nasser and M. Obata, "A Microcrack Model of Dilatancy in Brittle Materials," Journal of Applied Mechanics, in press.

4. PROFESSIONAL PERSONNEL ASSOCIATED WITH THE RESEARCH EFFORT; DEGREES AWARDED

Principal Investigator: S. Nemat Nasser

Postdoctoral Research Associates and Visiting Scholars:

MAKOTO ISHIDA, Visiting Professor, (Kyushu University, Fukuoka, and Kurume Institute of Technology, Kurume, Japan)

MAKOTO OBATA, (Postdoctoral Research Associate, Department of Applied Mechanics and Engineering Sciences, University of California, San Diego, La Jolla, California)

BENJAMIN LORET (Research Associate, Ecole Polytechnique, Palaiseau, France)

MORTEZA M. MEHRABADI (Associate Professor, Department of Mechanical Engineering, Tulane University, New Orleans, Louisiana)

DONG-TEAK CHUNG (Postdoctoral Research Associate, Department of Applied Mechanics and Engineering Sciences, University of California, San Diego, La Jolla, California)

Graduate Students	Degrees Awarded (AFOSR SUPPORT)
H. HORII,	Ph.D., Northwestern University
MUNEO HORI,	M.S., Northwestern University
JAE-YOUN CHANG,	M.S., Northwestern University

Other Graduate Students (Partially supported)

JAE-YOUN CHANG
MUNEO HORI

Other Researchers Who Have Been Involved in the Project:

JOHN E. STARRETT, Principal Development Engineer

5. INTERACTIONS (COUPLING ACTIVITIES)

A. Participation of Principal Investigator at Meetings -- Papers Presented; Lectures at Seminars (Under AFOSR-86-0035 only)

"Generalization of the Mandel-Spencer Double Slip Model," International Symposium on Physical Basis and Modeling of Finite Deformation of Aggregates, Paris, France, September 30-October 2, 1985.

"Failure in Compression," Ecole Polytechnique, Palaiseau, France, September 30-October 2, 1985.

"Failure in Compression," University of California, Santa Barbara, March 3, 1986.

"Micromechanically Based Constitutive Modeling of Inelastic Response of Solids," Proceedings of the ARO Workshop on Constitutive Models, Virginia Polytechnic Inst. March 24-26, 1986.

"Failure in Compression, " U.S. Army Research Office Workshop on Dynamic Deformation and Fracture, Leesburg, Virginia, May 12-15, 1986.

"Failure in Compression," NSF Workshop, Assessment of Experimental Techniques Applicable to Rock Fracture, Park City, Utah, May 29-30, 1986.

"Mechanics of Failure in Compression," Invited Plenary Contribution, Paper 211, Sixth European Conference on Fracture, Amsterdam, The Netherlands, June 15-20, 1986.

"Mechanics of Failure in Compression," Tohoku University, Sendai, Japan, June 27, 1986.

B. Consultative and Advisory Functions to Other Agencies or Laboratories

--Member of DARPA Panel on Material Modeling and Large Scale Computations, 1983-Present

International Symposium on Physical Basis and Modelling of Finite Deformation of Aggregates Paris, France September 30-October 4, 1985	--- Member of Scientific Committee - Co-Editor of Proceedings - Synthesizer
CISM Seminar, Simplified Analysis of Inelastic Structures Subjected to Statical or Dynamical Loadings Ecole Polytechnique, Paris, France, October 7-10, 1985	--- Synthesizer - Organizer of Discussions

CHAPTER II

A UNIFIED ANALYSIS OF VARIOUS PROBLEMS RELATING TO CIRCULAR HOLES WITH EDGE CRACKS*

by

M. Isida
S. Nemat-Nasser

Table of Contents

* Engineering Fracture Mechanics, in press.

CHAPTER II

A UNIFIED ANALYSIS OF VARIOUS PROBLEMS RELATING TO CIRCULAR HOLES WITH EDGE CRACKS

M. Isida* and S. Nemat-Nasser

Department of Applied Mechanics and Engineering Sciences

University of California, San Diego, La Jolla, CA 92093

Abstract

A unified method of analysis is developed for various problems relating to elastic plates containing circular holes with edge cracks. The method is based on the analysis of a unit rectangular region containing a circular hole with edge cracks, where the boundary conditions of the outer edges are suitably adjusted in order to treat various problems including periodic arrays of holes with edge cracks. The method is applied to five problems, and accurate values of the stress intensity factors are obtained. These analytical values of the stress intensity factors are fitted by polynomials which are convenient for practical applications.

* Present address: Department of Mechaical Engineering, Kurume Institute of Technology, 2228 Mukuno Kamitsumachi, Kurume 830, Japan.

NOMENCLATURE

x, y	Cartesian coordinates
z	complex coordinate $= x + iy$
$2b, 2c$	length and width of rectangular region
γ	aspect ratio of rectangular region $= \frac{c}{b}$
a	hole radius
α	normalized hole radius $= \frac{a}{c}$
ℓ	crack length
L	normalized crack length $= \frac{\ell}{a}$
β	crack length parameter $= (1+L)^{-1}$
E	Young's modulus of material
ν	Poisson's ratio of material
κ	$\kappa = \frac{3-\nu}{1+\nu}$ (plane stress), $= 3 - 4\nu$ (plane strain)
G	shear modulus $= \frac{E}{2(1+\nu)}$
$\sigma_x, \sigma_y, \tau_{xy}$	stress components in Cartesian coordinates
σ_0	reference stress
σ_1, σ_2	principal stresses at infinity
λ	ratio of principal stresses at infinity $= \frac{\sigma_2}{\sigma_1}$ $(\sigma_1 \neq 0)$
P_x, P_y	resultant force components in Cartesian coordinates
u, v	displacement components in Cartesian coordinates
$\phi(z), \psi(z)$	complex stress potentials
$\phi_1(z), \psi_1(z)$	complex stress potentials in Laurent expansion
$p_m(s_m)$	densities of distributed force doublets
$q_m(s_m)$	weighting functions of force doublet densities

M	subdivision number of crack
N_1	subdivision number of side $\overline{EF}$
N_2	subdivision number of side $\overline{FG}$
h_1	length of intervals on side $\overline{EF}$
h_2	length of intervals on side $\overline{FG}$
K_I	Mode I stress intensity factor
F_ℓ	dimensionless stress intensity factor $= \dfrac{K_I}{\sigma_0(\pi\ell)^{1/2}}$
F_a	dimensionless stress intensity factor $= \dfrac{K_I}{\sigma_0(\pi a)^{1/2}}$
K_{Ic}	critical stress intensity factor

1. INTRODUCTION

Since the pioneering work of Griffith [1], it has been commonly accepted that brittle failure is often caused by the formation and growth of tension cracks which usually nucleate at micro-defects such as preexisting cracks, voids, and other micro-heterogeneities. Recent analytical and experimental work [2-11] has clearly shown that, even under overall compressive farfield loads, brittle failure is usually a result of nucleation and growth of micro-tension cracks. An important class of micro-defects which may be a source of crack nucleation, is micro-cavities which are commonly present in most solids such as rocks, ceramics, metals, bones, etc. To be able to examine the physical consequences of strength degradation by crack nucleation and growth at preexisting cavities, one requires a solution of the problem of crack growth from the walls of cavities under prescribed farfield stresses. In the two-dimensional case, the elasticity problem of cracks extending from the edges of a circular hole has been solved by Bowie [12] for an infinitely extended medium. The more general problem of cracks emanating from an elliptical hole in a plane has been treated by several authors [13-16] where some of the results have been put in a form convenient for design purposes [17,18].

In this paper we consider a class of elasticity problems relating to circular holes with edge-cracks, and solve these problems by a unified method. This method is such that the results can be rendered as accurate as desired. The basic problem is formulated for a rectangular region containing a circular hole with two edge-cracks emanating from the hole. Various cases are then studied by adjusting the boundary conditions on the outer boundaries of the rectangular region. In this manner, solutions are

obtained for a finite region, for a strip containing an array of holes with edge-cracks, and for a sheet containing doubly-periodic holes and edge-cracks. These results are fitted by polynomials which are convenient for practical applications.

2. THEORETICAL ANALYSIS

2.1 Description of the problem

Consider a rectangular region containing a central circular hole and a pair of equal cracks, emanating from the hole in the x-direction; see Fig.1-1 for notation and definition of various geometric quantities. A variety of problems including periodic arrays of holes with edge cracks can be analysed by adjusting the boundary conditions of this rectangular region. We consider a class of problems for which the boundary conditions are symmetric about both coordinate axes. We solve this class of problems using suitably symmetric stress potentials defined on the first quadrant, OEFGO in Fig.1-1, and by enforcing the desired boundary conditions.

This paper deals with the following five problems:

(1) Uniform normal loads along $\overline{EF}$ and along $\overline{FG}$, (Fig.1-1).

(2) Infinite strip in the x-direction with a periodic array of holes and edge cracks aligned in the x-direction. This case corresponds to a rectangular specimen subjected to uniform displacement u without shear along $\overline{EF}$, (Fig.1-2).

(3) Infinite strip in the y-direction with a periodic array of holes and edge cracks aligned in the x-direction. This case corresponds to a rectangular specimen subjected to uniform displacement v without shear along $\overline{FG}$, (Fig.1-3).

(4) Infinite solid with doubly periodic array of holes and edge cracks, (Fig.1-4).

(5) Infinite solid with zig-zag periodic array of holes and edge cracks, (Fig.1-5).

The conditions on the outer edges depend on the problem, and are summarized in Table 1. In this table, u and v are the components of the displacement, P_x and P_y are those of the resultant force transmitted across an arbitrary path from a fixed point (x_0, y_0) to a typical point (x, y), and σ_1 and σ_2 are the applied stresses in the x- and y-directions, respectively. The cracks are assumed to be traction-free for all the treated problems. Hence, the results are valid for combinations of σ_1 and σ_2 that satisfy this assumption.

2.2. Basic relations

In plane problems of elasticity, components of the stress, the displacement and the resultant force with respect to the Cartesian coordinates are expressed in terms of two complex potentials, $\phi(z)$ and $\psi(z)$, and their derivatives, as follows:

$$\frac{\sigma_y + \sigma_x}{2} = 2\,\mathrm{Re}[\phi'(z)]$$

$$\frac{\sigma_y - \sigma_x}{2} + i\tau_{xy} = \bar{z}\,\phi''(z) + \psi''(z) \tag{1}$$

$$2G\,(u - iv) = \kappa\,\bar{\phi}(\bar{z}) - \bar{z}\phi'(z) - \psi'(z) \tag{2}$$

$$P_y + iP_x = -\,\bar{\phi}(\bar{z}) - \bar{z}\phi'(z) - \psi'(z) \tag{3}$$

where G is the shear modulus, and κ is defined in terms of Poisson's ratio, ν, as follows:

$$\kappa = \frac{3 - \nu}{1 + \nu} \quad \text{(plane stress)}, \quad = 3 - 4\nu \quad \text{(plane strain)} \tag{4}$$

The analysis is performed by superposing two stress states. The first

one is introduced in order to satisfy the outer boundary conditions, and is represented by the complex potentials $\phi_1(z)$ and $\psi_1(z)$ having singularities within the hole. The second stress state is properly singular at crack tips, and is realized by distributing suitable force doublets along the cracks.

The above two stress states are established in such a manner that they automatically satisfy the traction-free conditions at the hole. These stress states include unknown parameters which are then determined from the boundary conditions on the cracks and the outer edges of the rectangular region.

2.3. Displacement and resultant force due to $\phi_1(z)$ and $\psi_1(z)$

The complex potentials $\phi_1(z)$ and $\psi_1'(z)$ for the first stress state are expressed as the following Laurent series:

$$\phi_1(z) = \sum_{n=0}^{N-1} [\, F_{2n} z^{-(2n+1)} + M_{2n} z^{2n+1} \,]$$

$$\psi_1'(z) = \sum_{n=0}^{N-1} [\, D_{2n} z^{-(2n+1)} + K_{2n} z^{2n+1} \,] \qquad (5)$$

The coefficients F_{2n}, M_{2n}, D_{2n} and K_{2n} ($n = 0,1,2,\cdots,N-1$) are real due to the symmetry of the problem. N is to be fixed at the stage of the boundary collocation procedure, as discussed in Section 2.5.

The traction-free conditions at the hole require that

$$D_0 = -2M_0 a^2$$

$$D_{2n} = -(2n-1) K_{2n-2} a^{4n} - (2n)^2 M_{2n} a^{4n+2} \quad (1 \le n \le N-1) \qquad (6)$$

$$F_{2n} = -K_{2n} a^{4n+2} - (2n+3) M_{2n+2} a^{4n+4} \quad (0 \le n \le N-1)$$

Substituting Eqns. (6) into Eqns. (5), the complex potentials for the first stress state are obtained as follows:

$$\phi_1(z) = M_0 z + \sum_{n=0}^{N-1}[M_{2n}\{z^{2n+1}-(2n+1)a^{4n}z^{-(2n-1)}\}-K_{2n}a^{4n+2}z^{-(2n+1)}]$$

$$\psi_1'(z) = -2M_0\, a^2 z^{-1} + \sum_{n=0}^{N-1}[K_{2n}\{z^{2n+1}-(2n+1)a^{4n+4}z^{-(2n+3)}\} \qquad (7)$$

$$-M_{2n}(2n)^2 a^{4n+2}z^{-(2n+1)}]$$

The boundary conditions of the present problems have been given in Table 1 in terms of stress and displacement components. But in the analysis, the stress conditions are replaced by those of the resultant force in order to increase the accuracy of the numerical results [19,20].

Using Eqns.(7) in Eqns.(2) and (3), we have the following expressions for the displacement and the resultant force components:

$$2G(u - iv)_{(1)} = M_0\{2a^2 z^{-1}+(\kappa-1)\bar{z}\}+ \sum_{n=1}^{N-1} M_{2n}[\kappa\bar{z}^{2n+1}-(2n+1)\bar{z}z^{2n}$$

$$+(2n+1)a^{4n}\{-\kappa\bar{z}^{-(2n-1)}-(2n-1)\bar{z}z^{-2n}\}+(2n)^2\, a^{4n+2}z^{-(2n+1)}]$$

$$+ \sum_{n=0}^{N-1} K_{2n}[-z^{2n+1}-a^{4n+2}\{\kappa z^{-(2n+1)}+(2n+1)\bar{z}z^{-(2n+2)}\}$$

$$+(2n+1)a^{4n+4}z^{-(2n+3)}] \qquad (8.1)$$

$$(P_y + iP_x)_{(1)} = M_0(2a^2 z^{-1} - 2\bar{z})+ \sum_{n=1}^{N-1} M_{2n}[-\bar{z}^{2n+1}-(2n+1)\bar{z}z^{2n}$$

$$+(2n+1)a^{4n}\{\bar{z}^{-(2n-1)}-(2n-1)\bar{z}z^{-2n}\}+(2n)^2\, a^{4n+2}z^{-(2n+1)}]$$

$$+ \sum_{n=0}^{N-1} K_{2n}[-z^{2n+1}+a^{4n+2}\{z^{-(2n+1)}-(2n+1)\bar{z}z^{-(2n+2)}\}$$

$$+(2n+1)a^{4n+4}z^{-(2n+3)}] \qquad (8.2)$$

The above expressions include 2N unknown coefficients M_{2n} and K_{2n} $(n = 0,1,2,\cdots,N-1)$ to be determined from the boundary conditions.

2.4. Displacement and resultant force due to force doublets

The second stress state is realized by distributing force doublets of arbitrary density on the cracks. The force doublets are established from stress states for concentrated forces acting in an infinite solid which contains a circular hole, and, therefore, the traction-free conditions at the hole edge are satisfied automatically. Expressions for the displacement and the resultant force components due to distributed force doublets have been derived by Isida and Noguchi [21], and are as follows:

$$2G\,(u - iv)_{(2)} = \frac{1}{2\pi}\sum_{m=1}^{2}\int_{-\ell/2}^{\ell/2} p_m(s_m)\left[-\frac{1}{s_m-w_1} + \frac{\kappa}{s_m-w_1} + \frac{w_1-\bar{w}_1}{(s_m-w_1)^2}\right.$$

$$+ \frac{1}{s_m-w_2} - \frac{\kappa}{s_m-\bar{w}_2} + \frac{\bar{w}_1-w_2}{(s_m-w_2)^2} - \frac{\kappa(\bar{w}_1-\bar{w}_2)}{(s_m-w_2)^2} - 2(w_1-w_2)(\bar{w}_1-w_2)\frac{a^2}{z^2}\frac{1}{(s_m-w_2)^3}$$

$$\left. + 2\left(\kappa z + \frac{a^2}{z}\right)\frac{1}{(s_m+w_3)^2}\right] \qquad (9.1)$$

$$(P_y + iP_x)_{(2)} = \frac{1}{2\pi}\sum_{m=1}^{2}\int_{-\ell/2}^{\ell/2} p_m(s_m)\left[-\frac{1}{s_m-w_1} - \frac{1}{s_m-w_1} + \frac{w_1-\bar{w}_1}{(s_m-w_1)^2}\right.$$

$$+ \frac{1}{s_m-w_2} + \frac{1}{s_m-\bar{w}_2} + \frac{\bar{w}_1-w_2}{(s_m-w_2)^2} + \frac{\bar{w}_1-\bar{w}_2}{(s_m-w_2)^2} - 2(w_1-w_2)(\bar{w}_1-w_2)\frac{a^2}{z^2}\frac{1}{(s_m-w_2)^3}$$

$$\left. + 2\left(-z + \frac{a^2}{z}\right)\frac{1}{(s_m+w_3)^2}\right] \qquad (9.2)$$

where $p_m(s_m)$ $(m = 1,2)$ are unknown density functions of the force doublets,

and the subscript m takes 1 for the right and 2 for the left crack, respectively; the following notation is also used (see Fig. 2):

$$w_1 = z - x_{0,m}\ ,\quad w_2 = \frac{a^2}{z} - x_{0,m}\ ,\quad w_3 = x_{0,m}$$

$$x_{0,m} = a + \frac{\ell}{2} \qquad (m=1) \tag{10}$$

$$x_{0,m} = -a - \frac{\ell}{2} \qquad (m=2)$$

The density functions $p_m(s_m)$ in Eqns. (9) are expressed as [22]

$$p_m(s_m) = q_m(s_m)\,[\,(\tfrac{\ell}{2})^2 - s_m^2\,]^{-\frac{1}{2}} \tag{11}$$

where the weighting functions $q_m(s_m)$ are regular.

Eqn. (11) actually defines force doublet densities with singularities at both ends, $s_m = \pm\ell/2$. It applies to the present problem, provided the resultant force conditions (instead of stress conditions) are used, as can be seen by the accurate results obtained even with small number of of subdivisions shown in Tables 2 to 4 of Section 3.2.

It is obvious from symmetry that

$$q_2(-s_2) = q_1(s_1) \tag{12}$$

Thus $q_1(s_1)$ is the only unknown function in the second stress state.

2.5. Boundary conditions based on resultant force and displacement

A piecewise linear approximation will be used to estimate the unknown weighting function $q_1(s_1)$. For the right crack, this is shown in Fig. 3, where equally spaced intervals are used. Eqns. (9.1) and (9.2) now reduce to linear expressions in f_j $(j = 1,2,\cdots,M)$ which are the values of the weighting function at the ends of these intervals.

We now have 2N unknown coefficients in the first stress state and M unknown weights, f_j, in the second stress state to be determined from the boundary conditions. Since both stress states satisfy the traction-free conditions on the hole, we have only to consider the boundary conditions on the crack and at the outer edges of the first quadrant. These conditions are satisfied by means of a boundary collocation procedure based on the displacements and the resultant forces. In the numerical computations, the traction-free conditions of the cracks are replaced by M relations, and those of the outer edges by 2N relations.

The traction-free conditions on the cracks are common to all considered problems. In order to obtain M relations from the traction-free conditions on crack $\overline{A_1B_1}$ (stated in terms of resultant force components P_y), we divide this crack into M unequal intervals, $\overline{D_1D_2}$, $\overline{D_2D_3}$,--- $\overline{D_MD_{M+1}}$, where D_2, D_3,---, D_M are the mid-points of previously defined equal intervals (Fig.3). Then the traction-free conditions are:

$$\text{Along crack } \overline{A_1B_1}: \qquad [P_y]_{D_k}^{D_{k+1}} = 0 \quad (k = 1,2,\text{---},M) \tag{13}$$

To impose the boundary conditions at the outer edges, $\overline{EF}$ and $\overline{FG}$ are divided into N_1 and N_2 equal intervals, respectively, as shown in Fig. 4. The corresponding interval lengths then are

$$h_1 = \frac{c}{N_1}, \quad h_2 = \frac{b}{N_2} \tag{14}$$

The integer N in Eqn. (8) is chosen such that

$$N = N_1 + N_2 \tag{15}$$

Now the boundary conditions for all five problems given in Table 1 are replaced by the following relations in term of the resultant force and the

displacement components:

Problem (1)

$$\text{Along } \overline{EF} : [P_x]_{S_k}^{S_{k+1}} = \sigma_1 h_1,\ [P_y]_{S_k}^{S_{k+1}} = 0 \quad (k = 1,2,---,N_1)$$

$$\text{Along } \overline{FG} : [P_x]_{S_k}^{S_{k+1}} = 0,\ [P_y]_{S_k}^{S_{k+1}} = \sigma_2 h_2 \quad (k = N_1+1, N_1+2, ---, N) \tag{16}$$

Problem (2)

$$\text{Along } \overline{EF} : [u]_{S_k}^{S_{k+1}} = 0,\ [P_x]_E^F = \sigma_1 c,\ [P_y]_{S_k}^{S_{k+1}} = 0 \quad (k = 1,2,---,N_1)$$

$$\text{Along } \overline{FG} : [P_x]_{S_k}^{S_{k+1}} = 0,\ [P_y]_{S_k}^{S_{k+1}} = \sigma_2 h_2 \quad (k = N_1+1, N_1+2, ---, N) \tag{17}$$

Problem (3)

$$\text{Along } \overline{EF} : [P_x]_{S_k}^{S_{k+1}} = \sigma_1 h_1,\ [P_y]_{S_k}^{S_{k+1}} = 0 \quad (k = 1,2,---,N_1)$$

$$\text{Along } \overline{FG} : [P_x]_{S_k}^{S_{k+1}} = 0,\ [v]_{S_k}^{S_{k+1}} = 0,\ [P_y]_F^G = \sigma_2 b \quad (k = N_1+1, N_1+2, ---, N) \tag{18}$$

Problem (4)

$$\text{Along } \overline{EF} : [u]_{S_k}^{S_{k+1}} = 0,\ [P_x]_E^F = \sigma_1 c,\ [P_y]_{S_k}^{S_{k+1}} = 0 \quad (k = 1,2,---,N_1)$$

$$\text{Along } \overline{FG} : [P_x]_{S_k}^{S_{k+1}} = 0,\ [v]_{S_k}^{S_{k+1}} = 0,\ [P_y]_F^G = \sigma_2 b \quad (k = N_1+1, N_1+2, ---, N) \tag{19}$$

Problem (5)

For convenience, N_2 is taken to be an even integer, say $2N_3$, and the following relations (20.1) and (20.2) are used :

$$\text{Along } \overline{EF} : [u]_{S_k}^{S_{k+1}} = 0, \quad [P_y]_{S_k}^{S_{k+1}} = 0 \qquad (k = 1,2,\cdots,N_1)$$

$$\text{Along } \overline{FG} : [P_y]_{S_k}^{S_{k+1}} = [P_y]_{S_{N_4-k}}^{S_{N_4+1-k}}, \quad [P_x]_{S_k}^{S_{k+1}} = [P_x]_{S_{N_4-k}}^{S_{N_4+1-k}}$$

$$[u]_{S_k}^{S_{k+1}} = [u]_{S_{N_4-k}}^{S_{N_4+1-k}}, \quad [v]_{S_k}^{S_{k+1}} = [v]_{S_{N_4-k}}^{S_{N_4+1-k}}$$

$$N_3 = N_2/2, \quad N_4 = 2N_1 + N_2 + 1 \qquad (k = N_1+1, N_1+2, \cdots, N_1+N_3)$$

(20.1)

For the total forces:

$$[P_x]_E^F - [P_x]_G^H = 2\sigma_1 c \ , \quad [P_y]_F^G = \sigma_2 b \qquad (20.2)$$

3. NUMERICAL ANALYSIS

3.1. Dimensionless stress intensity factors

The unknown quantities K_{2n}, M_{2n} $(n = 0,1,2,\cdots,N-1)$ and f_j $(j = 1,2,\cdots,M)$ are determined by solving the simultaneous relations consisting of Eqns. (13) and one of Eqns.(16) to (20) depending on the considered problem. The stress intensity factor at the crack tip is then calculated by

$$K_I = f_M \left(\frac{\pi \ell}{2}\right)^{1/2} \tag{21}$$

We consider the following two cases of uniaxial loading:

(a) Compression in the x-direction : $\sigma_1 = -\sigma_0$, $\sigma_2 = 0$

(b) Tension in the y-direction : $\sigma_1 = 0$, $\sigma_2 = \sigma_0$

where σ_0 is a positive reference stress.

Calculations have been performed for all possible combinations of the following values of the geometric parameters: b/c = 2, 1.75, 1.5, 1.25, 1, 1/1.25, 1/1.5, 1/1,75, 1/2; c/a = 5, 6, 7, 8, 9, 10; L/a = 0.5, 1., 1.5, 2.0, 2.5, 3.0, 3.5, 4.0, 4.5, 5.0, 5.5, 6.0, 6.5, 7.0.

The numerical results are summarized in terms of two dimensionless stress intensity factors: one is based on the hole radius; and the other is based on the crack length. These dimensionless stress intensity factors are:

$$F_\ell^{(i,x)} = \frac{K_I^{(i,x)}}{\sigma_0(\pi\ell)^{1/2}}, \quad F_a^{(i,x)} = \frac{K_I^{(i,x)}}{\sigma_0(\pi a)^{1/2}} \quad (\sigma_1 = -\sigma_0, \sigma_2 = 0) \tag{22a}$$

$$F_\ell^{(i,y)} = \frac{K_I^{(i,y)}}{\sigma_0(\pi\ell)^{1/2}}, \quad F_a^{(i,y)} = \frac{K_I^{(i,y)}}{\sigma_0(\pi a)^{1/2}} \quad (\sigma_1 = 0, \sigma_2 = \sigma_0) \tag{22b}$$

$$(i = 1, 2, 3, 4, 5)$$

Here, superscript i denotes the problem number, and superscript x or y designates the loading direction.

As a/c tends to zero, the quantities in Eqns. (22) for all five problems should converge to the results for an infinite solid containing a hole with edge cracks. The results for this limiting problem are also given in terms of the following dimensionless stress intensity factors:

$$F_{\ell,0}^{(x)} = \frac{K_{I,0}^{(x)}}{\sigma_0(\pi\ell)^{1/2}}, \quad F_{a,0}^{(x)} = \frac{K_{I,0}^{(x)}}{\sigma_0(\pi a)^{1/2}} \quad (\sigma_1 = -\sigma_0,\ \sigma_2 = 0) \tag{23a}$$

$$F_{\ell,0}^{(y)} = \frac{K_{I,0}^{(y)}}{\sigma_0(\pi\ell)^{1/2}}, \quad F_{a,0}^{(y)} = \frac{K_{I,0}^{(y)}}{\sigma_0(\pi a)^{1/2}} \quad (\sigma_1 = 0,\ \sigma_2 = \sigma_0) \tag{23b}$$

$$F_{\ell,0} = \frac{K_{I,0}}{\sigma_0(\pi\ell)^{1/2}}, \quad F_{a,0} = \frac{K_{I,0}}{\sigma_0(\pi a)^{1/2}} \quad (\sigma_1 = -\sigma_0,\ \sigma_2 = \lambda\sigma_1) \tag{23c}$$

where subscript x or y designates the loading direction, and $F_{\ell,0}$ and $F_{a,0}$ denote the values for biaxial loadings.

3.2. Accuracy of numerical results

The accuracy of the numerical results would be improved by increasing subdivision numbers M, N_1 and N_2. It is however desirable to use minimum values for these quantities, which still provide needed accuracy.

Reasonable values of M have been determined from test calculations of an infinite solid. Table 2 gives typical results for $\ell/a = 0.4$. As is seen, any M larger than 3 seems to give reliable values with errors less than one per cent. Calculations also have been done for several finite regions. Based on this information, M is taken to be 7 to 10 depending on the region geometry.

Other series of test calculations also have been done to determine reasonable values for N_1 and N_2. Tables 3 and 4 give the values of $F_a^{(i,x)}$ and $F_a^{(i,y)}$ for various values of N_1 $(=N_2)$, where $b=c$, $a/c=0.2$, $\ell/a=2$ and $M=6$. The convergence is excellent, and N_1, N_2 larger than 4 are likely to give reliable values with errors less than one per cent. On the basis of the above and similar results for other configurations, N_1 and N_2 are chosen to be 5 to 10 depending on the geometry.

Thus the number of unknowns to be determined from the boundary conditions is confined to less than 50 with good accuracy.

4. NUMERICAL RESULTS AND DISCUSSION

4.1. Infinite solid with a hole and cracks

Reliable solutions are available for an infinite solid containing a hole with edge cracks. However, we have reanalysed this problem because of its importance as a common limiting case for all other considered problems. The results also give useful information on the accuracy of the basic method, and help to fix the value of M to be used for each problem.

The numerical values of $F^{(x)}_{\ell,0}$ and $F^{(y)}_{\ell,0}$ are fitted by the following five-term polynomials for the range $0 \le \ell/a \le 7$:

(a) Compression in the x-direction

$$F^{(x)}_{\ell,0} = 0.0177 - 0.2329\beta + 1.0065\beta^2 - 1.0751\beta^3 + 1.4032\beta^4 \quad (\beta = \frac{1}{1+\ell/a}) \tag{24a}$$

(b) Tension in the y-direction

$$F^{(y)}_{\ell,0} = 1.0377 + 0.0061\beta + 2.5633\beta^2 - 3.0360\beta^3 + 2.7814\beta^4 \quad (\beta = \frac{1}{1+\ell/a}) \tag{24b}$$

(c) Biaxial loading

The results for biaxial loading are obtained by the linear combination of Eqns. (24a) and (24b) as follows:

$$K_{I,0} = (\pi\ell)^{1/2}(-\sigma_1 F^{(x)}_{\ell,0} + \sigma_2 F^{(y)}_{\ell,0}) = -\sigma_1(\pi\ell)^{1/2} F_{\ell,0} = -\sigma_1(\pi a)^{1/2} F_{a,0}$$

$$F_{\ell,0} = F^{(x)}_{\ell,0} - \lambda F^{(y)}_{\ell,0}, \quad F_{a,0} = F_{\ell,0}(\ell/a)^{1/2}, \quad \lambda = \sigma_2/\sigma_1 \quad (\sigma_1 \neq 0) \tag{24c}$$

The numerical values from Eqns. (24) based on the present analysis are

in excellent agreement with previous reliable values [17] shown in Table 5.

$F_{\ell,0}$ is usually convenient in theoretical considerations, but in analysing the test results, $F_{a,0}$ would be more useful since it is normalized by the hole radius which remains unchanged during crack extension.

4.2. Polynomial expressions of stress intensity factor

For applications, it is desirable to represent the numerical results by simple analytical expressions. We consider polynomial expressions in terms of the following dimensionless geometric parameters:

$$\alpha = \frac{a}{c}, \quad \beta = \frac{1}{1+L}, \quad \gamma = \frac{c}{b} \qquad (L = \frac{\ell}{a}) \tag{25}$$

Our computations show that the polynomial expressions must be such that the following conditions are satisfied:

(i) As $a/c \to 0$, the results for all five problems converge to those for an infinite solid, independent of the values of b/c.

(ii) Better accuracy is obtained by fitting polynomials to F_ℓ than to F_a.

(iii) For the tension applied in the y-direction (case (b)), the stress intensity factor becomes unbounded as $a + \ell \to b$.

The numerical values of $F_\ell^{(i,x)}$ and $F_\ell^{(i,y)}$ for problems (1) to (5) are fitted by polynomials of the three parameters defined by Eqns. (25). The results are summarized as follows:

(a) Compression in the x-direction ($\sigma_1 = -\sigma_0$, $\sigma_2 = 0$)

Case when $b \geq c$

$$F_\ell^{(i,x)} = F_{\ell,0}^{(x)} + \sum_{p=1}^{3} \sum_{q=0}^{3} \sum_{s=0}^{3} X_{pqs}^{(i,1)} \alpha^p \beta^q \gamma^s \tag{26a.1}$$

Case when $b \le c$

$$F_{\ell}^{(i,x)} = F_{\ell,0}^{(x)} + \sum_{p=1}^{3} \sum_{q=0}^{3} \sum_{s=0}^{3} X_{pqs}^{(i,2)} \alpha^p \beta^q \gamma^s \qquad (26a.2)$$

(b) Tension in the y-direction ($\sigma_1 = 0, \quad \sigma_2 = \sigma_0$)

Case when $b \ge c$

$$F_{\ell}^{(i,y)} = F_{\ell,0}^{(y)} + \sum_{p=1}^{3} \sum_{q=0}^{3} \sum_{s=0}^{3} Y_{pqs}^{(i,1)} \alpha^p \beta^q \gamma^s \, / \, (1 - \frac{a+\ell}{b})^{1/2} \qquad (26b.1)$$

Case when $b \le c$

$$F_{\ell}^{(i,y)} = F_{\ell,0}^{(y)} + \sum_{p=1}^{3} \sum_{q=0}^{3} \sum_{s=0}^{3} Y_{pqs}^{(i,2)} \alpha^p \beta^q \gamma^s \, / \, (1 - \frac{a+\ell}{b})^{1/2} \qquad (26b.2)$$

(c) Biaxial loading

The stress intensity factor for the biaxial loading is given by a linear combination of Eqns. (26a.1) to (26b.2) as follows:

$$K_I^{(i)} = (\pi \ell)^{1/2} (- \sigma_1 F_{\ell}^{(i,x)} + \sigma_2 F_{\ell}^{(i,y)}) \qquad (26c)$$

Note that X_{pqs} and Y_{pqs} for $p = 0$ are not included in Eqns. (26a.1) to (26b.2) in order to ensure that $F_{\ell}^{(i,x)}$ and $F_{\ell}^{(i,y)}$ tend to the results for an infinite solid as $\alpha = a/c \to 0$. Furthermore, Eqns. (26b.1) and (26b.2) are formulated in such a manner that the stress intensity factor becomes unbounded as $a + \ell \to b$.

Eqns. (26) yield the dimensionless stress intensity factor F_{ℓ}. To obtain F_a from these equations, we use the expression

$$F_a = F_{\ell} \left(\frac{\ell}{a} \right)^{1/2} \qquad (27)$$

The coefficients in the polynomials (26a.1) to (26b.2) for problems (1)

to (5) are given in Tables 6 to 10, respectively.

The numerical values from these expressions are compared with those from direct analysis in Figs. 5 to 9-2, for typical cases of the five treated problems. The agreement is quite good, and the proposed polynomials (26) are useful in applications.

5. SUMMARY AND CONCLUSIONS

A unified method of analysis for various problems relating to elastic plates containing circular holes with edge cracks is developed. The method is based on the analysis of a unit rectangular region containing a circular hole with edge cracks, where the boundary conditions of the outer edges are suitably adjusted in order to treat various problems including periodic arrays of holes with edge cracks.

The method is applied to five important problems, and accurate values of the stress intensity factors are obtained. These values are fitted by polynomials which are convenient for practical applications.

REFERENCES

[1] Griffith, A.A., *Phil. Trans. Roy. Soc. London*, **A221**, 163 (1921).

[2] McClintock, F.A. and Walsh, J.B., *Proc. 4th U.S. Nat. Congr. Appl. Mech. 1962*, ASME,**2**, 1015 (1963).

[3] Kachanov, M.L., *Mechanics of Materials 1*, 29 (1982).

[4] Ashby, M.F. and Hallam, S.D. (née Cooksley), *Acta Metall.*,**34**, 497 (1986).

[5] Isida, M. and Nemat-Nasser, N., On Mechanics of Crack Growth and Its Effects on the Overall Response of Brittle Porous Solid, to appear in *Acta Metallurgica* .

[6] Brace, W.F. and Bombolakis, E.G., *J. Geophys. Res.*, **68**, 3709 (1963).

[7] Hoek, E. and Bieniawski, Z.T., *Int. J. Frac. Mech.*, **1**, 137 (1965).

[8] Nemat-Nasser, S. and Horii H., *J. Geophys. Res.*, **87**, 6805 (1982).

[9] Nemat-Nasser, S. and Horii, H., *Proc. 6th Intern. Conf. Frac. (ICF6)*, New Delhi, India, 515 (1984).

[10] Horii, H. and Nemat-Nasser, S., *J. Geophys. Res.*, **90**, 3105 (1985).

[11] Nemat-Nasser, S. and Horii, H., Brittle Failure in Compression: Splitting, Faulting, and Brittle-Ductile Transition, to appear in *Phil. Trans. Roy. Soc. London*.

[12] Bowie, O.L., *J. Math. Phys.*, **35**, 60 (1956).

[13] Newman, J.C., Jr., *NASA TN*, D-6376 (1971).

[14] Nisitani, H. and Isida, M., *Trans. JSME*, **39**, 7 (1973).

[15] Isida, M. and Nakamura, Y., *Trans. JSME*, **46**, 947 (1980).

[16] Isida, M., Chen, D.H. and Nisitani, H., *Eng. Frac. Mech.*, **21**, 983 (1985).

[17] Sih, G.C., *Handbook of Stress Intensity Factors for Researchers*

and Engineers, Lehigh University, Bethlehem, P.A. (1973).

[18] Rook, D.P. and Cartwright, D.J., *Compendium of Stress Intensity Factors*, H.M. Stationary Office, England (1976).

[19] Isida, M., *Proc. 1st Congr. Numer. Meths. Frac. Mech.*, Swansea, England, 81 (1978).

[20] Isida, M. and Sato, R., *Trans. JSME*, **A50**, 1619 (1984).

[21] Isida, M. and Noguchi, H., *Trans. JSME*, **A49**, 147 (1983).

[22] Nisitani, H., *Japanese Papers for Japan-U.S. Seminar, Strength and Struc. Solid Mat.*, Minnowbrook, 28 (1974).

Figure captions

Fig. 1-1 Uniform normal loads along sides $\overline{EF}$ and $\overline{FG}$.

Fig. 1-2 Strip with a periodic array of holes and cracks in the x-direction.

Fig. 1-3 Strip with a periodic array of holes and cracks in the y-direction.

Fig. 1-4 Infinite solid with doubly periodic array of holes and cracks.

Fig. 1-5 Infinite solid with zig-zag periodic array of holes and cracks.

Fig. 2 Geometry of a circular hole with edge cracks.

Fig. 3 Subdivision of crack for numerical evaluation of weighting function.

Fig. 4 Subdivision of outer edges for numerical evaluation.

Fig. 5 $F_a^{(1,x)}$ for Problem (1), $b/c = 2$.

Fig. 6 $F_a^{(2,x)}$ for Problem (2), $b/c = 2$.

Fig. 7 $F_a^{(3,y)}$ for Problem (3), $b/c = 1$.

Fig. 8-1 $F_a^{(4,x)}$ for Problem (4), $b/c = 1$.

Fig. 8-2 $F_a^{(4,y)}$ for Problem (4), $b/c = 1$.

Fig. 9-1 $F_a^{(5,x)}$ for Problem (5), $b/c = 2$.

Fig. 9-2 $F_a^{(5,y)}$ for Problem (5), $b/c = 2$.

Table 1 Boundary conditions of outer edges

Problem	Side $\overline{EF}$	Side $\overline{FG}$
(1)	$\sigma_x = \sigma_1$ $\tau_{xy} = 0$	$\sigma_y = \sigma_2$ $\tau_{xy} = 0$
(2)	u = const. $[P_x]_E^F = \sigma_1 c$ $\tau_{xy} = 0$	$\sigma_y = \sigma_2$ $\tau_{xy} = 0$
(3)	$\sigma_x = \sigma_1$ $\tau_{xy} = 0$	v = const. $[P_y]_F^G = \sigma_2 b$ $\tau_{xy} = 0$
(4)	u = const. $[P_x]_E^F = \sigma_1 c$ $\tau_{xy} = 0$	v = const. $[P_y]_F^G = \sigma_2 b$ $\tau_{xy} = 0$
(5)	u = const. $[P_x]_E^F - [P_x]_G^H = 2\sigma_1 c$ $\tau_{xy} = 0$	$(\sigma_y)_x = (\sigma_y)_{b-x}$ $(\tau_{xy})_x = (\tau_{xy})_{b-x}$ $[u]_0^x = [u]_{b-x}^b$ $[v]_0^x = [v]_{b-x}^b$ $[P_y]_F^G = \sigma_2 b$

Table 2 Variation of $F^{(x)}_{\ell,0}$ and $F^{(y)}_{\ell,0}$ with various M for $\ell/a = 0.4$

M	$F^{(x)}_{\ell,0}$	$F^{(y)}_{\ell,0}$
2	0.332	1.949
3	0.334	1.955
4	0.337	1.964
5	0.338	1.968
6	0.339	1.969
7	0.339	1.969
8	0.340	1.974
9	0.339	1.969
10	0.339	1.972
11	0.339	1.973
12	0.339	1.971

Table 3 Variation of $F_a^{(i,x)}$ for the case when

b/c=1, a/c=0.2, ℓ/a=2, M=6

N_1, N_2	i=1	i=2	i=3	i=4	i=5
2	0.2426	0.0425	0.0733	0.0142	
3	0.2001	0.0528	0.0795	0.0185	
4	0.2156	0.0514	0.0793	0.0182	0.0346
5	0.2110	0.0517	0.0797	0.0182	
6	0.2130	0.0516	0.0795	0.0182	0.0345
7	0.2120	0.0516	0.0796	0.0182	
8	0.2125	0.0516	0.0795	0.0182	0.0345
9	0.2120	0.0516	0.0796	0.0182	
10	0.2119	0.0517	0.0795	0.0182	

Table 4 Variation of $F_a^{(i,y)}$ for the case when

N_1, N_2	i=1	i=2	i=3	i=4	i=5
2	2.490	2.191	2.265	2.070	
3	2.781	2.239	2.292	2.075	
4	2.863	2.233	2.294	2.077	2.148
5	2.829	2.236	2.298	2.077	
6	2.848	2.234	2.295	2.077	2.146
7	2.837	2.235	2.297	2.077	
8	2.843	2.235	2.296	2.077	2.146
9	2.838	2.235	2.297	2.077	
10	2.839	2.235	2.296	2.077	

Table 5 Comparison of $F_{\ell,0}$ from Eqns. (24) and previous analysis. (infinite solid)

	$\lambda = 0$		$\lambda = 0.1$		$\lambda = 0.2$	
L	Eqn.(24a)	Ref.[17]	Eqns.(24)	Ref.[17]	Eqns.(24)	Ref.[17]
0.01	1.079	1.074	0.750	0.747	0.422	0.420
0.02	1.040	1.041	0.718	0.718	0.397	0.396
0.04	0.968	0.968	0.659	0.658	0.350	0.348
0.06	0.903	0.902	0.605	0.603	0.307	0.305
0.08	0.843	0.842	0.555	0.554	0.268	0.266
0.10	0.788	0.788	0.510	0.509	0.232	0.231
0.15	0.672	0.671	0.414	0.413	0.156	0.155
0.20	0.577	0.577	0.336	0.336	0.096	0.095
0.25	0.500	0.500	0.273	0.273	0.046	0.046
0.30	0.436	0.437	0.221	0.221	0.006	0.006
0.40	0.338	0.339	0.142	0.142	-0.055	-0.055
0.50	0.268	0.269	0.085	0.086		
0.60	0.217	0.217	0.044	0.044		
0.80	0.148	0.147	-0.011	-0.010		
1.00	0.106	0.105				
1.20	0.079	0.077				
1.50	0.053	0.051				
2.00	0.029	0.029				
3.00	0.011	0.011				

Table 6 Coefficients of polynomials (26.1) to (26.2)

for Problem (1) (X_{3qs}, Y_{3qs} = 0)

p	q	s	$X^{(1,1)}_{pqs}$	$X^{(1,2)}_{pqs}$	$Y^{(1,1)}_{pqs}$	$Y^{(1,2)}_{pqs}$
1	0	0	-7.4715E-01	-2.4215E+00	5.7012E+00	2.2056E+01
1	0	1	2.3737E+00	3.8558E+00	2.6320E+01	-4.3445E+01
1	0	2	-5.3173E-01	-1.4332E+00	-2.5258E+01	1.9673E+01
1	0	3	0.0000E+00	0.0000E+00	0.0000E+00	0.0000E+00
1	1	0	-1.9973E+00	1.8117E+00	-1.2146E+02	-5.6748E+01
1	1	1	-6.1593E+00	-2.0771E+00	-5.4035E+01	1.2814E+02
1	1	2	3.2767E+00	6.2703E-01	1.3601E+02	-5.8552E+01
1	1	3	0.0000E+00	0.0000E+00	0.0000E+00	0.0000E+00
1	2	0	2.4177E+01	0.0000E+00	3.5453E+02	-1.5351E+02
1	2	1	-1.7526E+01	0.0000E+00	5.5240E+01	1.9721E+02
1	2	2	-2.9660E+00	0.0000E+00	-3.6728E+02	-8.9138E+01
1	2	3	0.0000E+00	0.0000E+00	0.0000E+00	0.0000E+00
1	3	0	-2.0392E+01	0.0000E+00	-1.6091E+02	2.7113E+02
1	3	1	6.2492E+00	0.0000E+00	-3.0702E+02	-4.1494E+02
1	3	2	1.7132E+01	0.0000E+00	4.7679E+02	1.9012E+02
1	3	3	0.0000E+00	0.0000E+00	0.0000E+00	0.0000E+00
2	0	0	4.5632E+00	3.3112E+01	5.5254E+01	-1.2963E+02
2	0	1	-2.5129E+00	-5.0744E+01	-1.8464E+02	2.8193E+02
2	0	2	-1.4135E+01	1.8632E+01	2.9894E+01	-1.6561E+02
2	0	3	0.0000E+00	0.0000E+00	0.0000E+00	0.0000E+00
2	1	0	-5.0766E+00	-2.6862E+01	4.3826E+02	8.1074E+02
2	1	1	4.0657E+01	4.4293E+01	-1.0866E+02	-1.5208E+03
2	1	2	5.2748E+01	-1.3934E+01	3.7345E+02	8.1247E+02
2	1	3	0.0000E+00	0.0000E+00	0.0000E+00	0.0000E+00
2	2	0	-1.1439E+02	0.0000E+00	-2.3193E+03	-5.1824E+02
2	2	1	8.4083E+01	0.0000E+00	2.5729E+03	8.2030E+02
2	2	2	-1.2571E+02	0.0000E+00	-1.6524E+03	-4.7128E+02
2	2	3	0.0000E+00	0.0000E+00	0.0000E+00	0.0000E+00
2	3	0	1.4261E+02	0.0000E+00	1.8022E+03	-4.2400E+02
2	3	1	-1.0036E+02	0.0000E+00	-1.8598E+03	9.4728E+02
2	3	2	4.1161E+01	0.0000E+00	8.7650E+02	-4.6230E+02
2	3	3	0.0000E+00	0.0000E+00	0.0000E+00	0.0000E+00

Table 7 Coefficients of polynomials (26a.1) to (26b.2) for Problem (2)

p	q	s	$X^{(2,1)}_{pqs}$	$X^{(2,2)}_{pqs}$	$Y^{(2,1)}_{pqs}$	$Y^{(2,2)}_{pqs}$
1	0	0	4.4980E-02	1.7911E-01	-3.4397E+01	-9.7220E-01
1	0	1	1.4205E+00	1.1863E-02	1.3797E+02	-6.0517E+00
1	0	2	-1.3067E+00	-4.6399E-03	-1.2161E+02	1.2914E+00
1	0	3	0.0000E+00	0.0000E+00	1.6083E+00	0.0000E+00
1	1	0	1.0267E+00	1.0965E+00	1.5796E+02	1.9387E+01
1	1	1	-8.1648E+00	-2.6270E+00	-4.8040E+02	1.4744E+01
1	1	2	7.6367E+00	7.6423E-01	4.0362E+02	-6.0552E+00
1	1	3	0.0000E+00	0.0000E+00	-2.3961E+01	0.0000E+00
1	2	0	-2.3842E+01	-1.3997E+00	-4.7568E+02	-5.1005E+01
1	2	1	6.1551E+01	4.7890E+00	2.5405E+02	-1.5115E+01
1	2	2	-4.1235E+01	-1.6465E+00	-2.7887E+02	1.1186E+01
1	2	3	0.0000E+00	0.0000E+00	5.3624E+02	0.0000E+00
1	3	0	5.0970E+01	0.0000E+00	-2.7518E+02	4.2245E+01
1	3	1	-1.1814E+02	0.0000E+00	2.7326E+03	-1.1905E+00
1	3	2	7.2459E+01	0.0000E+00	-1.3206E+03	-5.5917E+00
1	3	3	0.0000E+00	0.0000E+00	-1.3142E+03	0.0000E+00
2	0	0	1.1656E+00	-3.4406E+00	2.2052E+02	0.0000E+00
2	0	1	-1.8971E+01	2.4326E+00	-4.0462E+02	0.0000E+00
2	0	2	1.5030E+01	-7.8577E-01	-7.2028E+02	0.0000E+00
2	0	3	0.0000E+00	0.0000E+00	1.0938E+03	0.0000E+00
2	1	0	2.2888E+01	1.5467E+01	-6.3733E+02	0.0000E+00
2	1	1	6.9402E+01	-1.0844E+01	1.3699E+03	0.0000E+00
2	1	2	-8.2563E+01	3.4696E+00	1.2412E+03	0.0000E+00
2	1	3	0.0000E+00	0.0000E+00	-2.7180E+03	0.0000E+00
2	2	0	-9.0318E-02	-6.2833E+00	1.8033E+03	0.0000E+00
2	2	1	-2.4824E+02	-6.1725E+00	9.3307E+02	0.0000E+00
2	2	2	2.4491E+02	4.4776E-01	6.8139E+03	0.0000E+00
2	2	3	0.0000E+00	0.0000E+00	-9.8197E+03	0.0000E+00
2	3	0	-1.3510E+02	0.0000E+00	4.0440E+03	0.0000E+00
2	3	1	4.9533E+02	0.0000E+00	-1.6234E+04	0.0000E+00
2	3	2	3.7369E+02	0.0000E+00	-2.3441E+04	0.0000E+00
2	3	3	0.0000E+00	0.0000E+00	3.7646E+04	0.0000E+00
3	0	0	0.0000E+00	0.0000E+00	-2.2984E+02	0.0000E+00
3	0	1	0.0000E+00	0.0000E+00	-4.3422E+02	0.0000E+00
3	0	2	0.0000E+00	0.0000E+00	2.6958E+03	0.0000E+00
3	0	3	0.0000E+00	0.0000E+00	-2.8198E+03	0.0000E+00
3	1	0	0.0000E+00	0.0000E+00	-8.0843E+02	0.0000E+00
3	1	1	0.0000E+00	0.0000E+00	2.6784E+03	0.0000E+00
3	1	2	0.0000E+00	0.0000E+00	4.2135E+03	0.0000E+00
3	1	3	0.0000E+00	0.0000E+00	-2.3381E+03	0.0000E+00
3	2	0	0.0000E+00	0.0000E+00	9.7915E+03	0.0000E+00
3	2	1	0.0000E+00	0.0000E+00	-4.0365E+04	0.0000E+00
3	2	2	0.0000E+00	0.0000E+00	-2.8534E+04	0.0000E+00
3	2	3	0.0000E+00	0.0000E+00	5.6549E+04	0.0000E+00
3	3	0	0.0000E+00	0.0000E+00	-2.4737E+04	0.0000E+00
3	3	1	0.0000E+00	0.0000E+00	6.3754E+04	0.0000E+00
3	3	2	0.0000E+00	0.0000E+00	1.1662E+05	0.0000E+00
3	3	3	0.0000E+00	0.0000E+00	-1.5932E+05	0.0000E+00

Table 8 Coefficients of polynomials (26a.1) to (26b.2)

for Problem (3) (X_{33s}, Y_{33s} = 0)

p	q	s	$X^{(3,1)}_{pqs}$	$X^{(3,2)}_{pqs}$	$Y^{(3,1)}_{pqs}$	$Y^{(3,2)}_{pqs}$
1	0	0	4.6011E-03	8.0875E-01	-1.5119E+00	-1.0891E+01
1	0	1	-1.0581E-01	-1.3423E+00	-1.3759E+01	1.7244E+01
1	0	2	1.5066E-01	0.0000E+00	9.1954E+00	-1.4304E+01
1	0	3	0.0000E+00	0.0000E+00	0.0000E+00	3.9456E+00
1	1	0	-3.5730E+00	-2.0032E+00	-4.9449E+01	1.1683E+01
1	1	1	3.8074E+00	4.6367E+00	1.5889E+02	-8.5217E+00
1	1	2	-1.2534E-01	0.0000E+00	-8.1243E+01	5.4158E+00
1	1	3	0.0000E+00	0.0000E+00	0.0000E+00	-2.1868E+00
1	2	0	2.0181E+01	5.6744E+00	2.4158E+02	0.0000E+00
1	2	1	-2.9163E+01	-6.9607E+00	-4.7704E+02	0.0000E+00
1	2	2	6.0356E+00	0.0000E+00	1.6456E+02	0.0000E+00
1	2	3	0.0000E+00	0.0000E+00	0.0000E+00	0.0000E+00
1	3	0	-2.5633E+01	0.0000E+00	-2.5499E+02	0.0000E+00
1	3	1	4.5789E+01	0.0000E+00	3.6793E+02	0.0000E+00
1	3	2	-1.4734E+01	0.0000E+00	-4.5176E+01	0.0000E+00
1	3	3	0.0000E+00	0.0000E+00	0.0000E+00	0.0000E+00
2	0	0	-3.3853E-01	-1.0764E+01	1.5635E+01	-5.6818E+01
2	0	1	5.3594E+00	2.0515E+01	5.6553E+01	1.4930E+02
2	0	2	-5.2904E+00	0.0000E+00	-3.7740E+01	-9.7176E+01
2	0	3	0.0000E+00	0.0000E+00	0.0000E+00	1.9697E+01
2	1	0	8.8234E+00	-1.5910E+01	-1.9539E+02	5.8317E+01
2	1	1	-4.0061E+01	-3.5513E+01	2.7947E+01	-2.2321E+02
2	1	2	3.7302E+01	0.0000E+00	-5.3576E+01	1.6611E+02
2	1	3	0.0000E+00	0.0000E+00	0.0000E+00	-3.4682E+01
2	2	0	-7.1578E+01	-6.9348E+00	7.3457E+02	0.0000E+00
2	2	1	1.4890E+02	4.9963E+01	-1.6397E+03	0.0000E+00
2	2	2	-8.0834E+01	0.0000E+00	1.4676E+03	0.0000E+00
2	2	3	0.0000E+00	0.0000E+00	0.0000E+00	0.0000E+00
2	3	0	9.9964E+01	0.0000E+00	-9.6305E+02	0.0000E+00
2	3	1	-2.0570E+02	0.0000E+00	3.0293E+03	0.0000E+00
2	3	2	9.3005E+01	0.0000E+00	-2.5766E+03	0.0000E+00
2	3	3	0.0000E+00	0.0000E+00	0.0000E+00	0.0000E+00
3	0	0	0.0000E+00	5.2036E+01	0.0000E+00	0.0000E+00
3	0	1	0.0000E+00	-8.4383E+01	0.0000E+00	0.0000E+00
3	0	2	0.0000E+00	0.0000E+00	0.0000E+00	0.0000E+00
3	0	3	0.0000E+00	0.0000E+00	0.0000E+00	0.0000E+00
3	1	0	0.0000E+00	5.4394E+01	0.0000E+00	0.0000E+00
3	1	1	0.0000E+00	1.4518E+02	0.0000E+00	0.0000E+00
3	1	2	0.0000E+00	0.0000E+00	0.0000E+00	0.0000E+00
3	1	3	0.0000E+00	0.0000E+00	0.0000E+00	0.0000E+00
3	2	0	0.0000E+00	-1.1444E+02	0.0000E+00	0.0000E+00
3	2	1	0.0000E+00	-8.3128E+01	0.0000E+00	0.0000E+00
3	2	2	0.0000E+00	0.0000E+00	0.0000E+00	0.0000E+00
3	2	3	0.0000E+00	0.0000E+00	0.0000E+00	0.0000E+00

Table 9 Coefficients of polynomials (26a.1) to (26b.2)

for Problem (4) (X_{23s}, X_{3qs}, Y_{23s}, Y_{3qs} = 0)

p	q	s	$X_{pqs}^{(4,1)}$	$X_{pqs}^{(4,2)}$	$Y_{pqs}^{(4,1)}$	$Y_{pqs}^{(4,2)}$
1	0	0	-3.2587E-01	1.2001E-02	-6.6054E+00	-4.7946E+00
1	0	1	3.7426E-01	3.8127E-02	-2.6497E-01	-1.9074E+00
1	0	2	3.6561E-02	4.8180E-02	0.0000E+00	0.0000E+00
1	0	3	0.0000E+00	0.0000E+00	0.0000E+00	0.0000E+00
1	1	0	8.0086E-01	-6.7988E-01	2.5899E+01	2.3497E+01
1	1	1	-1.9838E+00	-6.4505E-01	-1.3825E+00	-7.0045E-01
1	1	2	1.1054E-01	1.6759E-01	0.0000E+00	0.0000E+00
1	1	3	0.0000E+00	0.0000E+00	0.0000E+00	0.0000E+00
1	2	0	5.8229E-01	8.1387E-01	-2.2990E+01	-2.7635E+01
1	2	1	1.2307E+00	2.5439E+00	-4.4066E+00	4.2335E+00
1	2	2	2.7677E-01	-1.0634E+00	0.0000E+00	0.0000E+00
1	2	3	0.0000E+00	0 0000E+00	0.0000E+00	0.0000E+00
1	3	0	0.0000E+00	0.0000E+00	0.0000E+00	0.0000E+00
1	3	1	0.0000E+00	0.0000E+00	0.0000E+00	0.0000E+00
1	3	2	0.0000E+00	0.0000E+00	0.0000E+00	0.0000E+00
1	3	3	0.0000E+00	0.0000E+00	0.0000E+00	0.0000E+00
2	0	0	1.4991E+00	-1.4935E+00	2.5284E+01	1.8234E+01
2	0	1	1.0240E+00	3.0513E+00	-2.2889E+00	1.6523E+00
2	0	2	-2.7217E+00	-1.8975E+00	0.0000E+00	0.0000E+00
2	0	3	0.0000E+00	0.0000E+00	0.0000E+00	0.0000E+00
2	1	0	-1.2694E+01	6.5026E+00	-1.3826E+02	-1.0653E+02
2	1	1	9.0147E+00	-6.9495E+00	2.7114E+01	1.4958E+01
2	1	2	7.1809E+00	4.6407E+00	0.0000E+00	0.0000E+00
2	1	3	0.0000E+00	0.0000E+00	0.0000E+00	0.0000E+00
2	2	0	5.1746E+00	-9.5870E+00	1.4436E+02	1.3627E+02
2	2	1	-1.9962E+00	9.1101E-01	-1.1742E+01	-3.5588E+01
2	2	2	-1.3561E+01	-2.9050E+00	0.0000E+00	0.0000E+00
2	2	3	0.0000E+00	0.0000E+00	0.0000E+00	0.0000E+00

Table 10 Coefficients of polynomials (26a.1) to (26b.2)

for Problem (5) (X_{3qs}, Y_{3qs} = 0)

p	q	s	$X^{(5,1)}_{pqs}$	$X^{(5,2)}_{pqs}$	$Y^{(5,1)}_{pqs}$	$Y^{(5,2)}_{pqs}$
1	0	0	1.7531E-01	3.0014E-01	3.0181E+01	-6.5174E+00
1	0	1	-1.1768E-01	-6.4930E-01	-6.3848E+01	2.8785E+00
1	0	2	-4.6124E-02	5.5971E-01	2.6805E+01	-2.3563E+00
1	0	3	0.0000E+00	-1.1408E-01	0.0000E+00	0.0000E+00
1	1	0	-2.5995E+00	2.8194E+00	-2.4054E+02	-7.4074E+00
1	1	1	7.0347E+00	-4.2148E+00	5.4821E+02	4.1677E+01
1	1	2	-4.3277E+00	8.1776E-01	-2.8360E+02	-1.4110E+01
1	1	3	0.0000E+00	7.8482E-02	0.0000E+00	0.0000E+00
1	2	0	0.0000E+00	-2.9033E+00	3.9446E+02	5.5070E+01
1	2	1	0.0000E+00	3.0314E+00	-9.3436E+02	-1.2007E+02
1	2	2	0.0000E+00	2.2003E+00	5.1613E+02	4.5461E+01
1	2	3	0.0000E+00	-1.2209E+00	0.0000E+00	0.0000E+00
1	3	0	0.0000E+00	0.0000E+00	0.0000E+00	0.0000E+00
1	3	1	0.0000E+00	0.0000E+00	0.0000E+00	0.0000E+00
1	3	2	0.0000E+00	0.0000E+00	0.0000E+00	0.0000E+00
1	3	3	0.0000E+00	0.0000E+00	0.0000E+00	0.0000E+00
2	0	0	2.5910E+00	-6.2418E-01	-6.2190E+01	8.3148E+01
2	0	1	-8.5914E+00	-8.1785E-01	2.1830E+01	-1.1222E+02
2	0	2	5.7373E+00	1.4816E+00	6.2948E+01	4.4637E+01
2	0	3	0.0000E+00	-8.6639E-01	0.0000E+00	0.0000E+00
2	1	0	8.9134E+00	-3.3216E+00	8.4793E+02	-3.2857E+02
2	1	1	-1.6126E+01	8.0049E+00	-1.4123E+03	4.1580E+02
2	1	2	6.9518E+00	-2.5632E+00	4.5535E+02	-1.6118E+02
2	1	3	0.0000E+00	1.4334E+00	0.0000E+00	0.0000E+00
2	2	0	0.0000E+00	1.7599E+01	-1.6084E+03	1.1821E+02
2	2	1	0.0000E+00	-2.9872E+01	3.1919E+03	-5.7679E+01
2	2	2	0.0000E+00	7.1522E+00	-1.4621E+03	1.7903E+01
2	2	3	0.0000E+00	-1.5332E+00	0.0000E+00	0.0000E+00
2	3	0	0.0000E+00	0.0000E+00	0.0000E+00	0.0000E+00
2	3	1	0.0000E+00	0.0000E+00	0.0000E+00	0.0000E+00
2	3	2	0.0000E+00	0.0000E+00	0.0000E+00	0.0000E+00
2	3	3	0.0000E+00	0.0000E+00	0.0000E+00	0.0000E+00

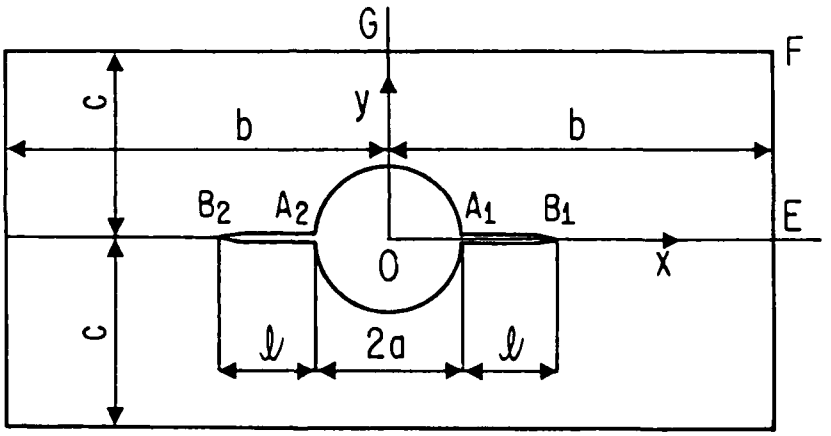

Figure 1

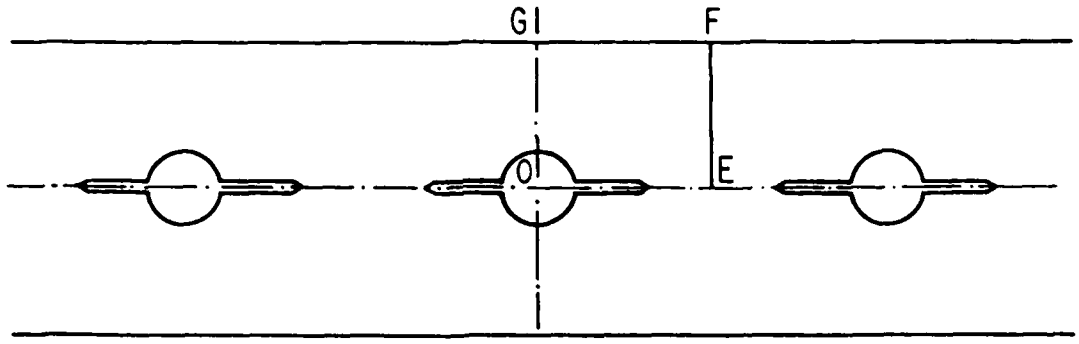

Figure 1-2

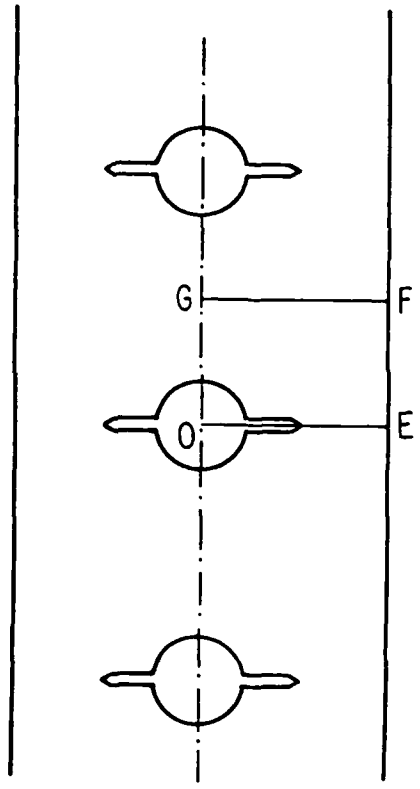

Figure 1-3

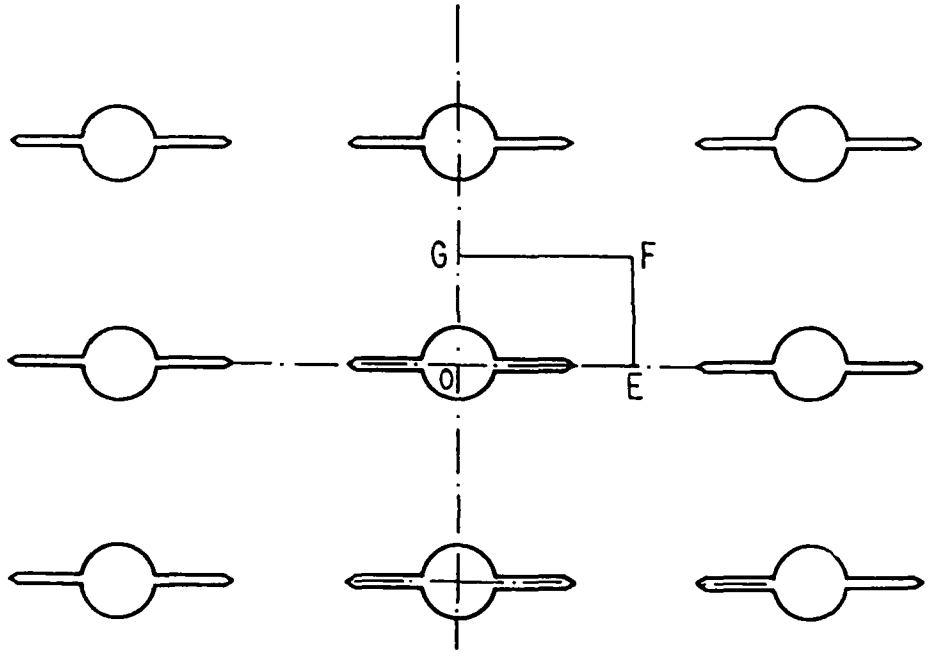

Figure 1-4

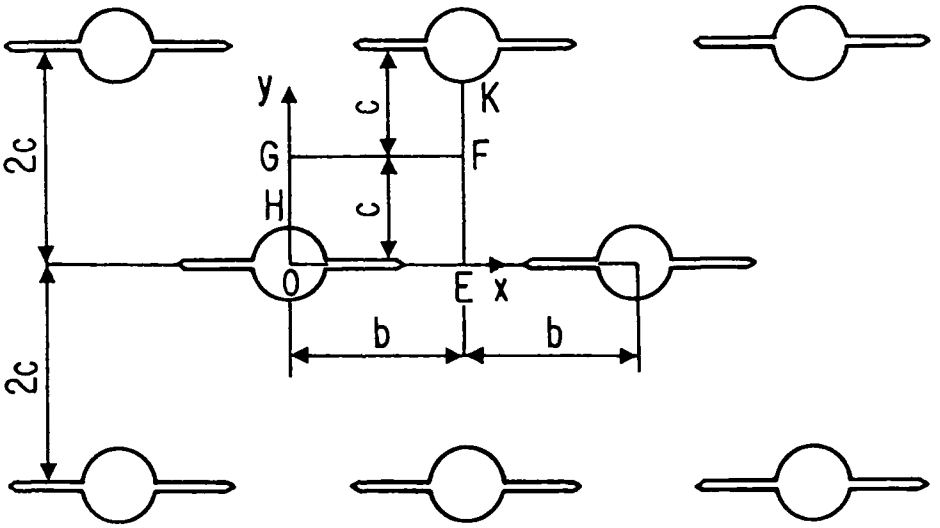

Figure 1-5

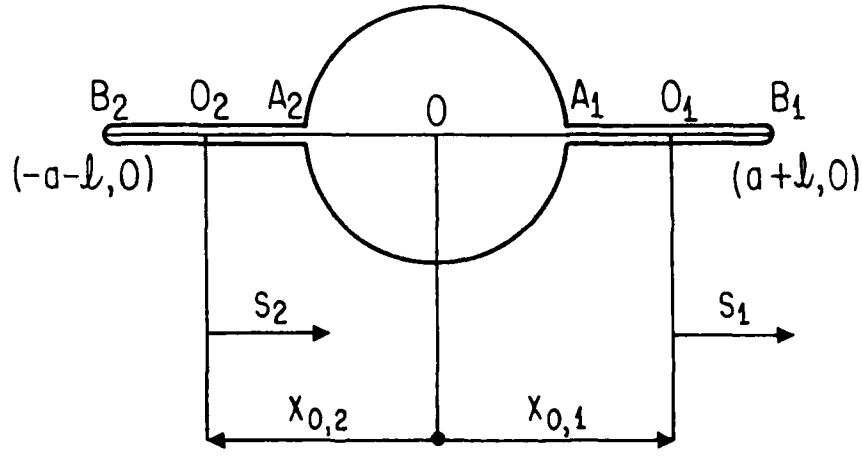

Figure 2

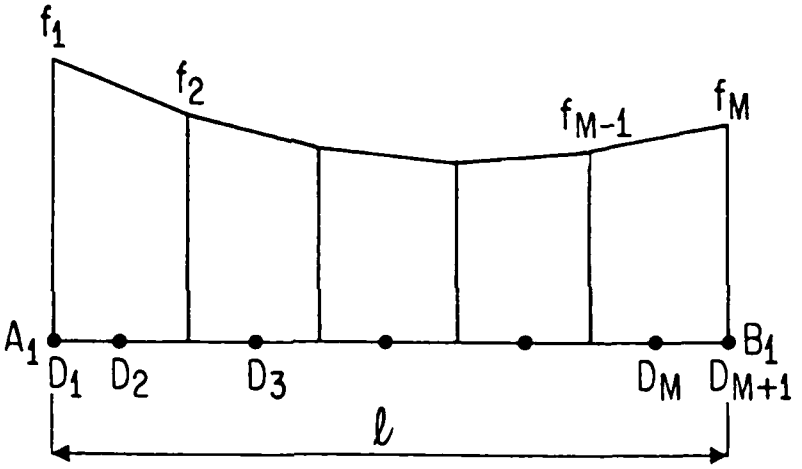

Figure 3

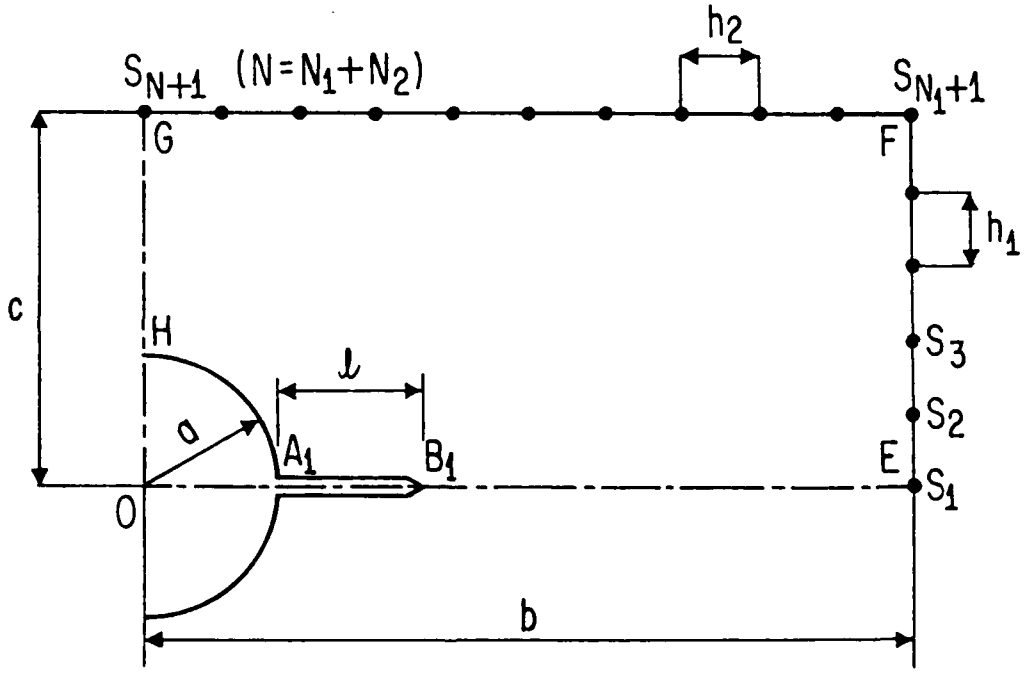

Figure 4

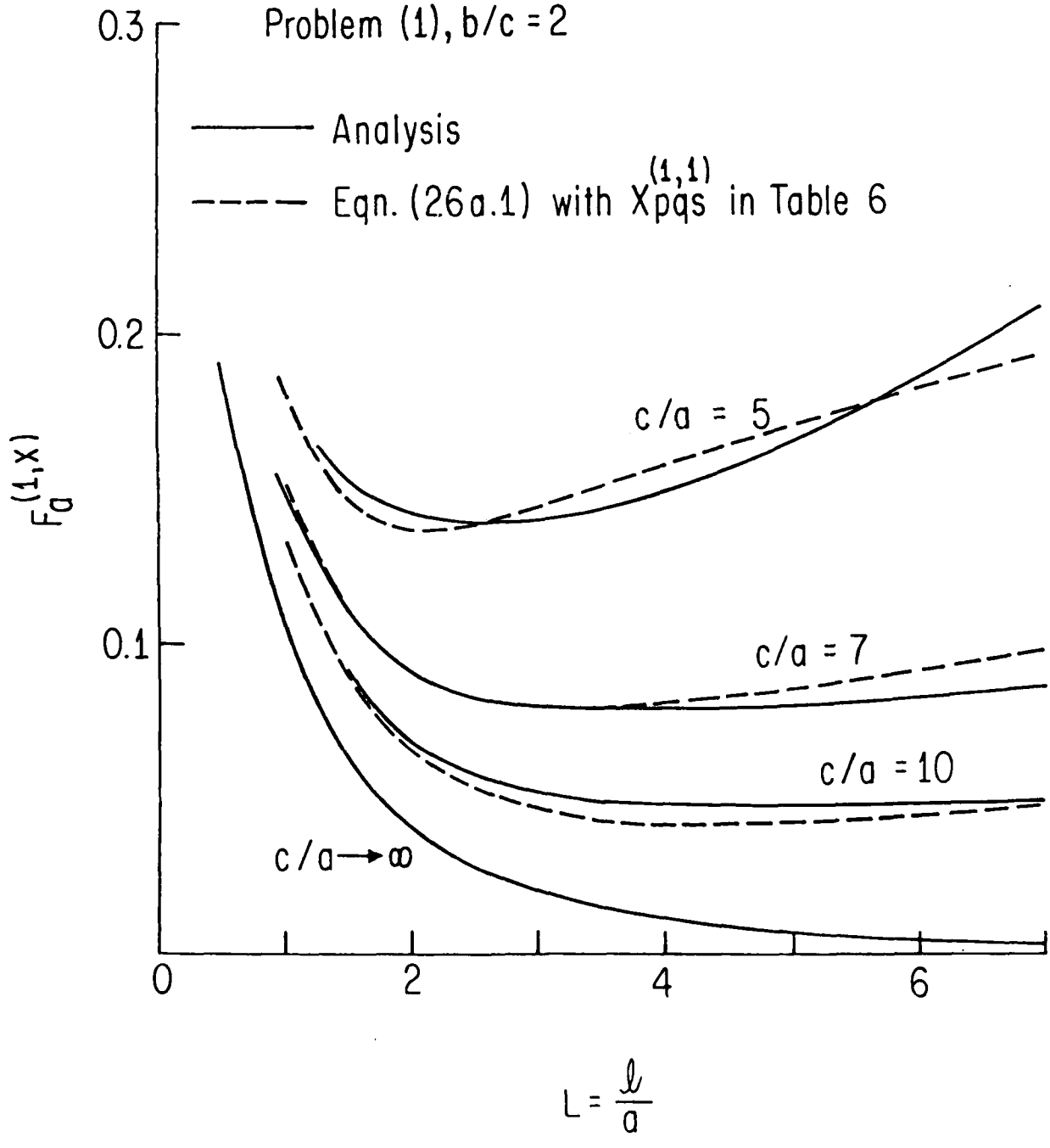
Problem (1), b/c = 2
Analysis
Eqn. (26a.1) with $X_{pqs}^{(1,1)}$ in Table 6
0.3
0.2
0.1
$F_a^{(1,x)}$
c/a = 5
c/a = 7
c/a = 10
c/a → ∞
0
2
4
6
$L = \frac{\ell}{a}$

Figure 5

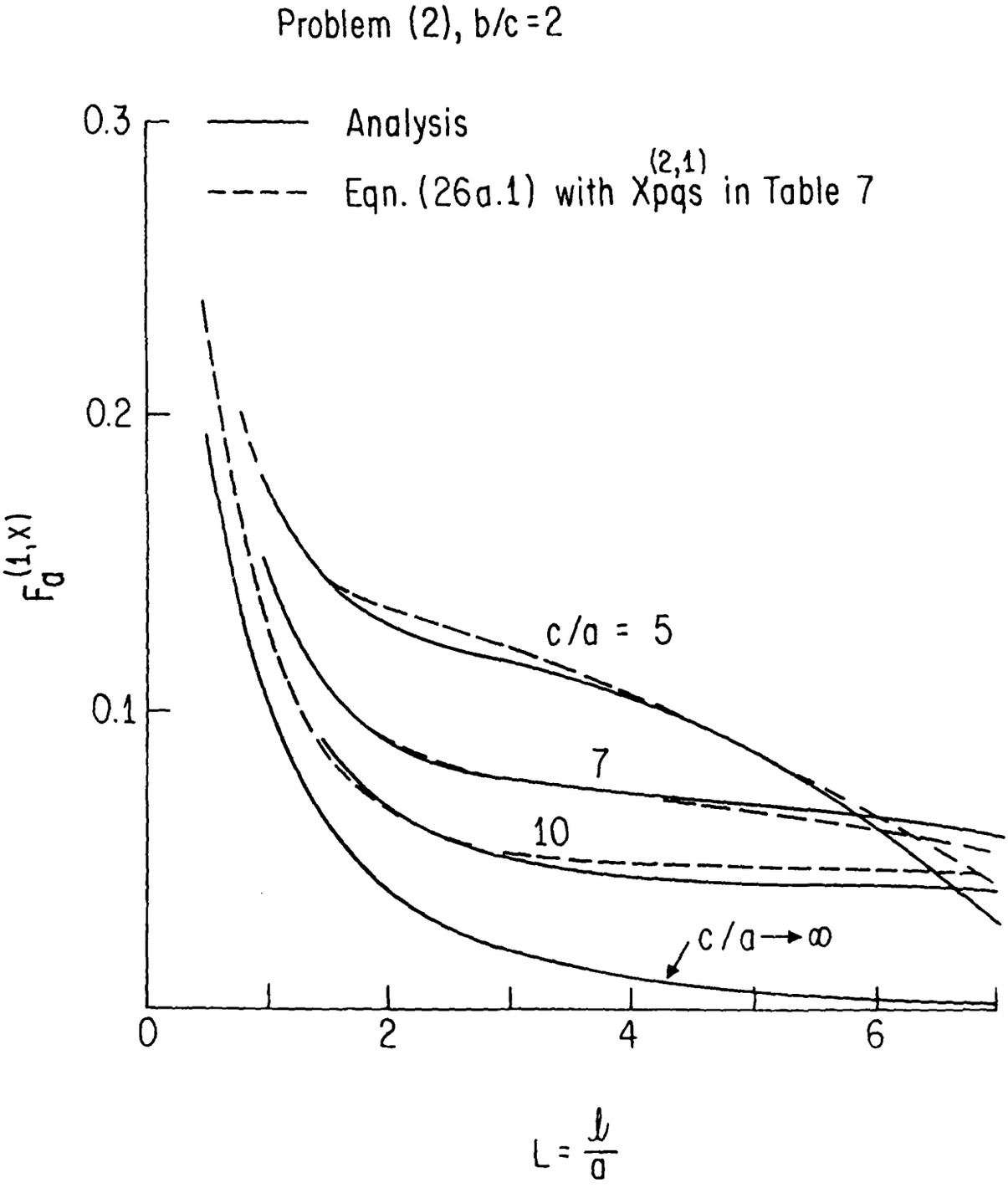
Problem (2), b/c = 2
Analysis
Eqn. (26a.1) with $X_{pqs}^{(2,1)}$ in Table 7
0.3
0.2
0.1
$F_a^{(1,X)}$
c/a = 5
7
10
c/a → ∞
0
2
4
6
$L = \frac{l}{a}$

Figure 6

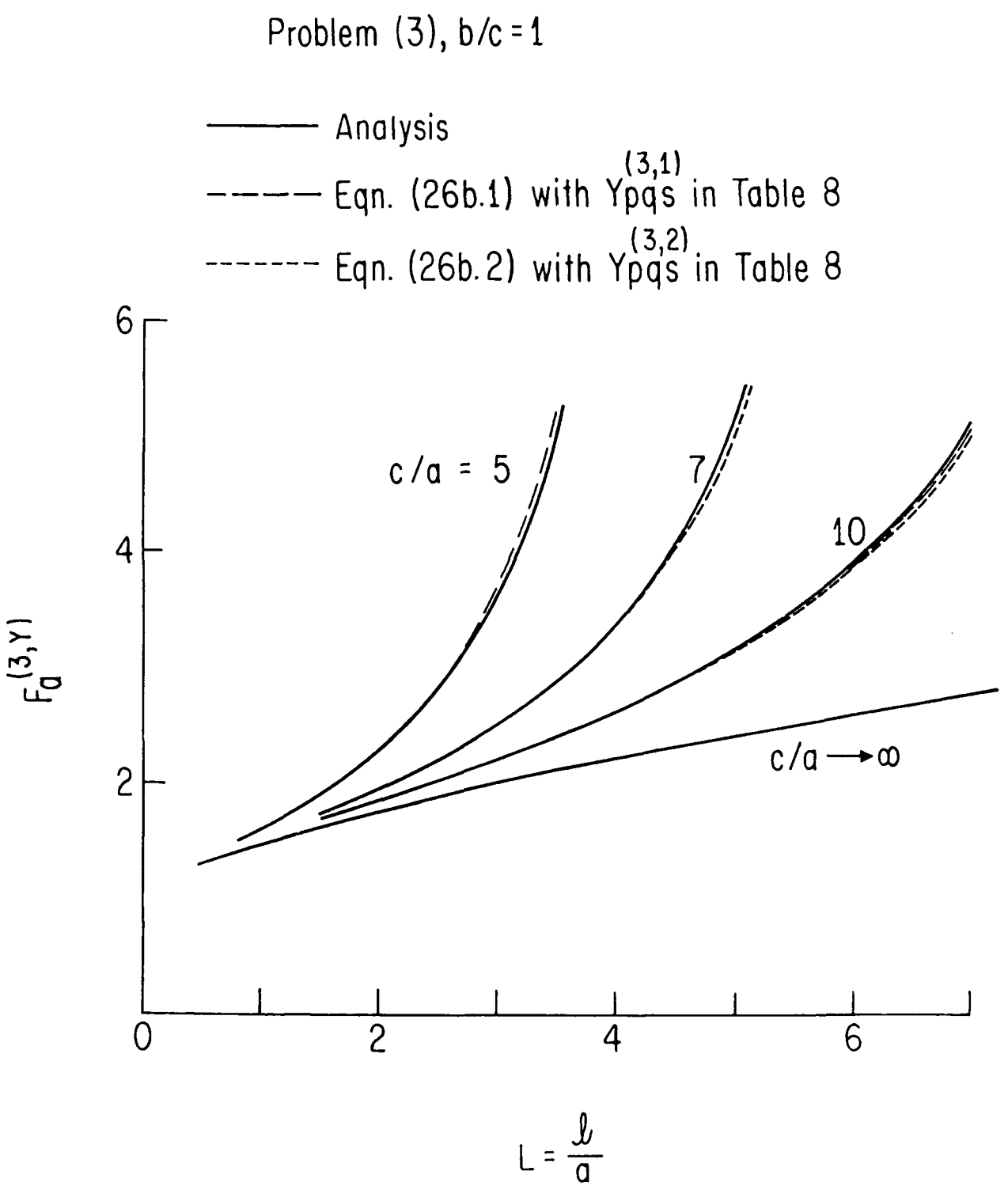
Problem (3), b/c = 1
Analysis
Eqn. (26b.1) with $Y_{pqs}^{(3,1)}$ in Table 8
Eqn. (26b.2) with $Y_{pqs}^{(3,2)}$ in Table 8
$F_a^{(3,Y)}$
6
4
2
0
2
4
6
c/a = 5
7
10
c/a → ∞
$L = \frac{\ell}{a}$

Figure 7

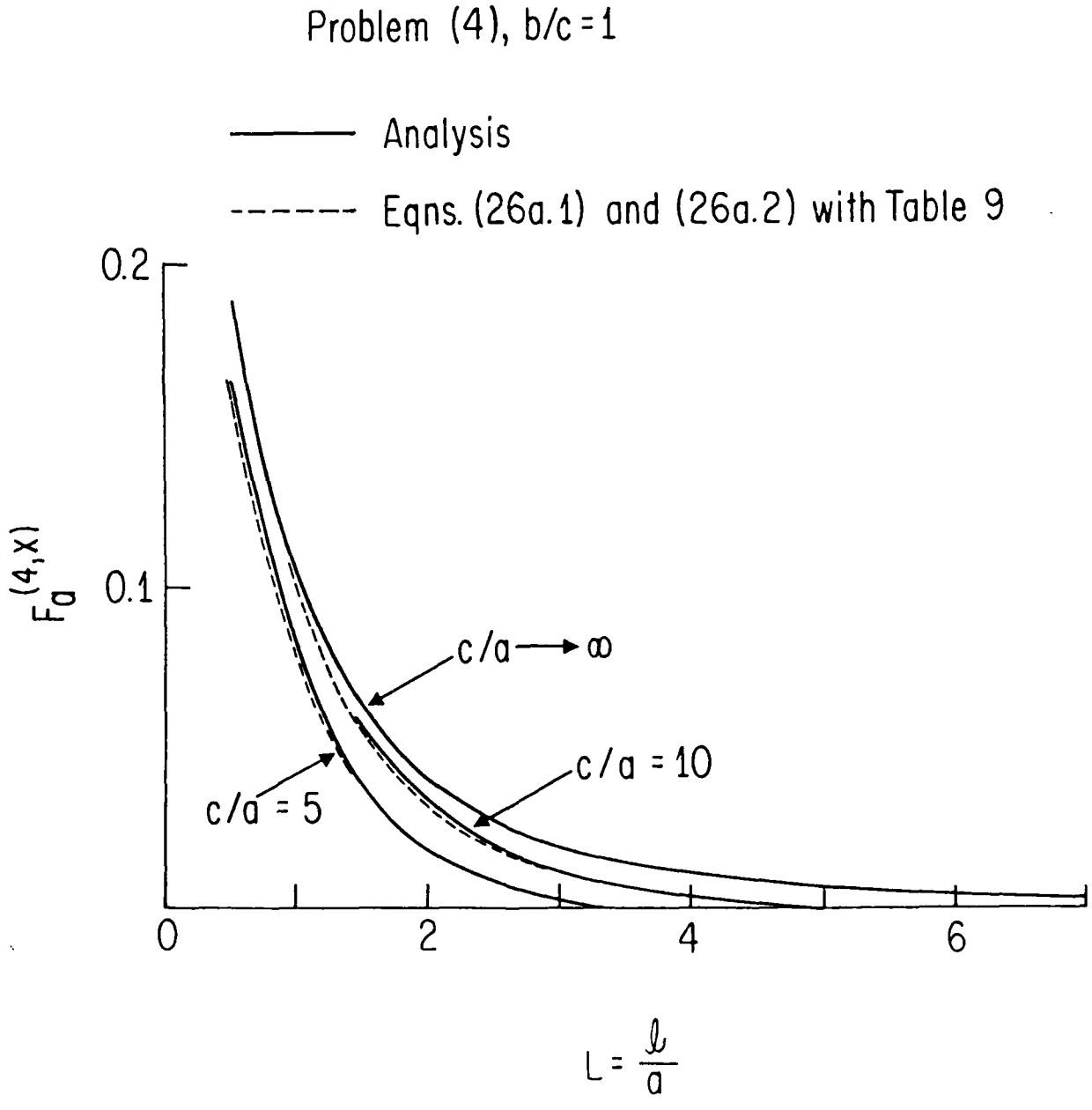
Problem (4), b/c = 1
Analysis
Eqns. (26a.1) and (26a.2) with Table 9
0.2
0.1
$F_a^{(4,x)}$
c/a → ∞
c/a = 10
c/a = 5
0
2
4
6
$L = \frac{\ell}{a}$

Figure 8-1

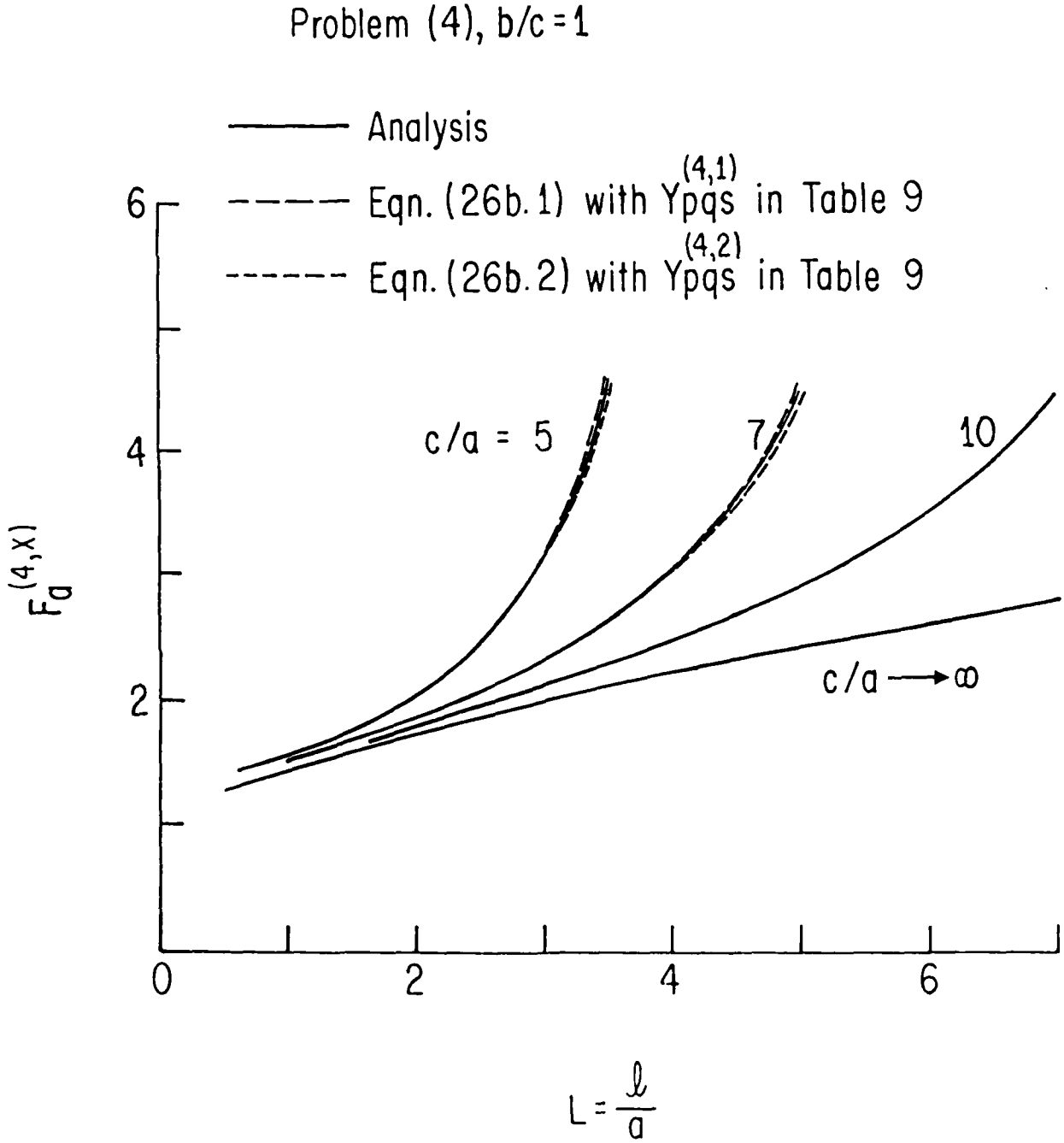
Problem (4), b/c = 1
Analysis
Eqn. (26b.1) with $Y_{pqs}^{(4,1)}$ in Table 9
Eqn. (26b.2) with $Y_{pqs}^{(4,2)}$ in Table 9
c/a = 5
7
10
c/a → ∞
$F_a^{(4,X)}$
0
2
4
6
$L = \frac{\ell}{a}$

Figure 8-2

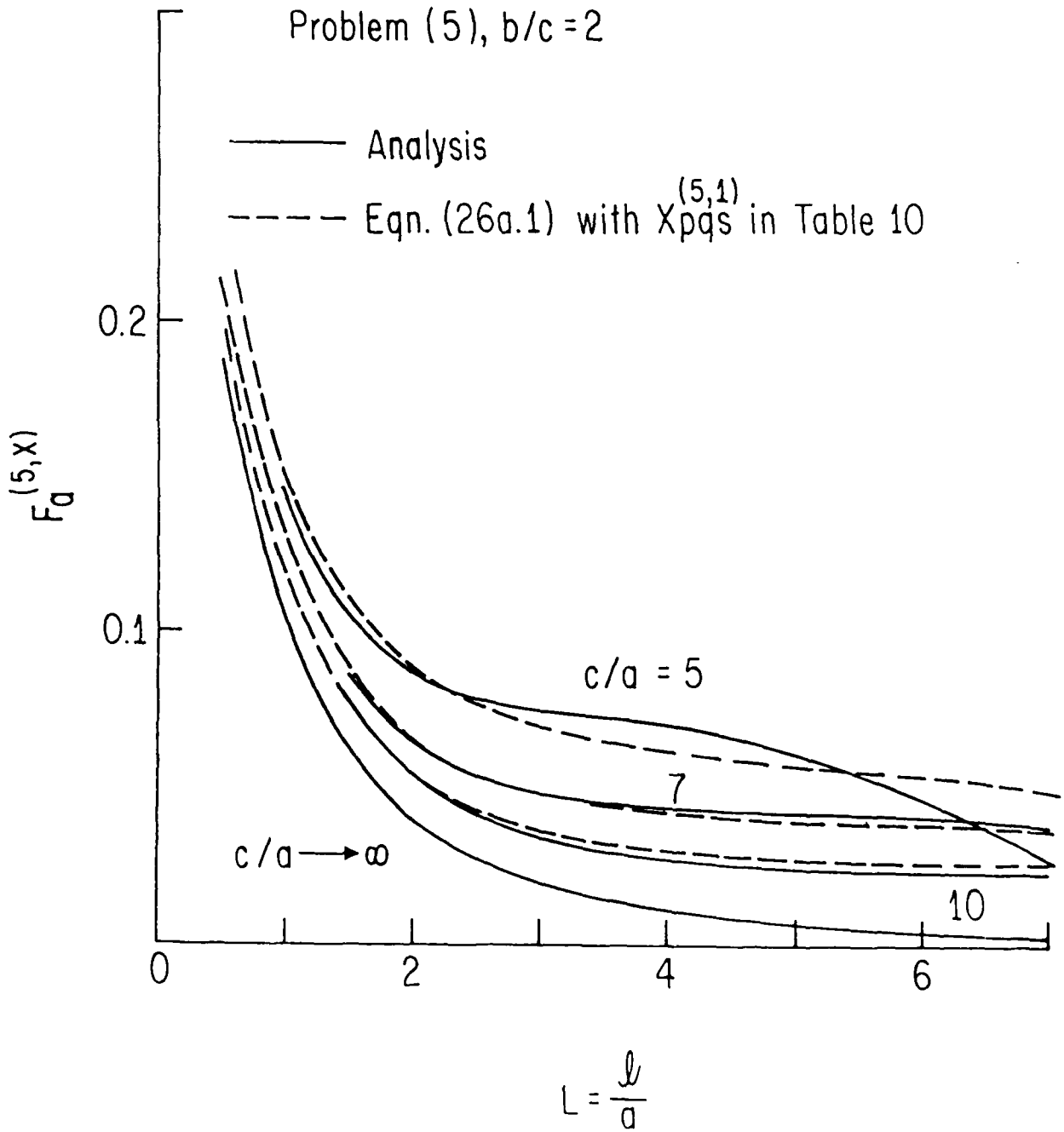
Problem (5), b/c = 2
Analysis
Eqn. (26a.1) with $X_{pqs}^{(5,1)}$ in Table 10
$F_a^{(5,X)}$
0.2
0.1
c/a = 5
7
c/a → ∞
10
0
2
4
6
$L = \frac{\ell}{a}$

Figure 9-1

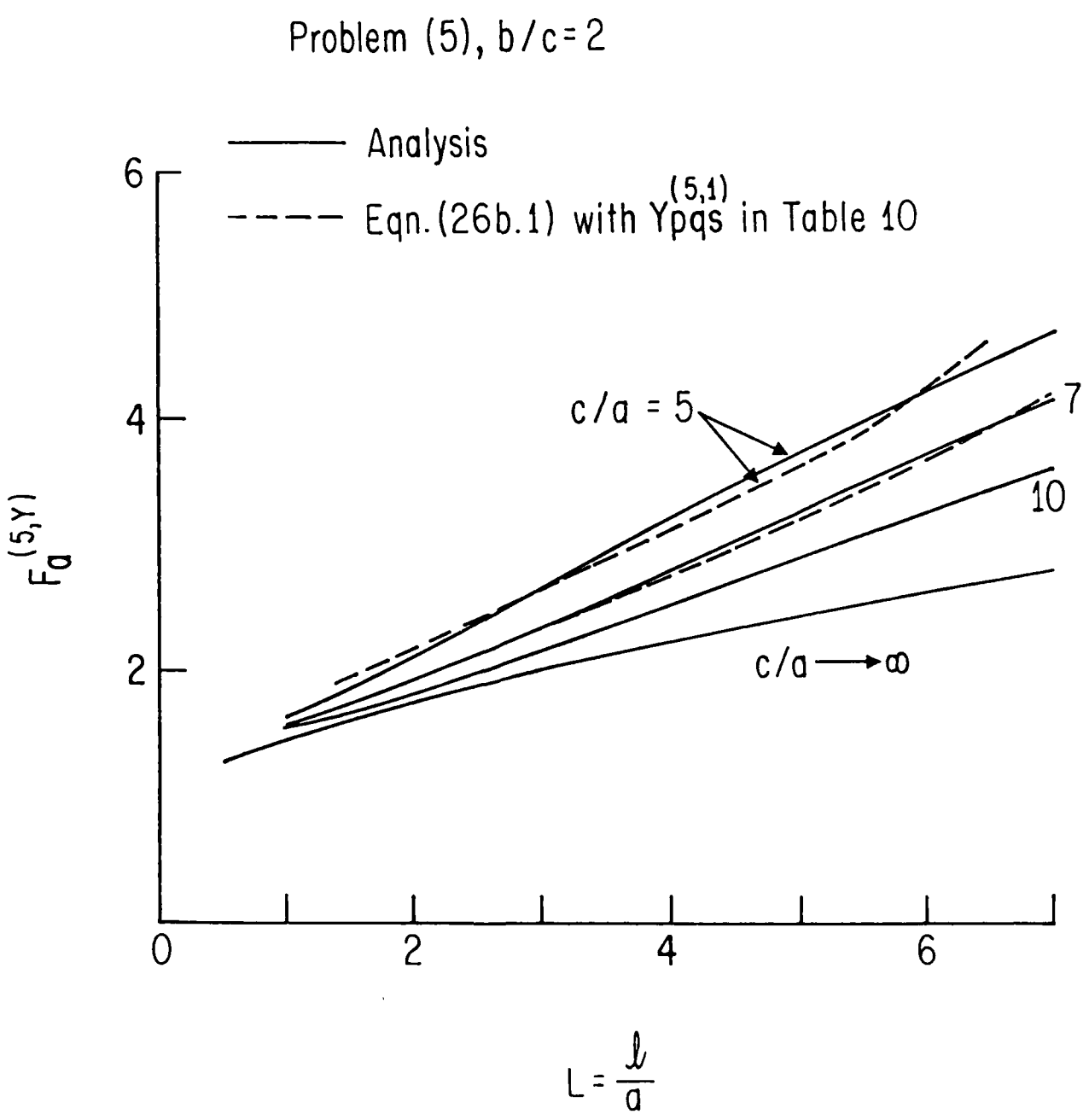
Problem (5), b/c = 2
Analysis
Eqn. (26b.1) with $Y_{pqs}^{(5,1)}$ in Table 10
$F_a^{(5,Y)}$
c/a = 5
7
10
c/a → ∞
0
2
4
6
$L = \frac{\ell}{a}$

Figure 9-2

CHAPTER III

ON MECHANICS OF CRACK GROWTH AND ITS EFFECTS ON THE OVERALL RESPONSE OF BRITTLE POROUS SOLIDS*

by

M. Isida
S. Nemat-Nasser

Table of Contents

* Acta Mettalurgica, in press.

CHAPTER III

ON MECHANICS OF CRACK GROWTH AND ITS EFFECTS ON THE OVERALL RESPONSE OF BRITTLE POROUS SOLIDS

M. Isida* and S. Nemat-Nasser

Department of Applied Mechanics and Engineering Sciences

University of California, San Diego, La Jolla, CA 92093

Abstract

This paper is concerned with crack growth in brittle porous solids under compression and its effects on the overall response of the material. As a mathematical model, we consider an elastic solid containing a zig-zag array of circular holes with a pair of edge cracks (two-dimensional problem), and solve this problem by using a theory which gives numerical results as accurate as desired. Based on the analytical results, we discuss the crack growth process and estimate the effective Young's moduli as well as the stress-strain relation for porous solids. Our computations show that the cracks emanating from the poles of the circular holes extend in the axial direction and grow -- in most cases in a stable manner, but for certain cases in an unstable manner during an intermediate loading state -- as the overall applied uniaxial compression increases, reaching a certain

---

* Present address: Department of Mechanical Engineering, Kurume Institute of Technology, 2228 Mukuno Kamitsumachi, Kurume 830, Japan.

limiting maximum length. This maximum crack length strongly depends on the ratio of the hole radius to the hole spacing in the loading direction. The effective Young's modulus in the direction of the crack growth is basically determined by the initial porosity, and is little affected by the crack length or its growth regime, i.e., whether stable or unstable. We find that the overall axial stress-strain curve remains monotonic, exhibiting no peak stress or strain softening, as cracks extend in the axial direction and reach their limiting length with increasing axial stress.

1. INTRODUCTION

For a large class of brittle materials, failure often involves the formation and growth of tension cracks. Under farfield overall tensile forces, such tension cracks initiate at preexisting flaws or defects, or at inclusions or other material heterogeneities which serve as stress concentrators. Tensile failure of this kind has been extensively studied since the pioneering work of Griffith [1]. It is also known that failure of brittle materials under farfield compressive forces is often caused by the formation and growth of tensile microcracks at preexisting flaws or other heterogeneities. In this case, even though the overall farfield stresses may be compressive, the presence of defects may produce high tensile stresses at the local level, leading to the formation of tension cracks. Brittle failure of this kind is rather complex and has received attention of researchers only recently.

Various mathematical models have been considered in order to explain and analytically quantify brittle failure in compression. A noteworthy model is a straight preexisting crack inclined with respect to the maximum overall farfield compression, producing tension cracks at its tips due to the relative frictional sliding of its faces; see [2-11]. Recently, Nemat-Nasser and Horii [8,9], and Horii and Nemat-Nasser [10,11], have analyzed the elasticity problem associated with this model by considering a preexisting thin straight flaw (or a set of such flaws) endowed with both frictional and cohesive resistance, and embedded in a linearly elastic solid. By examining the growth of tension cracks which emanate from the tips of such a flaw, as well as from the tips of an interacting set of such flaws which are suitably arranged, these authors show that the model does capture the essential features observed experimentally, i.e., axial

splitting in uniaxial compression, and faulting when the axial compression is accompanied by some moderate confining pressures. In addition, by including the possibility of the formation of a plastic zone at the crack tips, Horii and Nemat-Nasser [9-11] show how the model can be used to explain the process of brittle-ductile transition. These authors also report on a set of model experiments which seem to corroborate their analytical predictions.

Microcracks may also nucleate at pores in a porous solid and grow under farfield compressive stresses. This suggests an alternative model for the analysis of failure in compression of brittle solids containing micro-cavities. To be able to examine the physical consequences of a model of this kind, one requires a solution of the problem of crack growth from the walls of cavities under prescribed farfield stresses. In the two-dimensional case, the elasticity problem of cracks extending from the edges of a circular hole has been solved by Bowie [12] for an infinitely extended medium. The more general problem of cracks emanating from an elliptical hole in a plane has been treated by several authors [13-16] where some of the results have been put in a form convenient for design purposes [17,18].

Recently, Sammis and Ashby [19] proposed to use edge-cracks emanating from circular (in two dimensions) or spherical (in three dimensions) cavities, as a basic model for the analysis of brittle failure in compression. With the aid of model experiments, these authors show that cracks can grow from pores and extend in the direction of maximum compression. However, since an exact solution for a finite body containing a circular cavity with edge-cracks does not exist, these authors use approximate estimates based on the beam theory. In particular, for a solid containing periodically distributed holes with edge-cracks, Sammis and Ashby

estimate the relation between the overall uniform axial stress and the axial strain, arriving at a stress-strain relation with a peak stress followed by a descending portion (i.e., "strain softening"). In this model, the cracks are assumed to initiate at the poles of the circular holes and to extend straight in the direction of axial compression. Since approximate expressions* based on strength-of-material considerations are used, it is not clear whether an exact solution of the associated elasticity problem would also produce a peak stress followed by "strain softening".

In this paper we solve the problem of a zig-zag array of circular holes with a pair of edge cracks. In the method used the results can be rendered as accurate as desired. Based on our numerical results, we discuss the crack growth process, the effective Young's moduli, and the stress-strain relation of porous solids. Our solution predicts a monotonically increasing axial stress-strain relation for this model problem even when the cracks grow axially in an unstable manner.

2. THEORETICAL ANALYSIS OF ZIG-ZAG ARRAY OF HOLES WITH EDGE CRACKS

As a mathematical model of porous solids with micro-cracks, we consider an infinite solid with a zig-zag periodic array of holes with edge cracks, as shown by Fig. 1. Due to symmetry, we solve this problem using suitably symmetric stress potentials defined on the rectangular region OEFGO; see

---

* In [19], the change in potential energy due to cracking is calculated for small crack lengths (i.e., $1 + L \simeq 1$ is used in equation (22) of [19]). The results are then used to calculate the elastic modulus of the cracked body for large crack lengths. This may be a major cause of the strain softening prediction in [19].

Fig. 2 for notation and definition of various geometric quantities. Figs. 3-1 and 3-2 show the two typical hole distributions corresponding to $b/c = 0.577$ and $b/c = 1$, which are the equilateral triangular array and the square array, respectively.

We consider the biaxial loading case in which

$$\sigma_1 = -\lambda_1\sigma_0, \quad \sigma_2 = -\lambda_2\sigma_0 \tag{1}$$

where σ_1 and σ_2 are the applied stresses at infinity in the x- and y-directions, respectively, and σ_0 is a positive reference stress.

The analytical procedure for the solution of this problem is outlined in Appendix 1. Here we discuss the numerical results.

The numerical values of the stress intensity factor K_I are given in terms of the following dimensionless quantity, F_I:

$$F_I(\lambda_1,\lambda_2) = \frac{K_I(\lambda_1,\lambda_2)}{\sigma_0(\pi a)^{\frac{1}{2}}} \tag{2}$$

Let E_x (in compression) and E_y (in tension) be the effective Young's moduli in the x- and y-directions for the porous solid with cracks. They are obtained from the displacements, u along $\overline{EF}$ and v along $\overline{FG}$, associated with cases $\lambda_1 = 1$, $\lambda_2 = 0$ and $\lambda_1 = 0$, $\lambda_2 = -1$, respectively. Their numerical results are given in terms of the "modulus-reduction-factors", C_x and C_y, which are defined by:

$$C_x = \frac{E_x}{E_0}, \quad C_y = \frac{E_y}{E_0} \tag{3a}$$

where

$$E_0 = E \ \text{(plane stress)}, \quad E_0 = \frac{E}{1-\nu^2} \ \text{(plane strain)} \tag{3b}$$

Note that E_y for compression is not the same as that for tension, once cracks in the x-direction are developed. In this case, E_y (compression) =

E_y (uncracked porous) > E_y (tension with cracks).

C_x and C_y depend on Poisson's ratio. (Numerical results presented by Fig. 8-1 to Fig. 13 have been obtained for plane strain with $\nu = 0.3$.)

3. CRACK GROWTH PROCESS IN BRITTLE POROUS SOLIDS UNDER COMPRESSION

3.1. Uniaxial Compression ($\lambda_1 = 1$, $\lambda_2 = 0$)

The solid curves in Figs. 4-1 to 4-3 give the dimensionless stress intensity factors $F_I(1,0)$ for various values of b/c in the case of uniaxial compression. In the range $b/c \leq 1$, which includes the two typical cases shown by Figs. 3-1 and 3-2, the value of $F_I(1,0)$ decreases monotonically with increasing values of L, i.e. an increase in the applied stress is required in order to extend the crack (at constant critical stress intensity factor). Thus the crack extension regime is stable in this range of b/c. F_I reduces to zero at a certain value of L, depending on the values of b/c and c/a. This trend becomes more pronounced as b/c increases.

For larger values of b/c, unstable crack growth may occur, as shown by Fig. 4-3. We observe that, for certain values of c/a, F_I which is first a decreasing function of L, may begin to increase with increasing crack length, L, after a certain crack length is attained. However, since the ascending portion of the F_I, L-curves are followed by a descending portion, the corresponding unstable crack growth is expected to cease and be followed by a stable one.

Since K_I is constant ($= K_{Ic}$) during the crack growth, we can define the normalized applied stress by the reciprocal of F_I, that is

$$\tilde{\sigma} = \frac{-\sigma_1(\pi a)^{\frac{1}{2}}}{K_{Ic}} \tag{4}$$

$\tilde{\sigma}$, L-curves for $b/c = 0.577$ and $b/c = 1/0.8$ are given in Figs. 5-1 and

5-2, respectively. In the range $b/c \leq 1$, $\tilde{\sigma}$ increases monotonically with increasing L, as shown in Fig. 5-1 for a typical case. Therefore the crack growth is stable in this range of b/c. For larger values of b/c, we observe an intermediate stage where $\tilde{\sigma}$ decreases with increasing L, as shown by Fig. 5-2. The crack growth behavior in this case depends on the test conditions. If the specimen is tested under a displacement-controlled machine, the $\tilde{\sigma}$, L-relations will be as shown in Fig. 5-2, consisting of an initial increasing stage, an intermediate decreasing stage, and a final increasing stage. In load-controlled tests, however, the crack will extend from $L = L_1$ to $L = L_2$ abruptly, and then $\tilde{\sigma}$ increases with increasing value of L, following the curve shown in Fig. 5-2. Therefore in this case, the crack growth is temporarily unstable.

As is seen in Figs 5-1 and 5-2, the crack growth, except for the unstable stage in Fig. 5-2, becomes more gradual as L increases, and L approaches a certain limiting value L_{max} when $\tilde{\sigma}$ tends to infinity. The value of L_{max} can be determined graphically from diagrams similar to Figs. 4-1 to 4-3, by finding the intersection of the F_I-curves with the L-axis.

The variation of L_{max} with b/c and c/a is displayed in Figs. 6-1 and 6-2, respectively. They show that L_{max} varies almost linearly with both b/c and c/a, and, hence, can be fitted by the linear relation

$$L_{max} = -1.025 + 0.003\frac{c}{a} + \frac{b}{c}\left(-0.061 + 0.981\frac{c}{a}\right) \qquad (5a)$$

Results from Eqn. (5a) are shown by dashed lines in Figs. 6-1 and 6-2.

Eqn.(5a) may also be expressed as

$$L_{max} = -1.025 + 0.003\frac{c}{a} + \frac{b}{a}\left(0.981 - 0.061\frac{a}{c}\right) \qquad (5b)$$

which shows that L_{max} is also linear in b/a for fixed values of c/a. In Fig. 6-3 we have plotted the numerical values of L_{max} for various c/a, taking b/a as the abscissa. It is seen that L_{max} is almost independent of c/a, and can be approximated by the following linear expression of b/a:

$$L_{max} = 0.97 \left(\frac{b}{a} - 1\right) \tag{5c}$$

Eqn. (5c) is sufficiently accurate, at least for the range of b/a and c/a shown in Figs. 6-1 and 6-2.

The above b/a - dependence of L_{max} in a limited range of b/c can be understood from the behavior of the stress flow around the crack tips, which is mainly affected by the relative horizontal hole spacing, b/a, and is little disturbed by the relative vertical spacing c/a.

3.2. Effect of Lateral Confining Pressure

The lateral confining pressure considerably reduces K_I and, hence, L_{max}. As an example, F_I and L_{max} for a one percent lateral compression are given by dashed curves in Figs. 4-1 to 4-3. In order to examine the effect of the lateral pressure on L_{max}, calculations are performed for various values of λ ($= \sigma_2/\sigma_1$) in the typical case of b/c = 0.577, and L_{max} is evaluated. The results are plotted against λ in Fig. 7, together with the curve for an infinite solid ($c/a \to \infty$) obtained as a limiting case of the present problem. L_{max} reduces to zero at a certain value of λ depending on c/a. These limiting values of λ for finite c/a are known as the ratio of the minimum and the maximum of the circumferential stress along the holes without cracks which are zig-zagly distributed [20]. The calculated curves in Fig. 7 are extended toward these limiting values by dashed lines.

4. MODULUS CHANGE AND STRESS-STRAIN RELATION

4.1. Compression in the Crack Growth Direction

Figs. 8-1 to 8-3 show the change in the elastic moduli due to crack extension for b/c = 0.577, 1 and 1/0.8, respectively. Values of the modulus reduction factor C_x are plotted by solid lines against the normalized crack length, L, for various values of the hole size parameter c/a. We find that C_x decreases for smaller values of L, and tends to be almost constant for larger values of L. Note that these curves are terminated at points where the corresponding limiting maximum crack length, L_{max}, is attained.

Since C_x depends on b/c and c/a in Figs. 8-1 to 8-3, it is of interest to check the relation between C_x and the porosity $f_H = \pi a^2/(2bc)$. In Fig. 9, we have plotted C_x against f_H for various values of b/c, where L is taken to be 1.5 for convenience. We find that C_x is not much affected by b/c. Thus we can conclude that, for all practical purposes, the modulus reduction factor C_x depends only on f_H, and is almost independent of b/c and L, unless b/c is extremely small.

The limiting values of C_x when $L \to 0$ are obtained by analysing a zig-zag array of holes without cracks [20]. Typical results are plotted in Fig. 10, and we find that $(C_x)_{L=0}$ also strongly depends on f_H and is little affected by b/c. These analytical values are fitted by the following polynomial with good accuracy:

$$(C_x)_{L=0} = 1 - 2.592\, f_H + 3.050\, f_H^2 - 3.354\, f_H^3 + \frac{b}{c}\left[- 0.828\, f_H + 1.586\, f_H^2 + 7.664\, f_H^3 \right] + \left(\frac{b}{c}\right)^2 \left[0.310\, f_H + 0.836\, f_H^2 - 11.680\, f_H^3 \right]$$

$$(0.25 \le b/c \le 1.33 \text{ and } f_H \le 0.5) \tag{6}$$

Let's make further comments on C_x for the two typical cases shown by Figs. 3-1 and 3-2. As is seen in Figs. 8-1 to 8-3, C_x remains almost constant after the crack length reaches a certain value which seems to be around 1.5. Fig. 11 shows the values of C_x for $L = 0$ and for $L \ge 1.5$. These are the upper and the lower bounds for C_x. The values for $L = 0$ are well fitted by the following polynomials:

$$(C_x)_{b/c=0.577, L=0} = 1 - 2.977\, f_H + 4.910\, f_H^2 \tag{7a}$$

$$(C_x)_{b/c=1, L=0} = 1 - 2.972\, f_H + 2.536\, f_H^2 \tag{7b}$$

In the special case of $b/c = 1$, $(C_x)_{L=0}$ can be also obtained by transformation of the results for a doubly periodic array of circular holes distributed with equal spacings in both directions [21] (see Appendix 2).

Now we consider the stress-strain relations for this problem. Let σ and ε be the axial compressive stress and strain, respectively. Then the strain when the crack length is L is given by the integral

$$\varepsilon_L = \int_{L=0}^{L} \frac{d\sigma}{E_x} \tag{8}$$

It is oberved from Figs. 8-1 to 8-3, that E_x remains nearly constant during the crack growth, in a wide range of values of b/c. In these cases we have

$$\varepsilon_L = \frac{\sigma_L}{E_x} \tag{9}$$

which is written in the dimensionless form

$$\tilde{\varepsilon}_L = \frac{\tilde{\sigma}_L}{C_x}, \quad C_x = \frac{E_x}{E_0} \tag{10}$$

where

$$\tilde{\varepsilon}_L = \frac{E_0(\pi a)^{1/2}\varepsilon_L}{K_{Ic}}, \quad \tilde{\sigma}_L = \frac{\sigma_L(\pi a)^{1/2}}{K_{Ic}} = \frac{1}{F_{I,L}} \tag{11}$$

It is to be emphasized that the linear relationship (10) holds approximately even for cases where the crack growth is temporarily unstable, as is seen in Figs. 5-2 and 8-3 for b/c = 1/0.8. Fig. 12 gives the $\tilde{\sigma}_L$, $\tilde{\varepsilon}_L$-relations for this case of b/c.

As stated above, our results do not show any significant reduction in the axial stiffness of the porous solid with axial crack growth, unless b/c is extremely small. Our numerical results produce monotonically increasing axial stress-strain relations without any peak stress, even when axial cracks grow in an unstable manner in the axial direction. The effect of such an axial crack growth on the axial strain and axial stiffness is of second order which does not change the character of the corresponding stress-strain relation.

4.2. Young's Modulus Transverse to Crack Growth Direction

The modulus reduction factor C_y, for tensile loading, is given by dashed curves in Figs. 8-1 to 8-3. As is expected, C_y decreases considerably with crack growth, and the tensile load-carrying capacity of the specimen reduces to zero when the adjacent cracks join. Thus C_y is zero when $a + \ell \to b$ or $L \to (b/c)(c/a)-1$. The curves obtained by numerical calculation may therefore be extended to their corresponding limiting values on the L-axis, as shown by dotted lines.

An abrupt drop in the value of C_y is observed in Figs. 8-1 to 8-3.

Fig. 13 gives the relation between C_y and f_H for L = 1.5. C_y is not

much affected by the variation in b/c, similarly to C_x. However, it should be noted that, unlike C_x, C_y suffers a considerable reduction with increasing L. Therefore, Fig. 13 should be regarded as an example for L = 1.5. C_y, for tensile loading, depends very strongly on L, as well as on f_H.

REFERENCES

1. Griffith, A.A., *Phil. Trans. Roy. Soc. London*, A221, 163 (1921).
2. McClintock, F.A. and Walsh, J.B., *Proc. 4th U.S. Nat. Congr. Appl. Mech. 1962* , ASME, 2, 1015 (1963).
3. Kachanov, M.L., *Mechanics of Materials 1*, 29 (1982).
4. Ashby, M.F. and Hallam, S.D. (née Cooksley), *Acta Metall.*,34, 497 (1986).
5. Steif, P.S., *Eng. Frac. Mech.*, 20, 463 (1984).
6. Brace, W.F. and Bombolakis, E.G., *J. Geophys. Res.*, 68, 3709 (1963).
7. Hoek, E. and Bieniawski, Z.T., *Int. J. Frac. Mech.*, 1, 137 (1965).
8. Nemat-Nasser, S. and Horii H., *J. Geophys. Res.*, 87, 6805 (1982).
9. Nemat-Nasser, S. and Horii, H., *Proc. 6th Intern. Conf. Frac. (ICF6)*, New Delhi, India, 515 (1984).
10. Horii, H. and Nemat-Nasser, S., *J. Geophys. Res.*, 90, 3105 (1985).
11. Nemat-Nasser, S. and Horii, H., Brittle Failure in Compression: Splitting, Faulting, and Brittle-Ductile Transition, to appear in *Phil. Trans. Roy. Soc. London*.
12. Bowie, O.L., *J. Math. Phys.*, 35, 60 (1956).
13. Newman, J.C., Jr., *NASA TN, D-6376* (1971).
14. Nisitani, H. and Isida, M., *Trans. JSME*, 39, 7 (1973).
15. Isida, M. and Nakamura, Y., *Trans. JSME*, 46, 947 (1980).
16. Isida, M., Chen, D.H. and Nisitani, H., *Eng. Frac. Mech.*, 21, 983 (1985).

17. Sih, G.C., *Handbook of Stress Intensity Factors for Researchers and Engineers*, Lehigh University, Bethlehem, P.A. (1973).

18. Rook, D.P. and Cartwright, D.J., *Compendium of Stress Intensity Factors*, H.M. Stationary Office, England (1976).

19. Sammis, C.G. and Ashby, M.F., *Acta Metall.*, 34, 511 (1986).

20. Isida, M. and Igawa, H., *Bulletin, Kurume Institute of Technology*, Japan,9, 29 (1985).

21. Nemat-Nasser, S., Iwakuma, T. and Hejazi, M., *Mechanics of Materials 1*, 239 (1982).

22. Isida, M., *Proc. 1st Congr. Numer. Meths. Frac. Mech.*, Swansea, England, 81 (1978).

23. Isida, M. and Sato, R., *Trans. JSME*, **A50**, 1619 (1984).

24. Muskhelishvili, N.I., *Some Basic Problems in the Mathematical Theory of Elasticity*, Nordhoff, Groningen, Holland (1953).

25. Isida, M. and Noguchi, H., *Trans. JSME*, **A49**, 147 (1983).

26. Nisitani, H., *Japanese Papers for Japan-U.S. Seminar, Strength and Struc. Solid Mat.*, Minnowbrook, 28 (1974).

APPENDIX 1 : ANALYSIS OF ZIG-ZAG ARRAY OF HOLES WITH EDGE CRACKS

Analytical Concept

Consider an infinite solid with a zig-zag periodic array of holes with edge cracks as shown by Fig. 1. Due to double symmetry, we solve this problem using stress potentials defined on the unit rectangular region in the first quadrant, OEFGO; see Fig.2.

The analysis is performed by superposing two stress states. The first one is represented by the complex potentials $\phi_1(z)$ and $\psi_1(z)$ having singularities within the hole. The second stress state is properly singular at the crack tips, and is realized by distributing suitable force doublets along the cracks.

The above two stress states are established in such a manner that they automatically satisfy the traction-free conditions at the hole.

The boundary conditions on the crack and at the outer edges of the unit region are given in terms of stresses and displacements. In the present analysis, the stress conditions are replaced by those of the resultant forces in order to increase the accuracy of the numerical results [22,23].

Displacements and Resultant Forces due to the First Stress State

In plane problems of elasticity, components of the stress, the displacement, and the resultant force with respect to the Cartesian coordinates are expressed in terms of two complex potentials, $\phi(z)$ and $\psi(z)$, as follows [24]:

$$\frac{\sigma_y + \sigma_x}{2} = 2\,\mathrm{Re}[\phi'(z)] \tag{A1.1}$$

$$\frac{\sigma_y - \sigma_x}{2} + i\tau_{xy} = \bar{z}\,\phi''(z) + \psi'(z)$$

$$2G\,(u - iv) = \kappa\,\bar{\phi}(\bar{z}) - \bar{z}\phi'(z) - \psi(z) \qquad \text{(A1.2)}$$

$$P_y + iP_x = -\,\bar{\phi}(\bar{z}) - \bar{z}\phi'(z) - \psi(z) \qquad \text{(A1.3)}$$

where G is the shear modulus, and κ is defined in terms of Poisson's ratio, ν, as follows:

$$\kappa = \frac{3 - \nu}{1 + \nu} \quad \text{(plane stress)}, \quad = 3 - 4\nu \quad \text{(plane strain)} \qquad \text{(A1.4)}$$

The complex potentials $\phi_1(z)$ and $\psi_1(z)$ for the first stress state are expressed as the following Laurent series:

$$\phi_1(z) = M_0 z + \sum_{n=0}^{N-1}[M_{2n}\{z^{2n+1} - (2n+1)a^{4n}z^{-(2n-1)}\} - K_{2n}a^{4n+2}z^{-(2n+1)}]$$

$$\psi_1(z) = -2M_0\,a^2z^{-1} + \sum_{n=0}^{N-1}[K_{2n}\{z^{2n+1} - (2n+1)a^{4n+4}z^{-(2n+3)}\} \qquad \text{(A1.5)}$$

$$-M_{2n}(2n)^2a^{4n+2}z^{-(2n+1)}]$$

Using Eqns.(A1.5) in Eqns.(A1.2) and (A1.3), we have the following expressions for the displacements and the resultant forces:

$$2G(u - iv)_{(1)} = M_0\{2a^2z^{-1} + (\kappa - 1)\bar{z}\} + \sum_{n=1}^{N-1} M_{2n}[\kappa\bar{z}^{2n+1} - (2n+1)\bar{z}z^{2n}$$

$$+(2n+1)a^{4n}\{-\kappa\bar{z}^{-(2n-1)} - (2n-1)\bar{z}z^{-2n}\} + (2n)^2\,a^{4n+2}z^{-(2n+1)}]$$

$$+ \sum_{n=0}^{N-1} K_{2n}[-z^{2n+1} - a^{4n+2}\{\kappa z^{-(2n+1)} + (2n+1)\bar{z}z^{-(2n+2)}\}$$

$$+(2n+1)a^{4n+4}z^{-(2n+3)}] \qquad \text{(A1.6a)}$$

$$(P_y + iP_x)_{(1)} = M_0(2a^2z^{-1} - 2\bar{z}) + \sum_{n=1}^{N-1} M_{2n}[-\bar{z}^{2n+1} - (2n+1)\bar{z}z^{2n}$$

$$+(2n+1)a^{4n}\{\bar{z}^{-(2n-1)} - (2n-1)\bar{z}z^{-2n}\} + (2n)^2\,a^{4n+2}z^{-(2n+1)}]$$

$$+ \sum_{n=0}^{N-1} K_{2n}[-z^{2n+1} + a^{4n+2}\{z^{-(2n+1)} - (2n+1)\bar{z}z^{-(2n+2)}\}$$

$$+(2n+1)a^{4n+4}z^{-(2n+3)}] \qquad \text{(A1.6b)}$$

The above expressions include 2N unknown coefficients M_{2n} and K_{2n} ($n = 0,1,2,\cdots,N-1$) to be determined from the boundary conditions.

Displacements and Resultant Forces due to the Second Stress State

The second stress state is realized by distributing force doublets of arbitrary densities on the cracks. The force doublets are established from stress states for concentrated forces acting in an infinite solid which contains a circular hole, and, therefore, the traction-free conditions at the hole edge are satisfied automatically. Expressions for the displacements and the resultant forces due to these distributed force doublets are as follows [25]:

$$2G\,(u - iv)_{(2)} = \frac{1}{2\pi}\sum_{m=1}^{2}\int_{-\ell/2}^{\ell/2} p_m(s_m)\left[-\frac{1}{s_m - w_1} + \frac{\kappa}{s_m - w_1} + \frac{w_1 - \bar{w}_1}{(s_m - w_1)^2}\right.$$

$$+ \frac{1}{s_m - w_2} - \frac{\kappa}{s_m - \bar{w}_2} + \frac{\bar{w}_1 - w_2}{(s_m - w_2)^2} - \frac{\kappa(\bar{w}_1 - \bar{w}_2)}{(s_m - w_2)^2} - 2(w_1 - w_2)(\bar{w}_1 - w_2)\frac{a^2}{z^2}\frac{1}{(s_m - w_2)^3}$$

$$\left. + 2\left(\kappa z + \frac{a^2}{z}\right)\frac{1}{(s_m + w_3)^2}\right] \qquad \text{(A1.7a)}$$

$$(P_y + iP_x)_{(2)} = \frac{1}{2\pi}\sum_{m=1}^{2}\int_{-\ell/2}^{\ell/2} p_m(s_m)\left[-\frac{1}{s_m - w_1} - \frac{1}{s_m - w_1} + \frac{w_1 - \bar{w}_1}{(s_m - w_1)^2}\right.$$

$$+ \frac{1}{s_m - w_2} + \frac{1}{s_m - \bar{w}_2} + \frac{\bar{w}_1 - w_2}{(s_m - w_2)^2} + \frac{\bar{w}_1 - \bar{w}_2}{(s_m - w_2)^2} - 2(w_1 - w_2)(\bar{w}_1 - w_2)\frac{a^2}{z^2}\frac{1}{(s_m - w_2)^3}$$

$$\left. + 2\left(-z + \frac{a^2}{z}\right)\frac{1}{(s_m + w_3)^2}\right] \qquad \text{(A1.7b)}$$

where $p_m(s_m)$ $(m=1,2)$ are unknown density functions of the force doublets, and the subscript m takes 1 for the right and 2 for the left crack, respectively; the following notation is also used (see Fig. A1-1):

$$w_1 = z - x_{0,m}\ ,\quad w_2 = \frac{a^2}{z} - x_{0,m}\ ,\quad w_3 = x_{0,m}$$

$$x_{0,m} = a + \frac{\ell}{2}\ \ (m=1)\ ,\quad x_{0,m} = -a - \frac{\ell}{2}\ \ (m=2) \tag{A1.8}$$

The density functions $p_m(s_m)$ in Eqns.(A1.7) are then expressed as [26]

$$p_m(s_m) = q_m(s_m)\left[\left(\frac{\ell}{2}\right)^2 - s_m^2\right]^{-1/2} \tag{A1.9}$$

It is obvious from symmetry that

$$q_2(-s_2) = q_1(s_1) \tag{A1.10}$$

Thus $q_1(s_1)$ is the only unknown function in the second stress state.

Boundary Conditions Based on Resultant Forces and Displacements

A piecewise linear approximation will be used to evaluate the unknown weighting function $q_1(s_1)$. For the right crack, this is shown in Fig. A1-2, where equally spaced intervals are used. Eqns. (A1.7a) and (A1.7b) now reduce to linear expressions in f_j $(j = 1,2,\cdots,M)$, which are the values of the weighting function at the ends of these intervals.

We now have 2N unknown coefficients in the first stress state and M unknown weights, f_j, in the second stress state to be determined from the boundary conditions. Since both stress states satisfy the traction-free conditions on the hole, we have only to consider the boundary conditions on the crack and at the outer edges of the unit rectangular region. These conditions are satisfied by means of a boundary collocation procedure based

on the displacements and the resultant forces. In the numerical computations, the traction-free conditions of the cracks are replaced by M relations, and those of the outer edges by 2N relations.

Since the cracks are assumed to be traction-free, the present analysis is valid for such combinations of σ_1 and σ_2 that satisfy this assumption.

In order to obtain M relations from the traction-free conditions on crack $\overline{A_1B_1}$ (stated in terms of resultant force, P_y), we divide this crack into M intervals, $\overline{D_1D_2}$, $\overline{D_2D_3}$,--- $\overline{D_MD_{M+1}}$, where D_2, D_3,---, D_M are the mid-points of the intervals shown in Fig. A1-2. Then the traction-free conditions are:

$$\text{Along crack } \overline{A_1B_1}: \qquad [P_y]_{D_k}^{D_{k+1}} = 0 \quad (k = 1,2,---,M) \qquad \text{(A1.11)}$$

The boundary conditions at the outer edges of the unit rectangular region are given by the following relations (A.12a) and (A1.12b):

Conditions for the side $\overline{EF}$:

$$u = \text{const.}, \quad \tau_{xy} = 0 \qquad \text{(for any } y\text{)}$$

Conditions for the side $\overline{FG}$: (A1.12a)

$$(\sigma_y)_x = (\sigma_y)_{b-x}, \quad (\tau_{xy})_x = (\tau_{xy})_{b-x},$$

$$[u]_0^x = [u]_{b-x}^b, \quad [v]_0^x = [v]_{b-x}^b \qquad \text{(for any } x\text{)}$$

Conditions for the total forces along the outer edges:

$$[P_x]_E^F - [P_x]_G^H = \sigma_1 c, \quad [P_y]_F^G = \sigma_2 b \qquad \text{(A1.12b)}$$

regarding the relation $[P_x]_F^K = -[P_x]_G^H$ in Fig. 1.

To impose these boundary conditions in numerical computations, $\overline{EF}$ and $\overline{FG}$ are divided into N_1 and N_2 equal intervals, respectively, as shown in Fig. 2, where N_2 is taken to be an even integer, say $2N_3$.
The corresponding lengths of the intervals on $\overline{EF}$ and $\overline{FG}$ are

$$h_1 = \frac{c}{2N_1}, \quad h_2 = \frac{b}{N_2} \qquad \text{(A1.13)}$$

The boundary conditions (A1.12) are then replaced by the following relations (A1.14a) and (A1.14b), in terms of the resultant forces and displacements:

Along $\overline{EF}$: $[u]_{S_k}^{S_{k+1}} = 0, \; [P_y]_{S_k}^{S_{k+1}} = 0 \quad (k = 1,2,\cdots,N_1)$

Along $\overline{FG}$: $[P_y]_{S_k}^{S_{k+1}} = [P_y]_{S_{N_4-k}}^{S_{N_4+1-k}}, \; [P_x]_{S_k}^{S_{k+1}} = [P_x]_{S_{N_4-k}}^{S_{N_4+1-k}}$

$$[u]_{S_k}^{S_{k+1}} = [u]_{S_{N_4-k}}^{S_{N_4+1-k}}, \; [v]_{S_k}^{S_{k+1}} = [v]_{S_{N_4-k}}^{S_{N_4+1-k}}$$

$$N_3 = N_2/2, \quad N_4 = 2N_1 + N_2 + 1 \qquad (k = N_1+1, N_1+2, \cdots, N_1+N_3)$$

(A1.14a)

For the total forces:

$$[P_x]_E^F - [P_x]_G^H = \sigma_1 c \ , \quad [P_y]_F^G = \sigma_2 b \tag{A1.14b}$$

In order to obtain the same number of simultaneous equations as there are unknowns, the integer N in Eqn. (A1.6) is chosen such that

$$N = N_1 + N_2 \tag{A1.15}$$

The unknown quantities K_{2n}, M_{2n} $(n = 0,1,2,\cdots,N-1)$ and f_j $(j = 1,2,\cdots,M)$ are determined by solving the simultaneous equations (A1.11) and (A1.14).

Accuracy of Results

The stress intensity factor at the crack tip is calculated by

$$K_I = f_M \left(\frac{\pi \ell}{2}\right)^{\frac{1}{2}} \tag{A1.16}$$

The numerical results are then represented in terms of the dimensionless stress intensity factors given by Eqn. (2).

The accuracy of the numerical results would be improved with increasing subdivision numbers M, N_1 and N_2. It is however desirable to use minimum values for these quantities which still provide needed accuracy.

Reasonable values of M have been determined from test calculations of an infinite solid containing a circular hole with edge cracks, as a special case of the present problem. Table A1-1 gives typical results of $F_I(1,0)$ for $\ell/a = 0.4$. As is seen, any M larger than 5 seems to give reliable values with errors less than one percent. In computations of the present problem, M is taken to be 7 to 10 depending on the geometric parameters.

Other series of test calculations have been done to determine reasonable values for N_1 and N_2. Table A1-2 gives an example for $b/c = 0.5$,

$c/a = 5$ and $\ell/a = 2$. $F_I(1,0)$, C_x, and C_y are given for various values of N_1 and N_2, whereas M is fixed to be 7. The convergence is excellent, especially when $N_1 = N_2$, i.e. $h_1 = h_2$. On the basis of the above and similar results for other configurations, N_1 and N_2 are chosen to be 5 to 10, holding the relation $h_1 \simeq h_2$.

Thus the number of unknowns to be determined from the boundary conditions is confined to less than 50 with good accuracy.

APPENDIX 2 : STIFFNESS REDUCTION FACTORS FOR ZIG-ZAG ARRAY OF HOLES

The computer program prepared in a previous work [20] has been employed to obtain the values of $(C_x)_{L=0}$. The numerical results are then fitted by Eqn. (6) in terms of b/c and f_H. Eqns. (7a) and (7b) are also proposed for the two typical arrays of holes.

The values for the special case of b/c = 1 can also be obtained by the transformation of the results for the doubly periodic array of circular holes distributed with equal spacings in both directions [21] (Fig. A2-1). The procedure will be outlined below.

The stress-strain relations for this problem can be written as follows:

$$\begin{aligned} \varepsilon_{11} &= D_{1111}\sigma_{11} + D_{1122}\sigma_{22} \\ \varepsilon_{22} &= D_{2211}\sigma_{11} + D_{2222}\sigma_{22} \\ \varepsilon_{12} &= D_{1212}\sigma_{12} \end{aligned} \tag{A2.1}$$

$$\begin{aligned} \sigma_{11} &= C_{1111}\varepsilon_{11} + C_{1122}\varepsilon_{22} \\ \sigma_{22} &= C_{2211}\varepsilon_{11} + C_{2222}\varepsilon_{22} \\ \sigma_{12} &= C_{1212}\varepsilon_{12} \end{aligned} \tag{A2.2}$$

where

$$\begin{aligned} D_{1111} &= D_{2222}, \quad D_{1122} = D_{2211} \\ C_{1111} &= C_{2222}, \quad C_{1122} = C_{2211} \end{aligned} \tag{A2.3}$$

and

$$\begin{aligned} D_{1111} &= \frac{C_{1111}}{C_{1111}^2 - C_{1122}^2} \\ D_{1122} &= \frac{-C_{1122}}{C_{1111}^2 - C_{1122}^2} \\ D_{1212} &= \frac{1}{C_{1212}} \end{aligned} \tag{A2.4}$$

Let D_{ijkl0} and C_{ijkl0} denote D_{ijkl} and C_{ijkl} for the unperforated solid under plane strain. They are given as follows:

$$D_{11110} = \frac{1}{E_0}, \quad D_{11220} = -\frac{\nu_0}{E_0}, \quad D_{12120} = \frac{1+\nu_0}{E_0} \tag{A2.5}$$

$$C_{11110} = \frac{E_0}{1-\nu_0^2}, \quad C_{11220} = -\nu_0 C_{11110}, \quad C_{12120} = \frac{E_0}{1+\nu_0} \tag{A2.6}$$

$$E_0 = \frac{E}{1-\nu^2}, \quad \nu_0 = \frac{\nu}{1-\nu} \tag{A2.7}$$

where E, ν are Young's moduluds and Poisson's ratio of the material under plane stress, and E_0, ν_0 denote their equivalent values under plane strain.

Values of C_{1111}/C_{11110} $(= f_1)$, C_{1122}/C_{11220} $(= f_2)$ and C_{1212}/C_{12120} $(= f_3)$ of this problem for $\nu = 0.3$ were given by Nemat-Nasser et al. in a previous paper [21], using the notation C^*_{2222}/C_{2222}, C^*_{2233}/C_{2233} and μ^*/μ, respectively.

Eqns. (A2.4) and (A2.6) enable us to calculate D_{ijkl} from f_1, f_2 and f_3 by the relations

$$D_{1111} = \frac{1}{E_0}\frac{(1-\nu_0^2)f_1}{f_1^2-f_2^2}$$

$$D_{1122} = -\frac{1}{E_0}\frac{\nu_0(1-\nu_0^2)f_2}{f_1^2-f_2^2} \tag{A2.8}$$

$$D_{1212} = \frac{1}{E_0}\frac{1+\nu_0}{f_3}$$

and the obtained values of $E_0 D_{ijkl}$ for $\nu = 0.3$ are given in Table A2-1.

Now we rotate the coordinate axes by $\pi/4$, and denote all quantities in the rotated system of coordinates by superimposed star. Then, the following equations determine D^*_{ijkl} from D_{ijkl}:

$$D^*_{1111} = D^*_{2222} = \frac{D_{1111} + D_{1122} + D_{1212}}{2}$$

$$D^*_{1122} = D^*_{2211} = \frac{D_{1111} + D_{1122} - D_{1212}}{2} \qquad \text{(A2.10)}$$

$$D^*_{1212} = D_{1111} - D_{1122}$$

The modulus reduction factor C_x for a zig-zag array of holes is given by $1/E_0 D^*_{1111}$. The obtained values are in close agreement with those from the direct analysis [20], as shown in Table A2-1.

Table A1-1.

Variation of $F_I(1,0)$ with various M for $c/a \to \infty$, $\ell/a = 0.4$.

M	$F_I(1,0)$
3	0.210
4	0.211
5	0.213
6	0.214
7	0.214
8	0.214
9	0.215
10	0.214
11	0.215
12	0.215

AD-A182 771 FLOW AND FAILURE OF ROCKS CONCRETE AND OTHER GEOMATERIALS(U) CALIFORNIA UNIV SAN DIEGO LA JOLLA DEPT OF APPLIED MECHANICS A S NEMAT-NASSER NOV 86 2/2

UNCLASSIFIED AFOSR-TR-87-0890 AFOSR-86-0035 F/G 8/7 NL

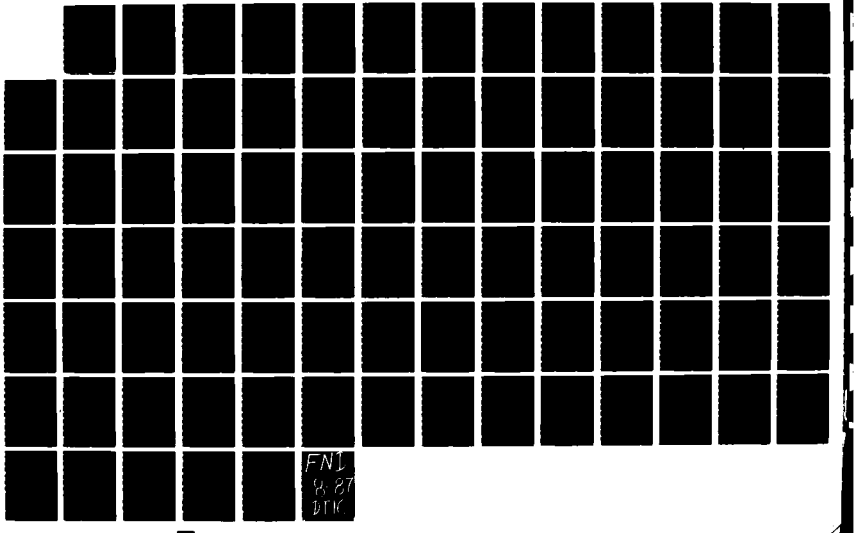

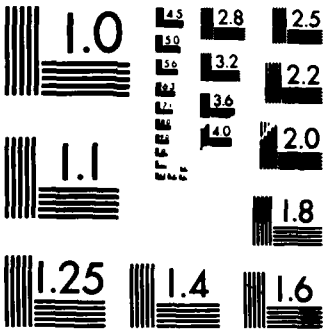

MICROCOPY RESOLUTION TEST CHART
NATIONAL BUREAU OF STANDARDS-1963-A

Table A1-2.

$F_I(1,0)$, C_x and C_x for b/c=0.5, c/a=5, ℓ/a=2, M=7, where N_{eq} (number of equations) $= M + 2(N_1+N_2)$ (plane strain, $\nu = 0.3$).

M	N_1	N_2	N_{eq}	$F_I(1,0)$	C_x	C_y
7	3	4	21	0.0343	0.908	0.550
7	4	4	23	0.0346	0.911	0.560
7	5	4	25	0.0338	0.891	0.484
7	5	6	29	0.0345	0.909	0.551
7	6	6	31	0.0345	0.909	0.552
7	7	6	33	0.0345	0.908	0.548
7	7	8	37	0.0345	0.909	0.551
7	8	8	39	0.0345	0.909	0.551
7	9	8	41	0.0345	0.908	0.551

Table A2-1. Comparison of $C_x = E_x/E_0$ for b/c = 1 from Refs. [20] and [21] ($\nu = 0.3$).

f_H	Doubly periodical holes			C_x for Zig-zag holes	
	E_0D_{1111}	$-E_0D_{1122}$	E_0D_{1212}	$\frac{1}{E_0D^*_{1111}}$	Ref. [20]
0.05	1.156	0.477	1.650	0.859	0.857
0.10	1.297	0.510	1.944	0.732	0.728
0.15	1.455	0.538	2.327	0.617	0.612
0.20	1.621	0.564	2.823	0.515	0.509
0.25	1.808	0.583	3.501	0.423	0.419
0.30	2.018	0.602	4.396	0.344	0.341
0.35					0.277
0.40	2.492	0.629	7.141	0.222	0.225
0.45					0.186
0.50	3.195	0.661	12.110	0.137	0.160

Figure captions

Fig. 1 Infinite solid with zig-zag periodic array of holes and cracks.

Fig. 2 Unit rectangular region and notation of geometric quantities.

Fig. 3-1 Equilateral triangular array of holes and cracks, $b/c = 0.577$.

Fig. 3-2 Square array of holes and cracks, $b/c = 1$.

Fig. 4-1 $F_I(1,0)$ and $F_I(1, 0.01)$ for $b/c = 0.577$.

Fig. 4-2 $F_I(1,0)$ and $F_I(1, 0.01)$ for $b/c = 1$.

Fig. 4-3 $F_I(1,0)$ and $F_I(1, 0.01)$ for $b/c = 1/0.8$.

Fig. 5-1 Relation between $\tilde{\sigma}$ and L for uniaxial compression, $b/c = 0.577$.

Fig. 5-2 Relation between $\tilde{\sigma}$ and L for uniaxial compression, $b/c = 1/0.8$.

Fig. 6-1 Relation between L_{max} and b/c for uniaxial compression.

Fig. 6-2 Relation between L_{max} and c/a for uniaxial compression.

Fig. 6-3 Relation between L_{max} and b/a for uniaxial compression.

Fig. 7 Relation between L_{max} and σ_2/σ_1 for biaxial compression, $b/c = 0.577$.

Fig. 8-1 C_x and C_y for $b/c = 0.577$.

Fig. 8-2 C_x and C_y for $b/c = 1$.

Fig. 8-3 C_x and C_y for $b/c = 1/0.8$.

Fig. 9 Relation between C_x and f_H for zig-zag holes with cracks, $L = 1.5$.

Fig. 10 Relation between C_x and f_H for zig-zag holes without cracks. $(L = 0)$.

Fig. 11 Relation between C_x and f_H for $b/c = 0.577$ and 1.

Fig. 12 Stress-strain curves for uniaxial compression, $b/c = 1/0.8$.

Fig. 13 Relation between C_y and f_H for $L = 1.5$.

Fig. A1-1 Geometry of a circular hole with edge cracks.

Fig. A1-2 Subdivision of crack for numerical evaluation of weighting function.

NOMENCLATURE

x, y	Cartesian coordinates
z	complex coordinate = $x + iy$
$2b$, $2c$	horizontal and vertical spacings of holes
a	hole radius
f_H	initial porosity = $\frac{\pi a^2}{2bc}$
ℓ	crack length
L	normalized crack length = $\frac{\ell}{a}$
L_{max}	maximum normalized crack length under uniaxial compression
E	Young's modulus of material
ν	Poisson's ratio of material
κ	$\kappa = \frac{3 - \nu}{1 + \nu}$ (plane stress), $= 3 - 4\nu$ (plane strain)
G	shear modulus = $\frac{E}{2(1+\nu)}$
E_0	$E_0 = E$ (plane stress), $E_0 = \frac{E}{1 - \nu^2}$ (plane strain)
E_x	Young's modulus of cracked porous solid; compression in the x-direction
E_y	Young's modulus of cracked porous solid; tension in the y-direction
C_x	modulus reduction factor in the x-direction = $\frac{E_x}{E_0}$
C_y	modulus reduction factor in the y-direction = $\frac{E_y}{E_0}$
σ_x, σ_y, τ_{xy}	stress components
σ_1, σ_2	applied stresses at infinity
σ_0	positive reference stress
λ_1	$-\frac{\sigma_1}{\sigma_0}$

λ_2	$-\frac{\sigma_2}{\sigma_0}$
λ	$\frac{\lambda_2}{\lambda_1}$ $(\lambda_1 \neq 0)$
P_x, P_y	resultant force components
u, v	displacement components
u_m	mean value of u along $\overline{EF}$
v_m	mean value of v along $\overline{FG}$
$\phi(z)$, $\psi(z)$	complex stress potentials
$q_m(s_m)$	weighting functions of force doublet densities
M	subdivision number for the crack
N_1	number of subdivisions of $\overline{EF}$
N_2	number of subdivisions of $\overline{FG}$
h_1	length of intervals on $\overline{EF} = \frac{c}{2N_1}$
h_2	length of intervals on $\overline{FG} = \frac{b}{N_2}$
K_I	Mode I stress intensity factor
F_I	dimensionless stress intensity factor $= \frac{K_I}{\sigma_0(\pi\ell)^{1/2}}$
K_{Ic}	critical stress intensity factor
$\bar{\sigma}$	normalized compressive stress $= \frac{-\sigma_1(\pi a)^{1/2}}{K_{Ic}}$
$\bar{\varepsilon}$	normalized compressive strain $= \frac{-\sigma_1(\pi a)^{1/2}}{K_{Ic}} \frac{E_0}{E_x}$

Figure 1

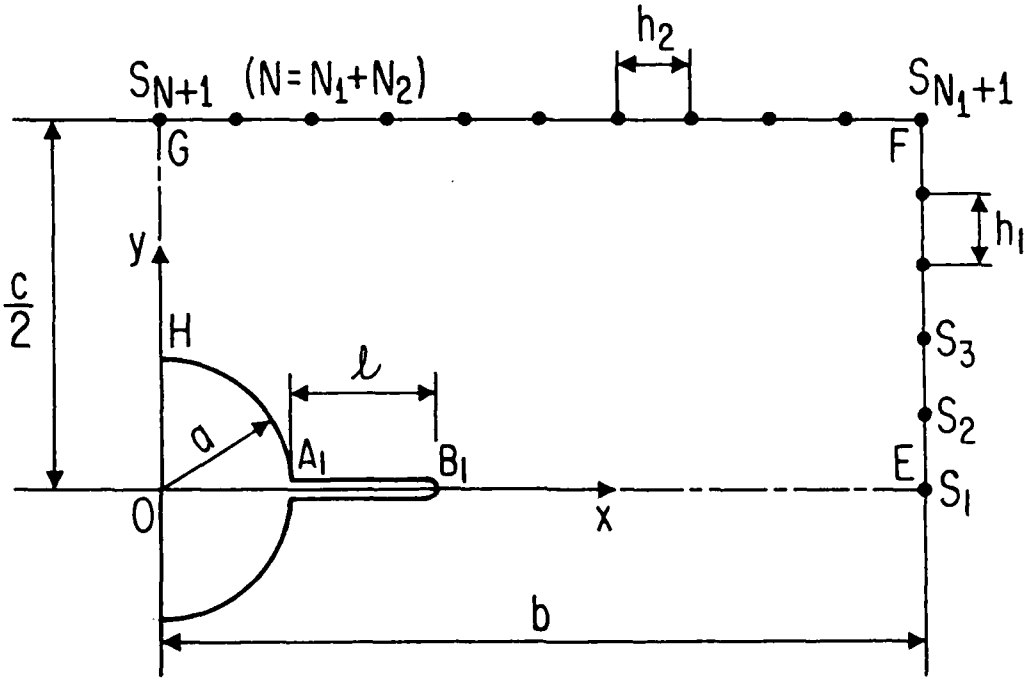

Figure 2

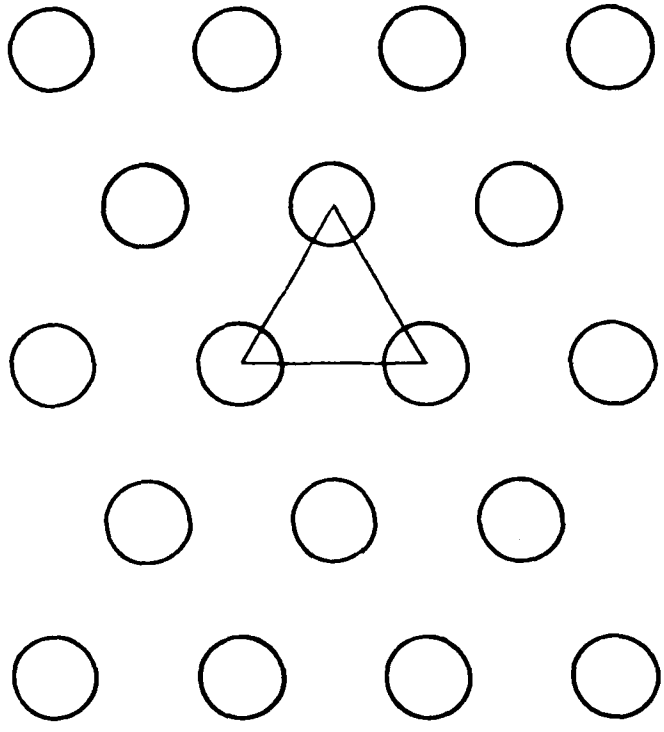

Figure 3-1

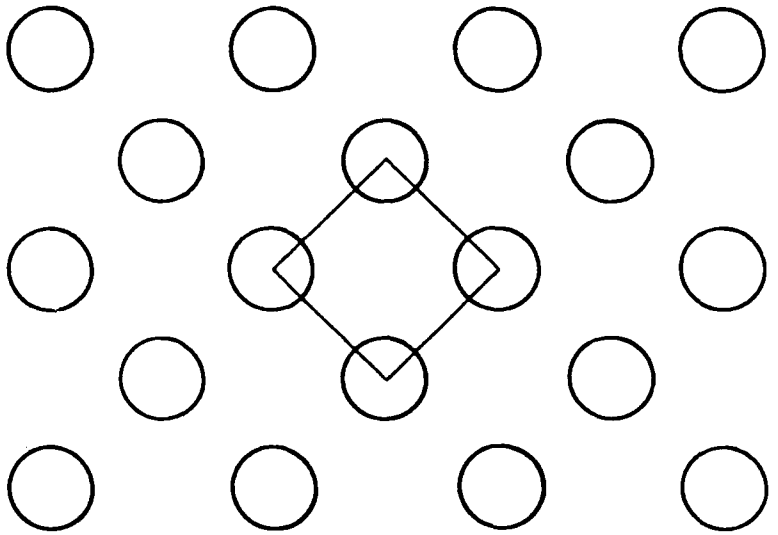

Figure 3-2

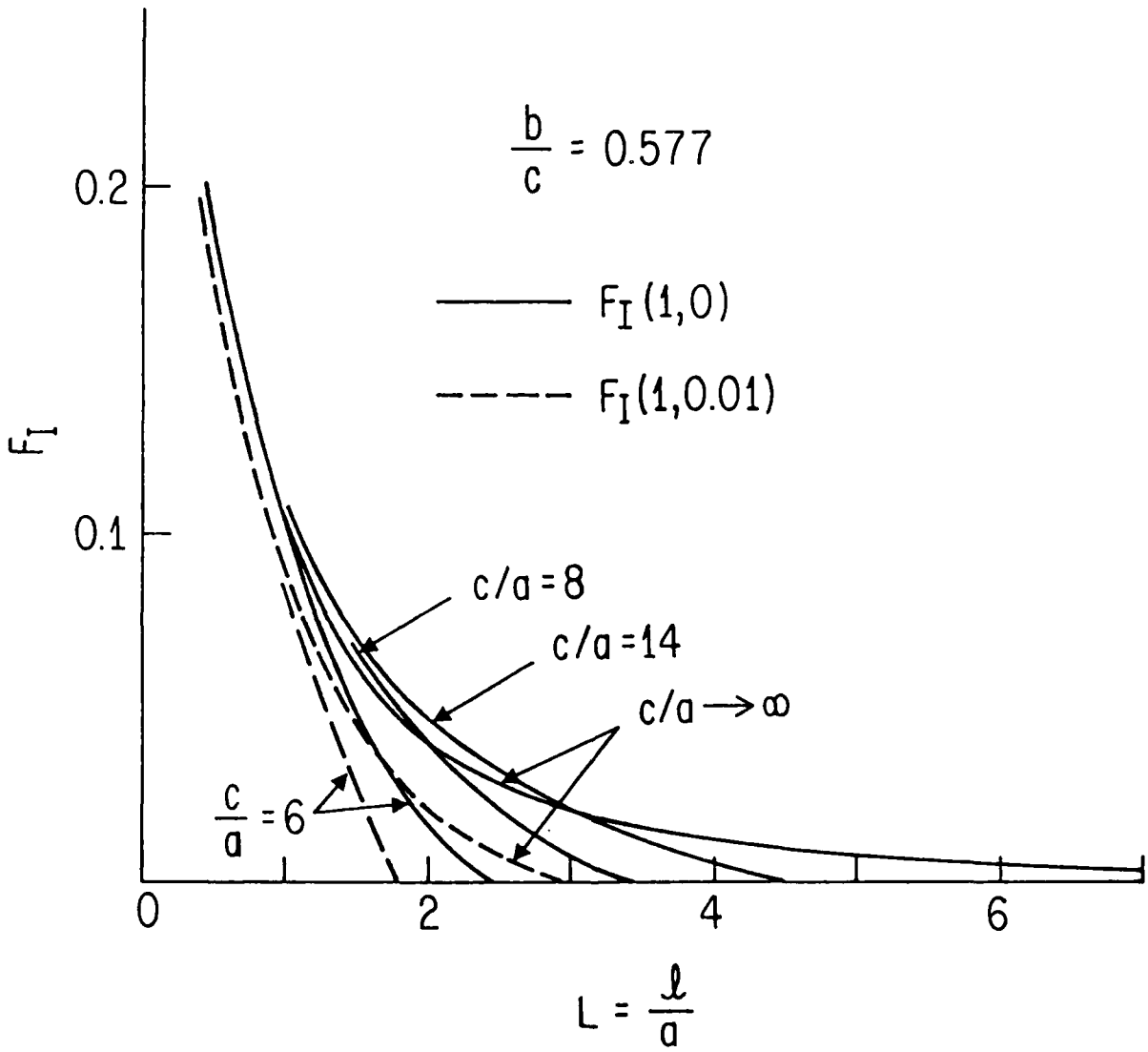

Figure 4-1

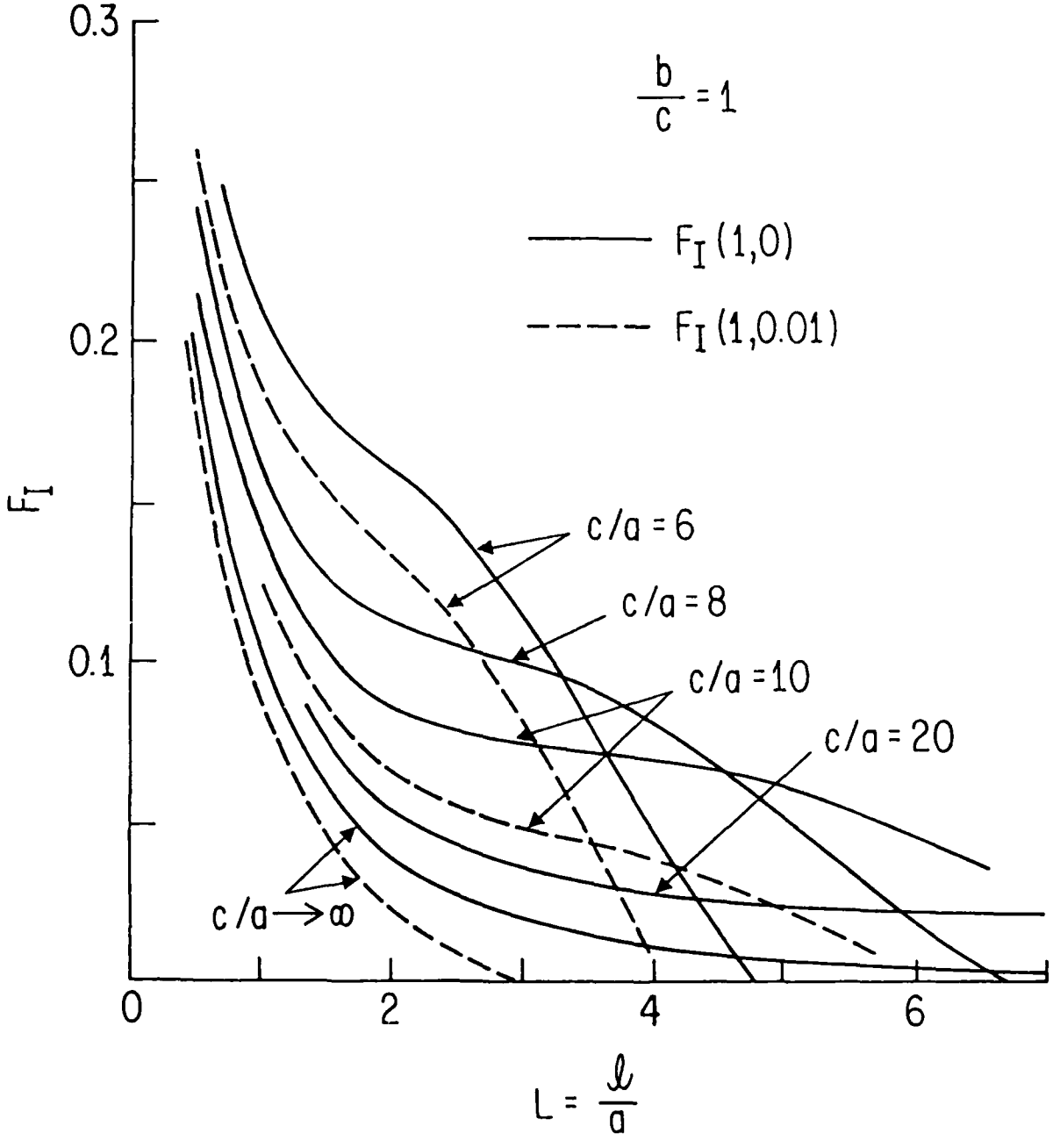
0.3
0.2
0.1
F_I
$\frac{b}{c} = 1$
$F_I(1,0)$
$F_I(1,0.01)$
c/a = 6
c/a = 8
c/a = 10
c/a = 20
c/a → ∞
0
2
4
6
$L = \frac{\ell}{a}$

Figure 4-2

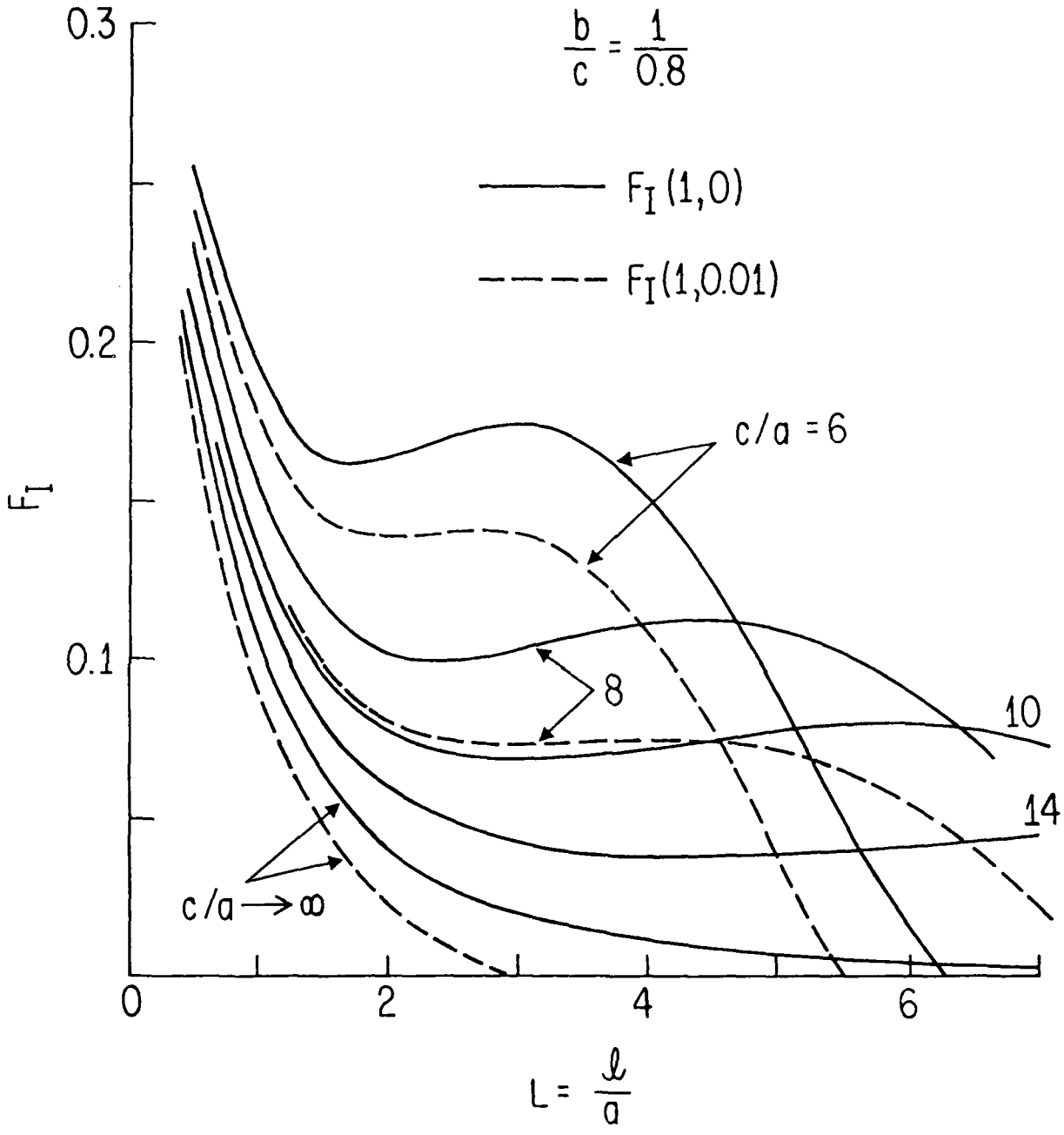

Figure 4-3

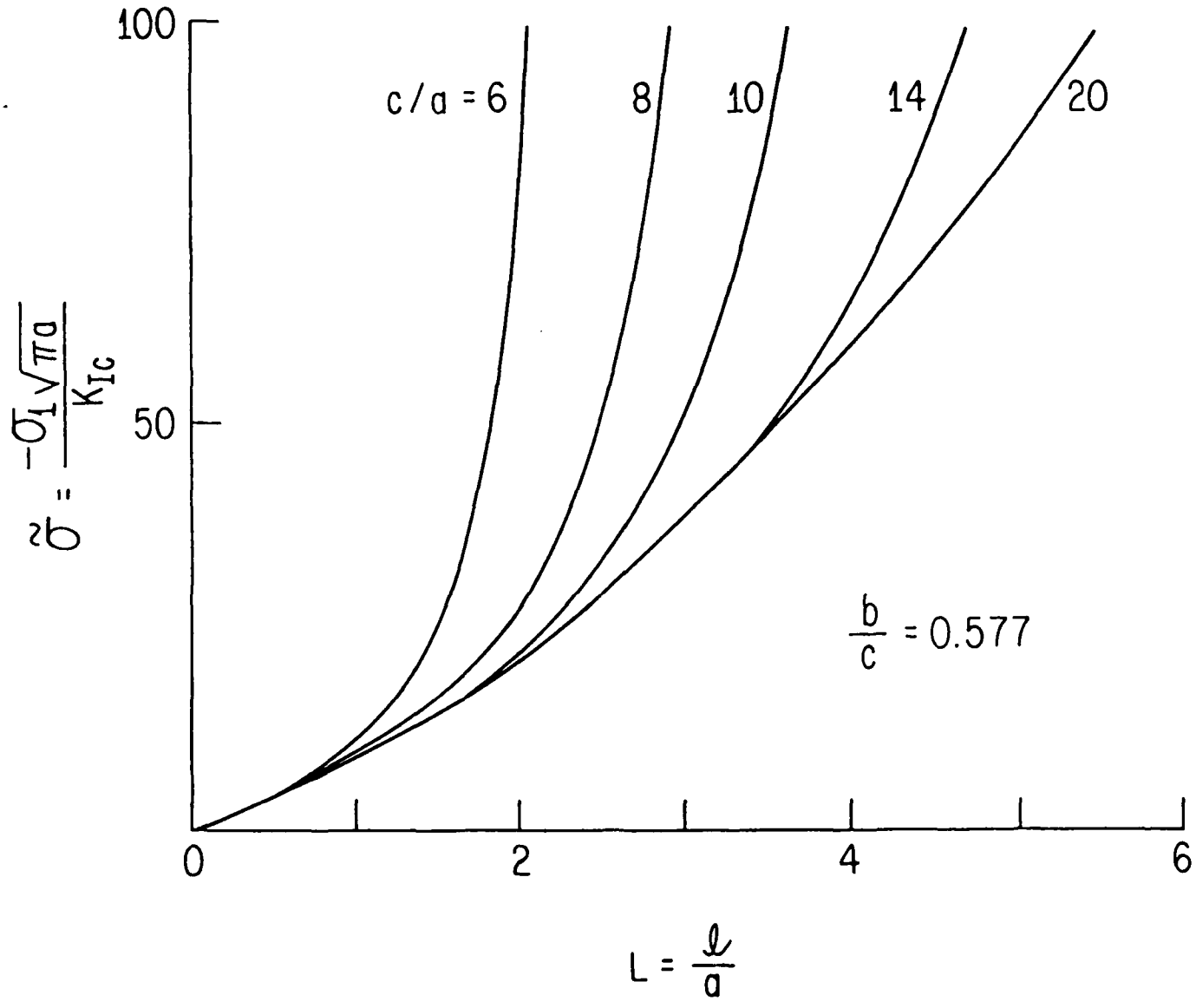
100
50
c/a = 6
8
10
14
20
$\sigma = \frac{-\sigma_1\sqrt{\pi a}}{K_{Ic}}$
$\frac{b}{c} = 0.577$
0
2
4
6
$L = \frac{\ell}{a}$

Figure 5-1

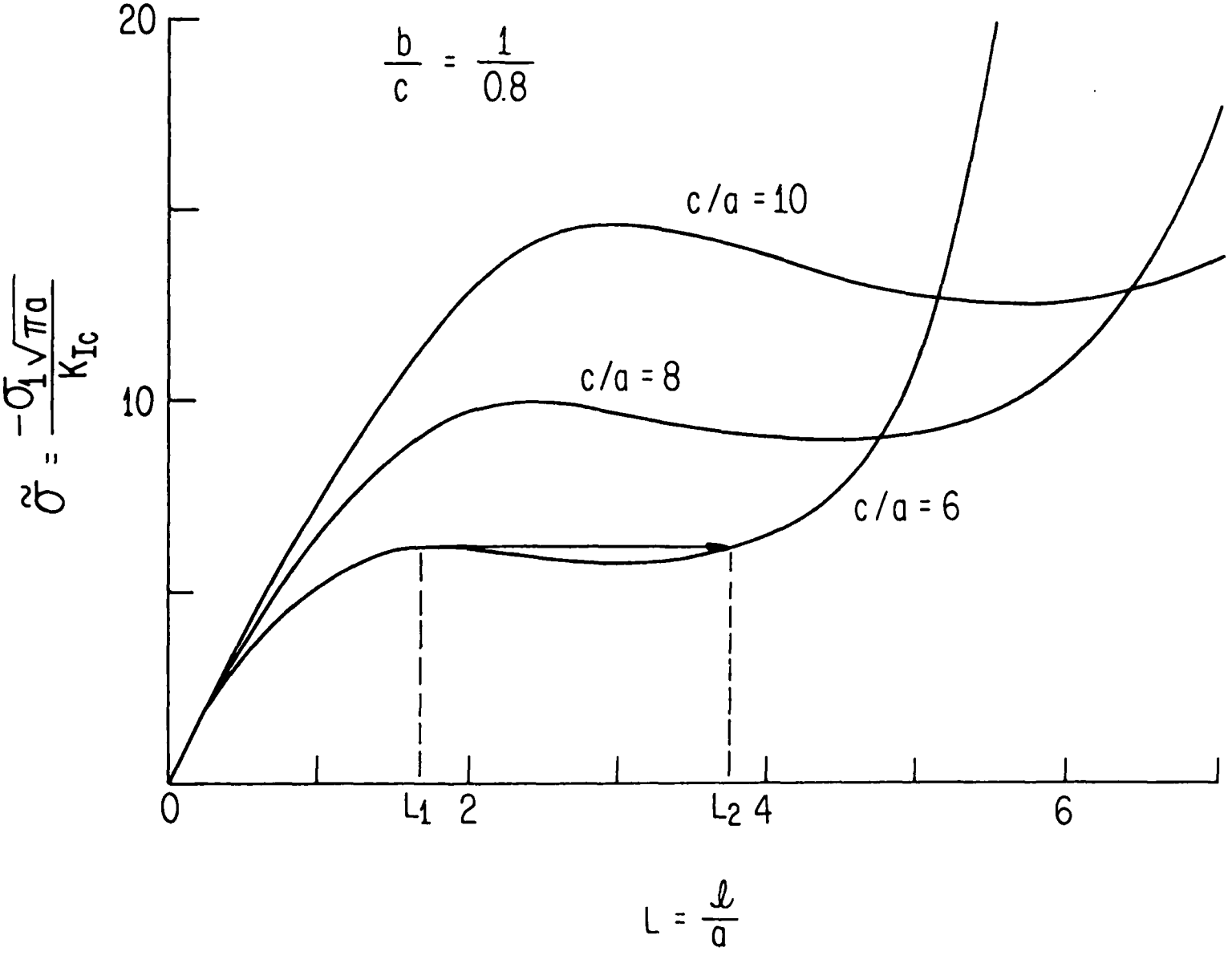
20
10
0
$\frac{b}{c} = \frac{1}{0.8}$
c/a = 10
c/a = 8
c/a = 6
$\sigma = \frac{-\sigma_1\sqrt{\pi a}}{K_{Ic}}$
L_1 2
L_2 4
6
$L = \frac{\ell}{a}$

Figure 5-2

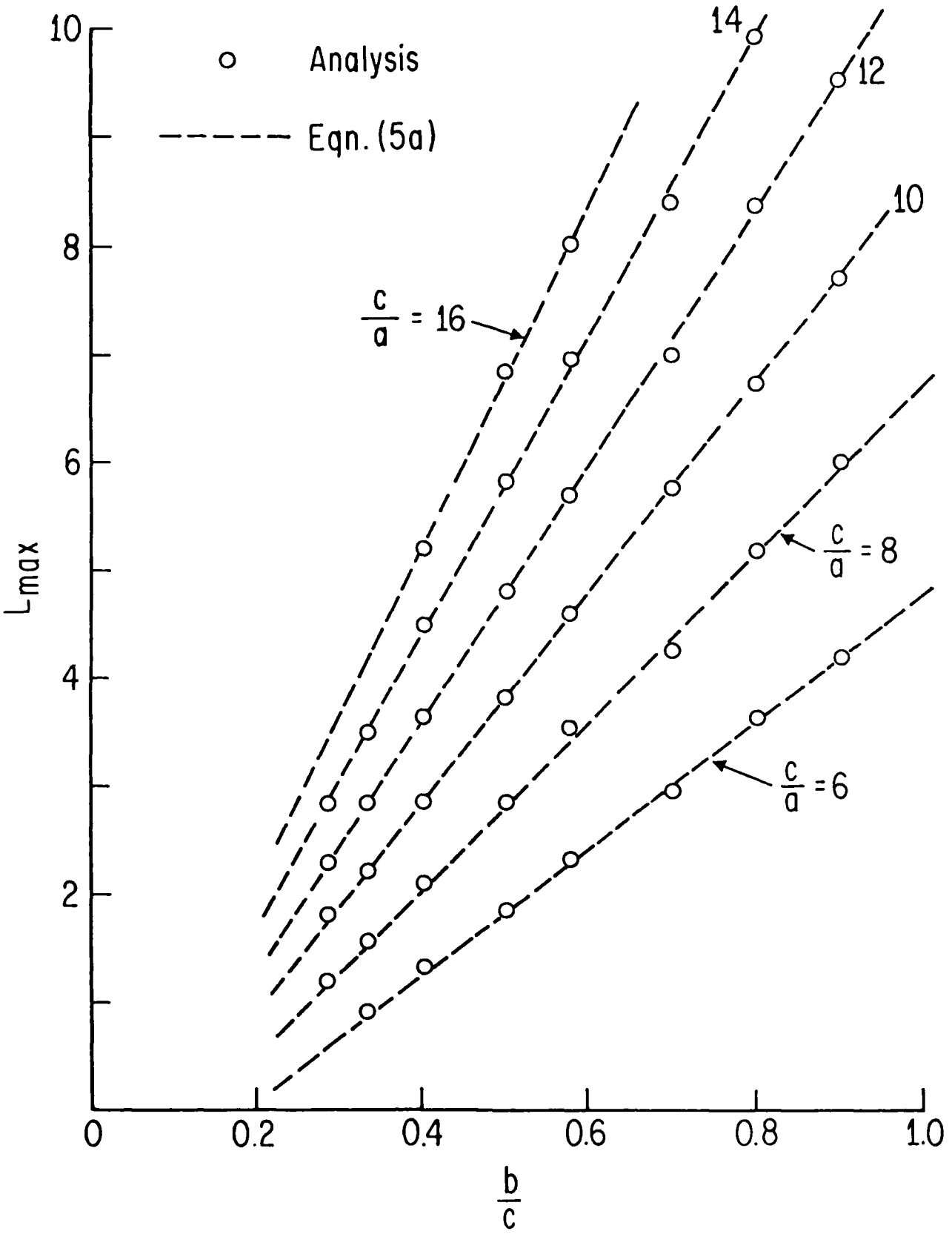
Analysis
Eqn. (5a)
14
12
10
c/a = 16
c/a = 8
c/a = 6
Lmax
b/c
0
0.2
0.4
0.6
0.8
1.0
2
4
6
8
10

Figure 6-1

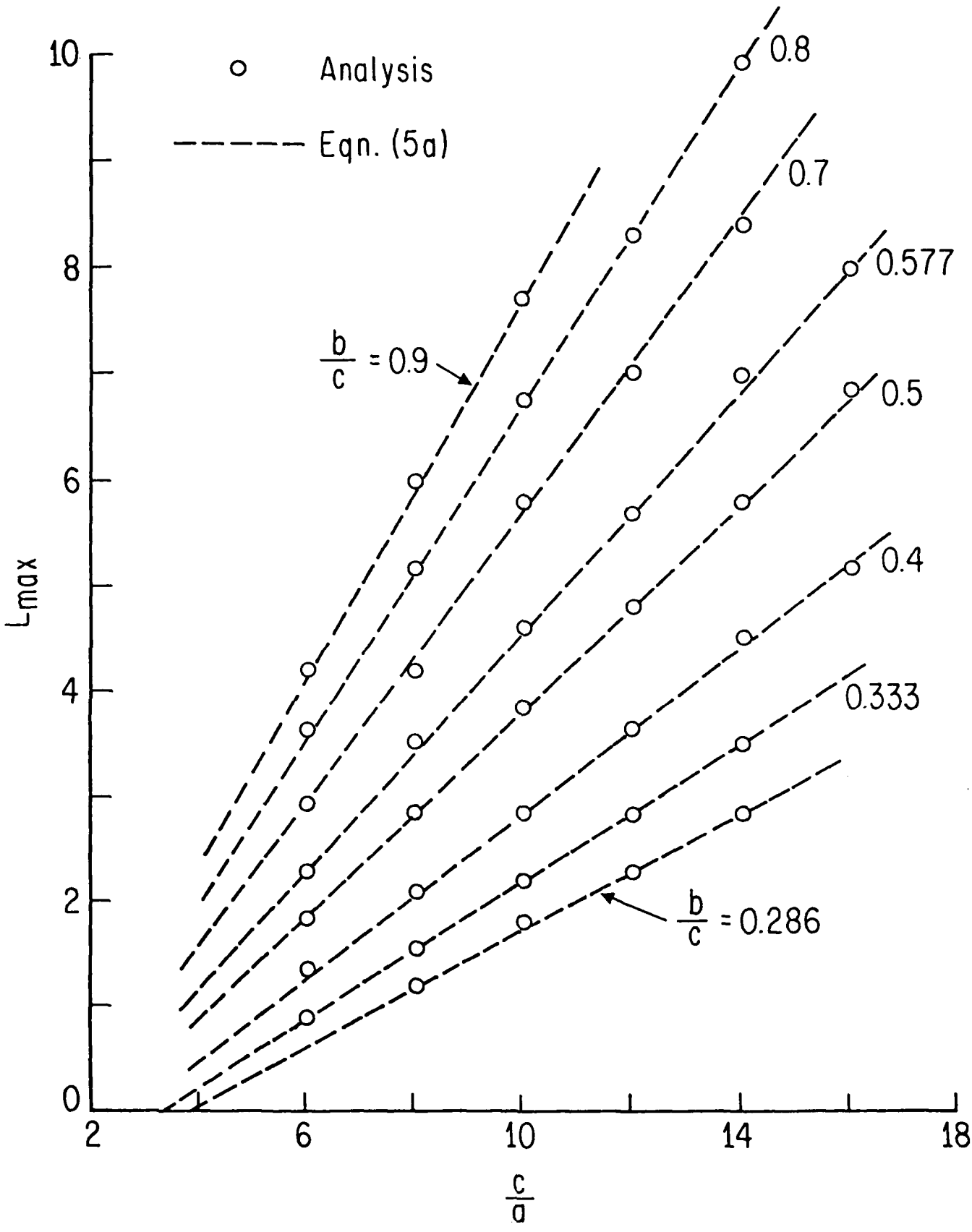
Analysis
Eqn. (5a)
0.8
0.7
0.577
0.5
0.4
0.333
b/c = 0.9
b/c = 0.286
Lmax
c/a
0
2
4
6
8
10
2
6
10
14
18

Figure 6-2

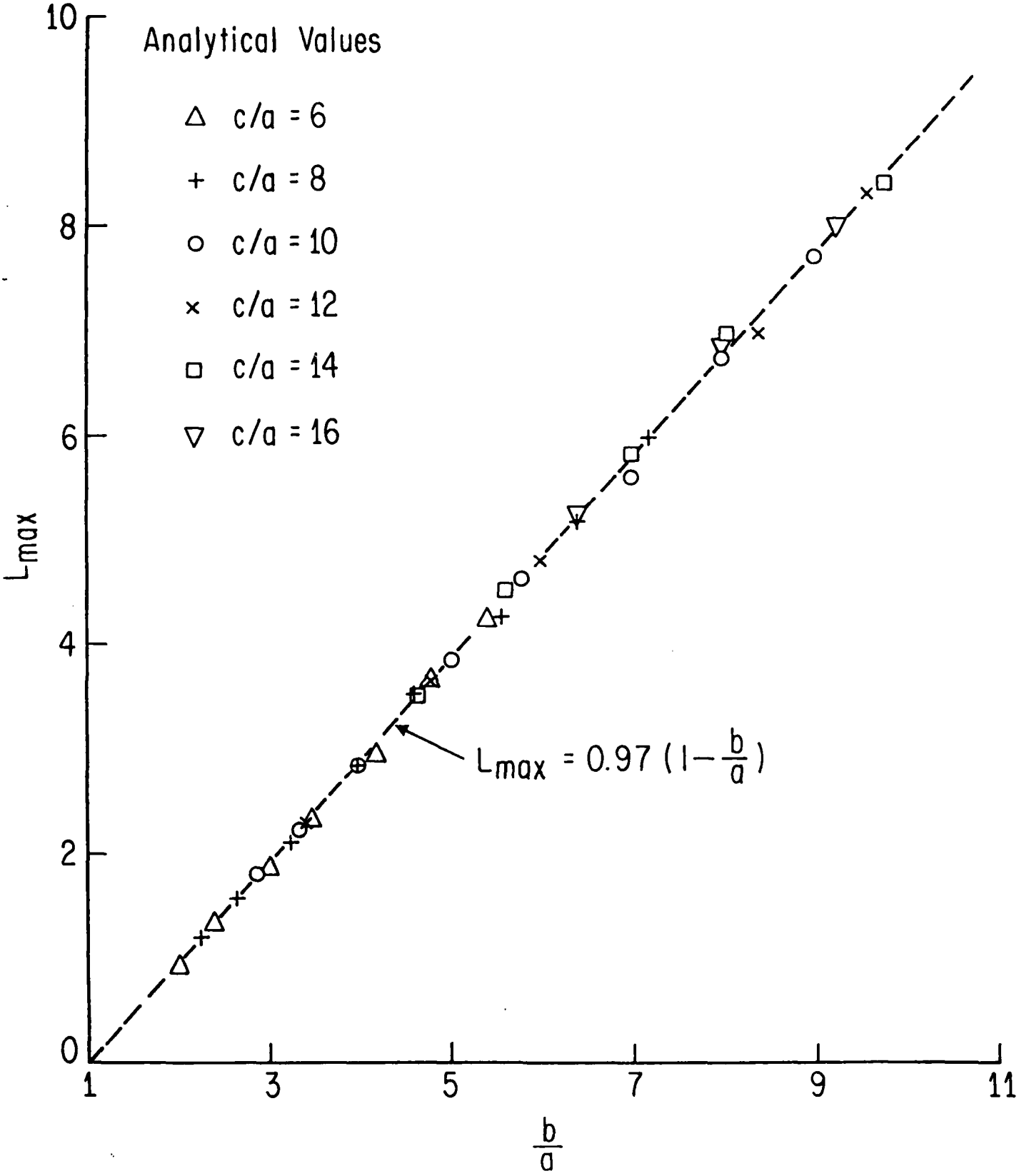
Analytical Values
△ c/a = 6
+ c/a = 8
○ c/a = 10
× c/a = 12
□ c/a = 14
▽ c/a = 16
$L_{max} = 0.97\left(1-\frac{b}{a}\right)$
L_{max}
$\frac{b}{a}$
0
2
4
6
8
10
1
3
5
7
9
11

Figure 6-3

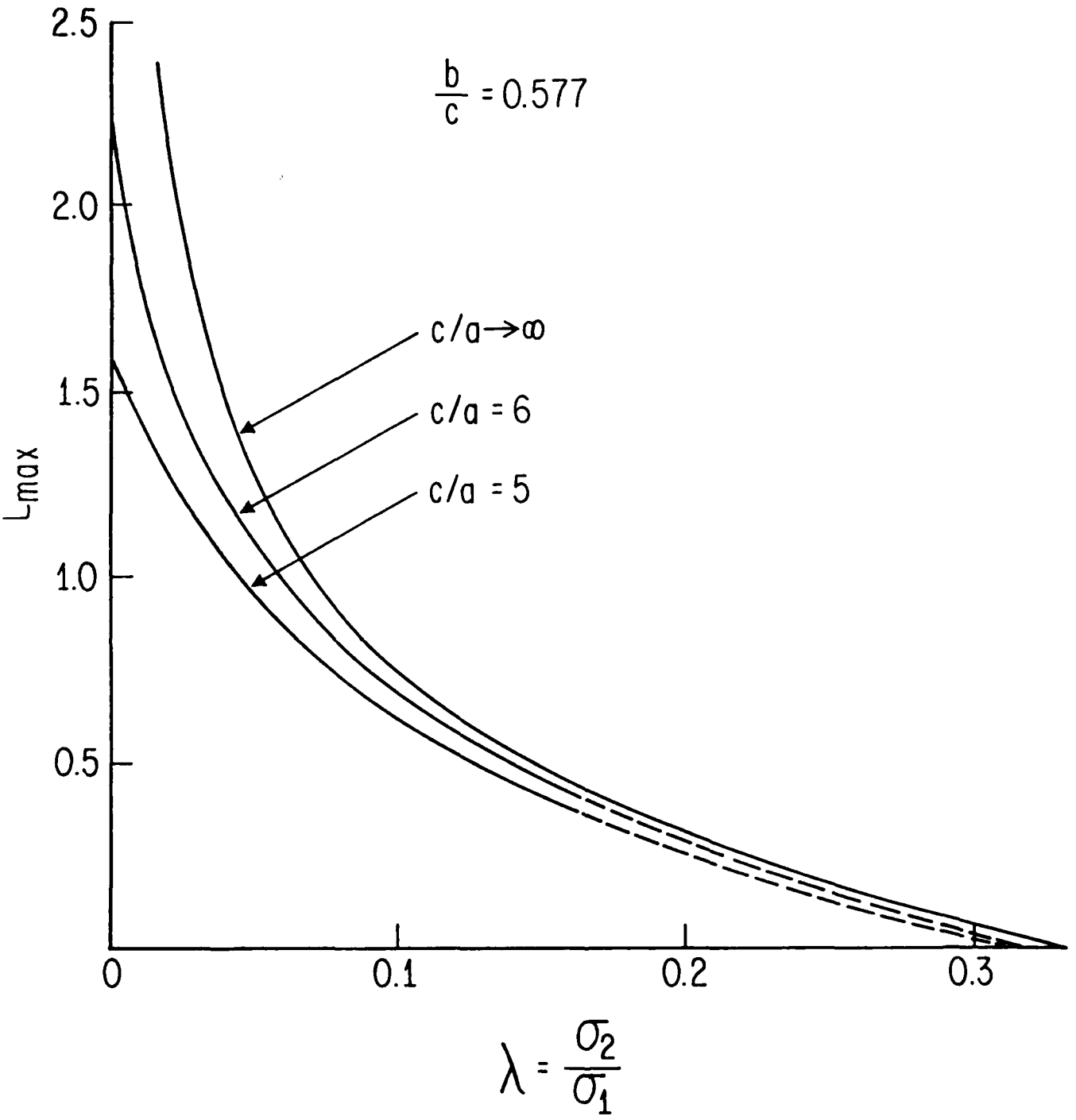
2.5
2.0
1.5
1.0
0.5
0
0.1
0.2
0.3
L_{max}
$\frac{b}{c} = 0.577$
$c/a \to \infty$
$c/a = 6$
$c/a = 5$
$\lambda = \frac{\sigma_2}{\sigma_1}$

Figure 7

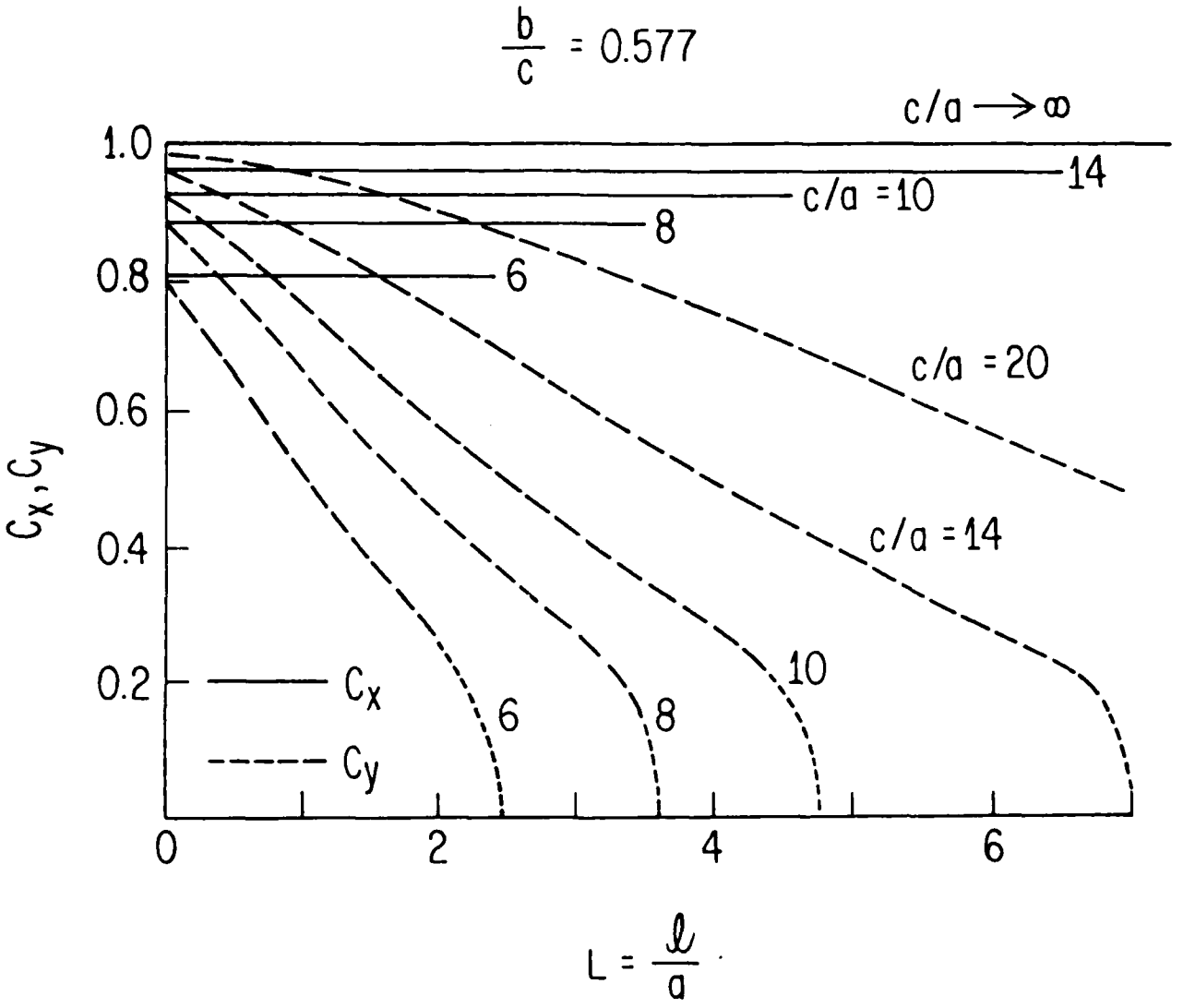
b/c = 0.577
c/a → ∞
14
c/a = 10
8
6
c/a = 20
c/a = 14
10
8
6
1.0
0.8
0.6
0.4
0.2
C_x, C_y
C_x
C_y
0
2
4
6
$L = \frac{\ell}{a}$

Figure 8-1

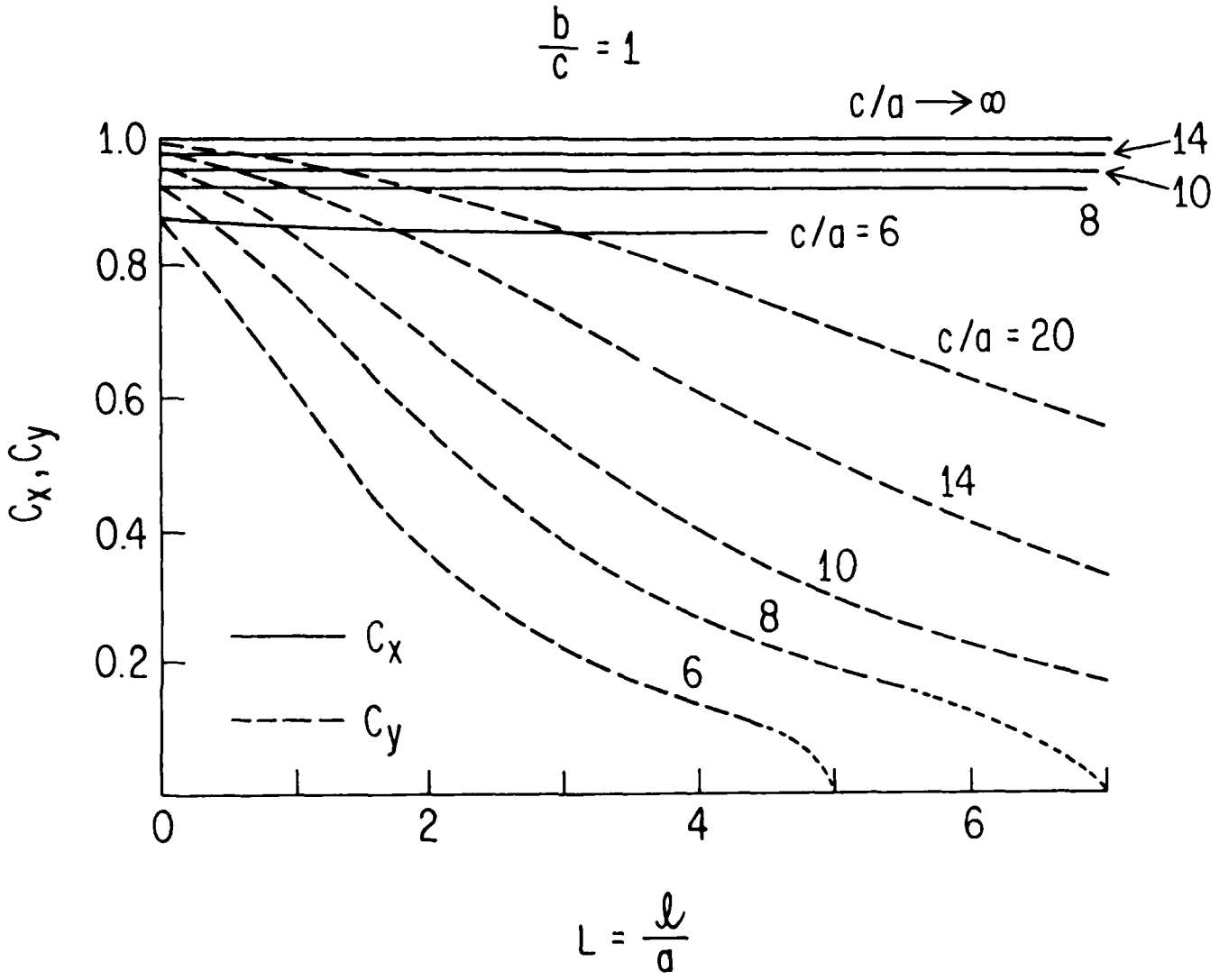
b/c = 1
c/a → ∞
14
10
8
c/a = 6
c/a = 20
14
10
8
6
1.0
0.8
0.6
0.4
0.2
C_x, C_y
C_x
C_y
0
2
4
6
$L = \frac{\ell}{a}$

Figure 8-2

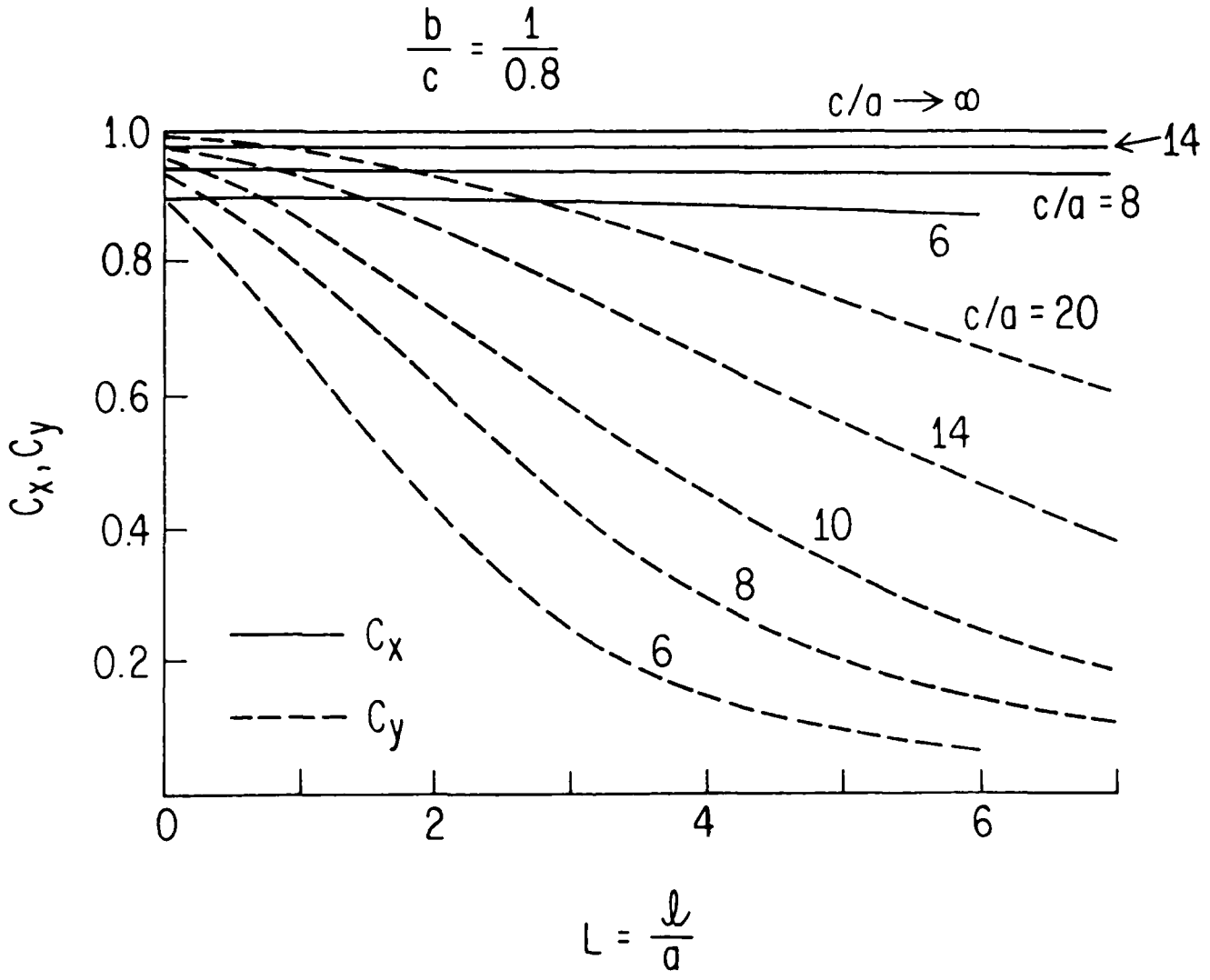

Figure 8-3

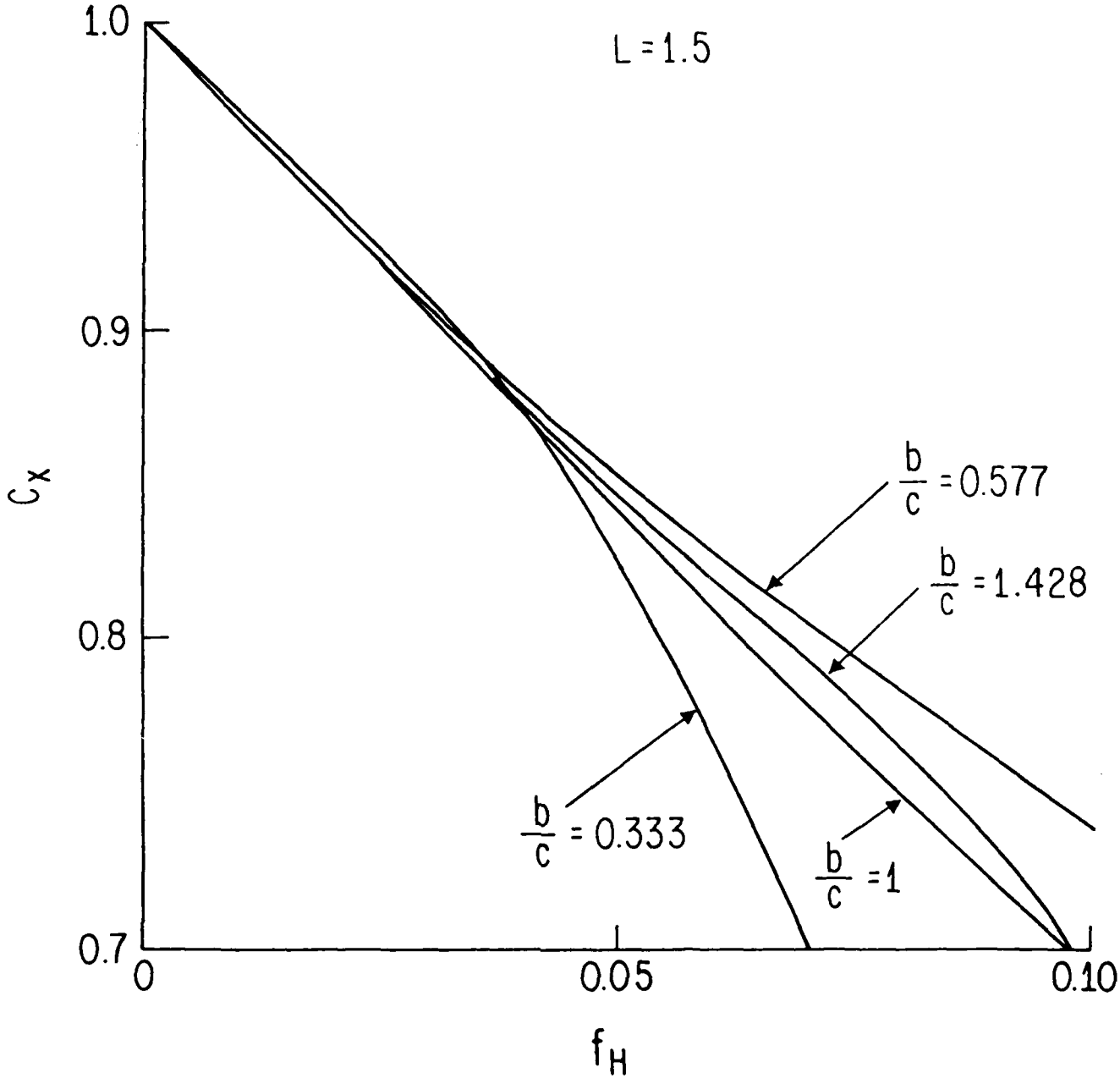
L = 1.5
1.0
0.9
0.8
0.7
C_x
0
0.05
0.10
f_H
$\frac{b}{c} = 0.577$
$\frac{b}{c} = 1.428$
$\frac{b}{c} = 0.333$
$\frac{b}{c} = 1$

Figure 9

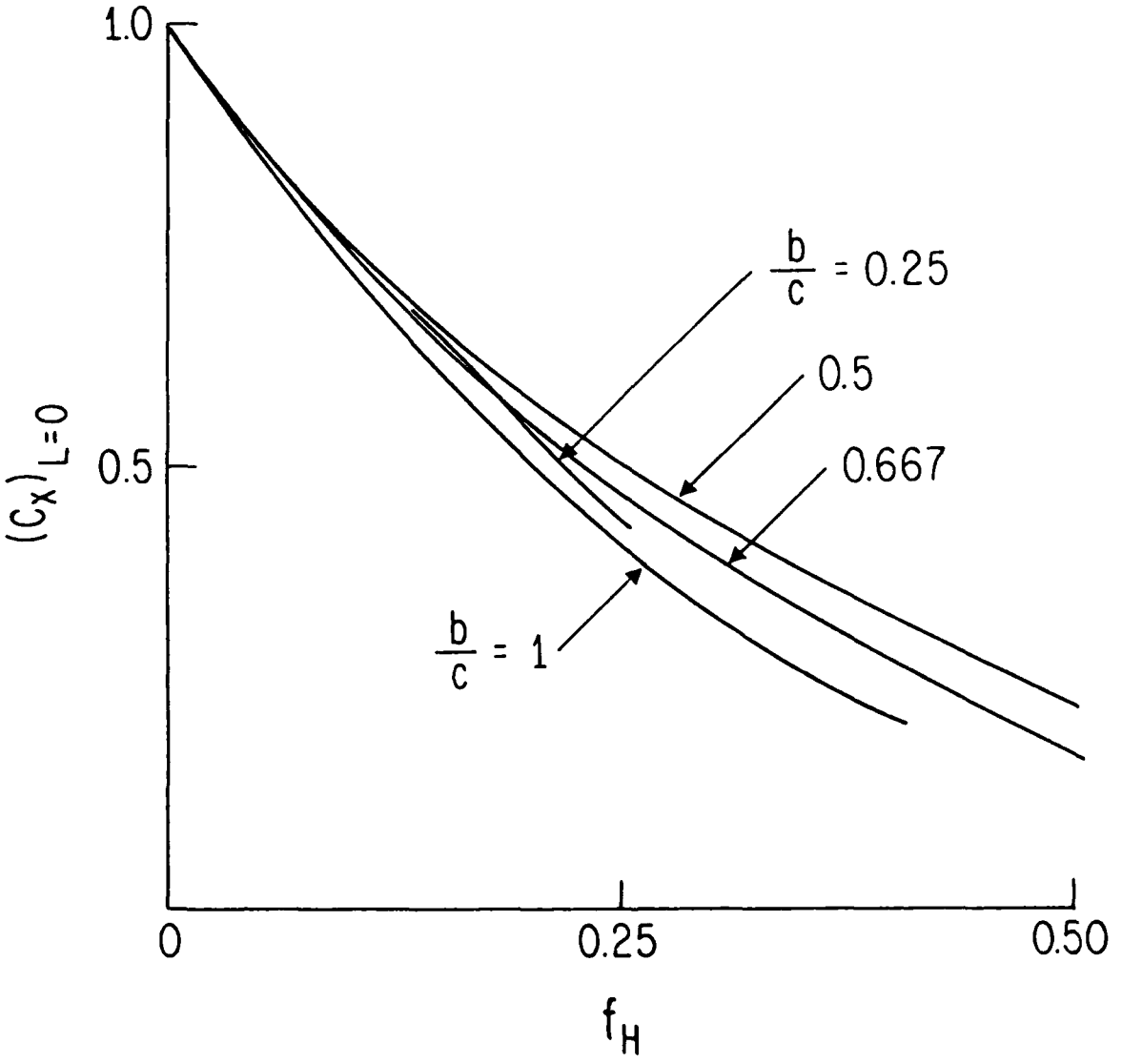

Figure 10

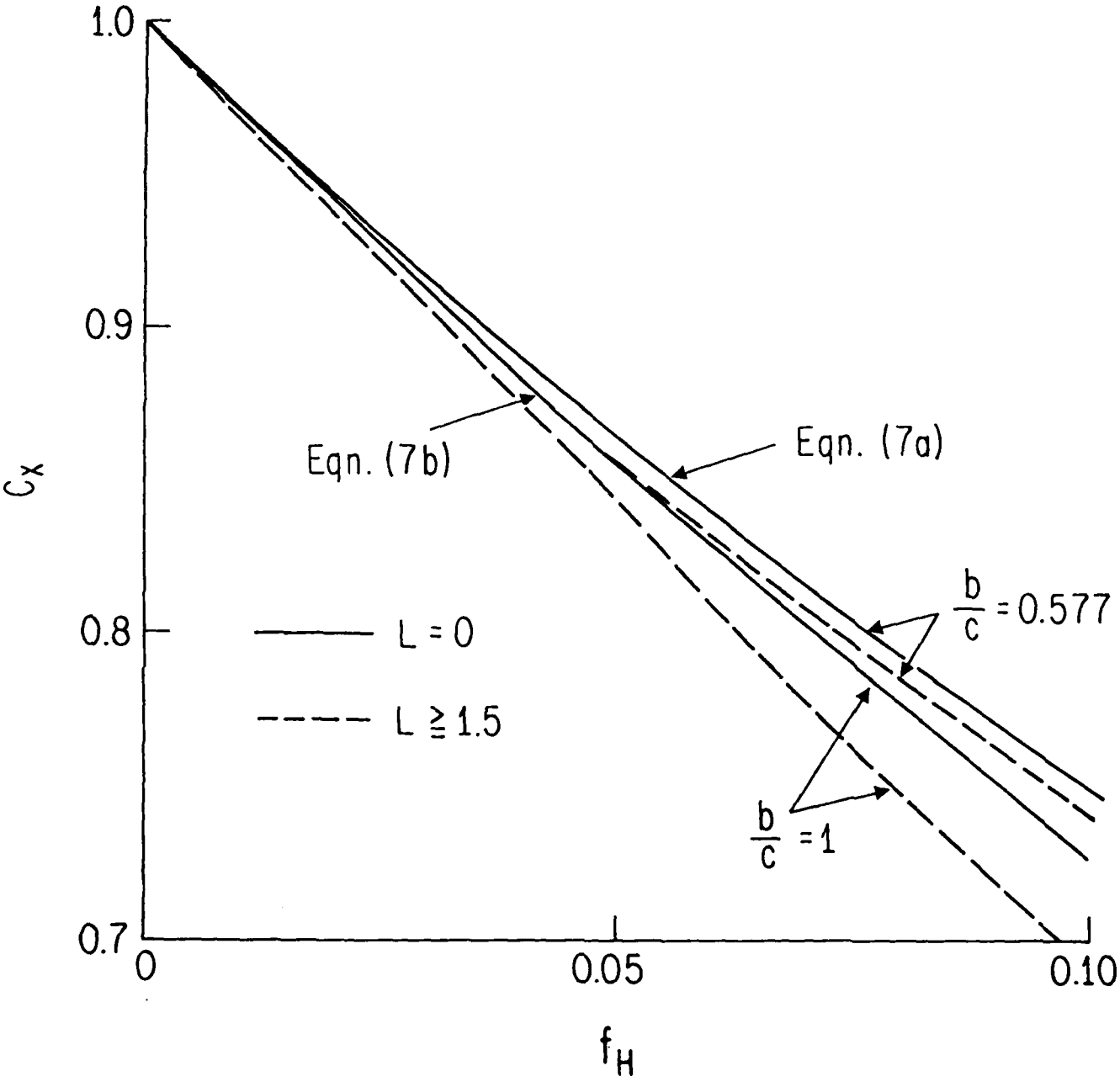
1.0
0.9
0.8
0.7
C_x
Eqn. (7b)
Eqn. (7a)
L = 0
L ≧ 1.5
$\frac{b}{c} = 0.577$
$\frac{b}{c} = 1$
0
0.05
0.10
f_H

Figure 11

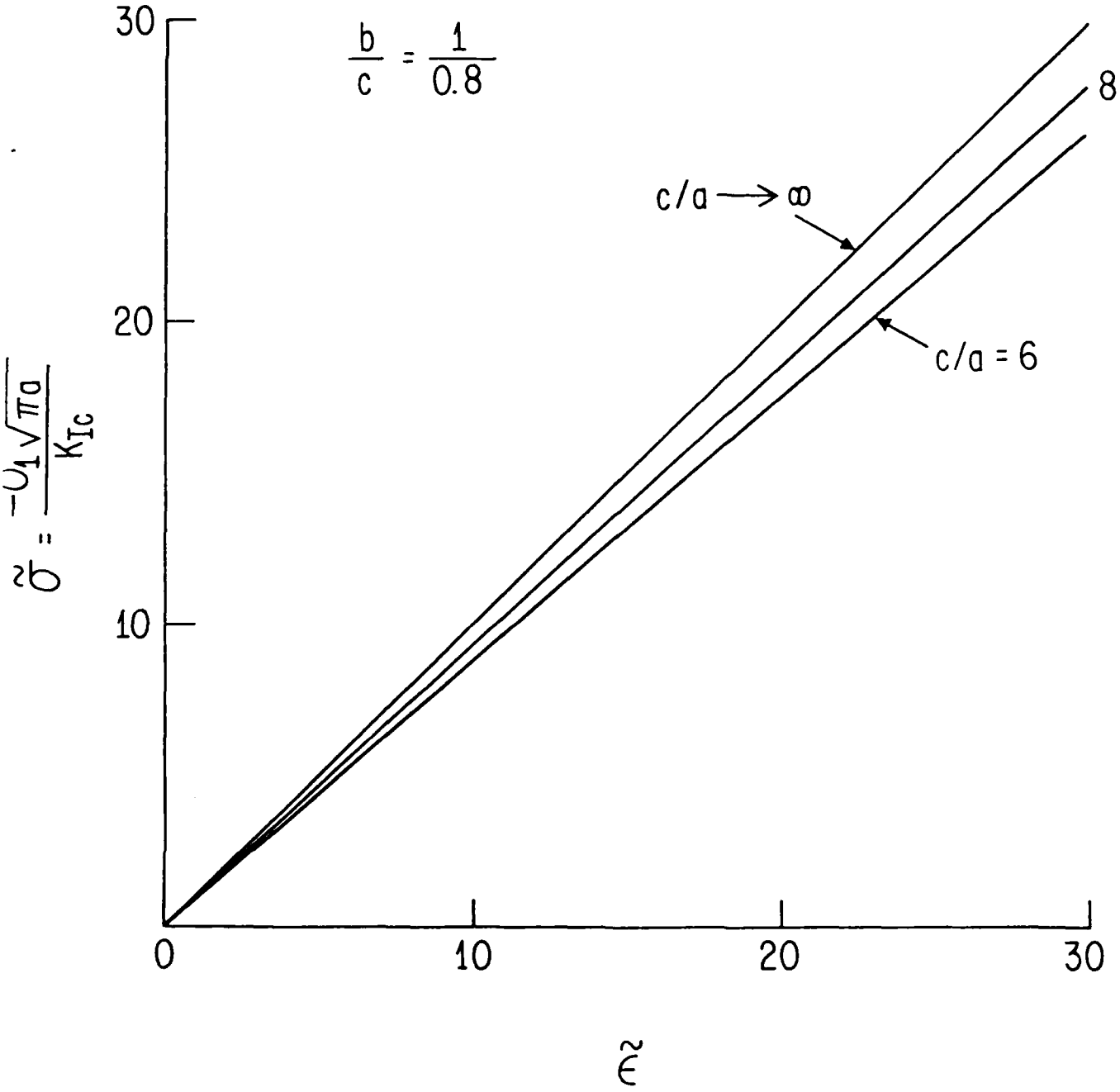
30
20
10
0
10
20
30
$\frac{b}{c} = \frac{1}{0.8}$
8
c/a → ∞
c/a = 6
$\tilde{\sigma} = \frac{-U_1\sqrt{\pi a}}{K_{Ic}}$
$\tilde{\epsilon}$

Figure 12

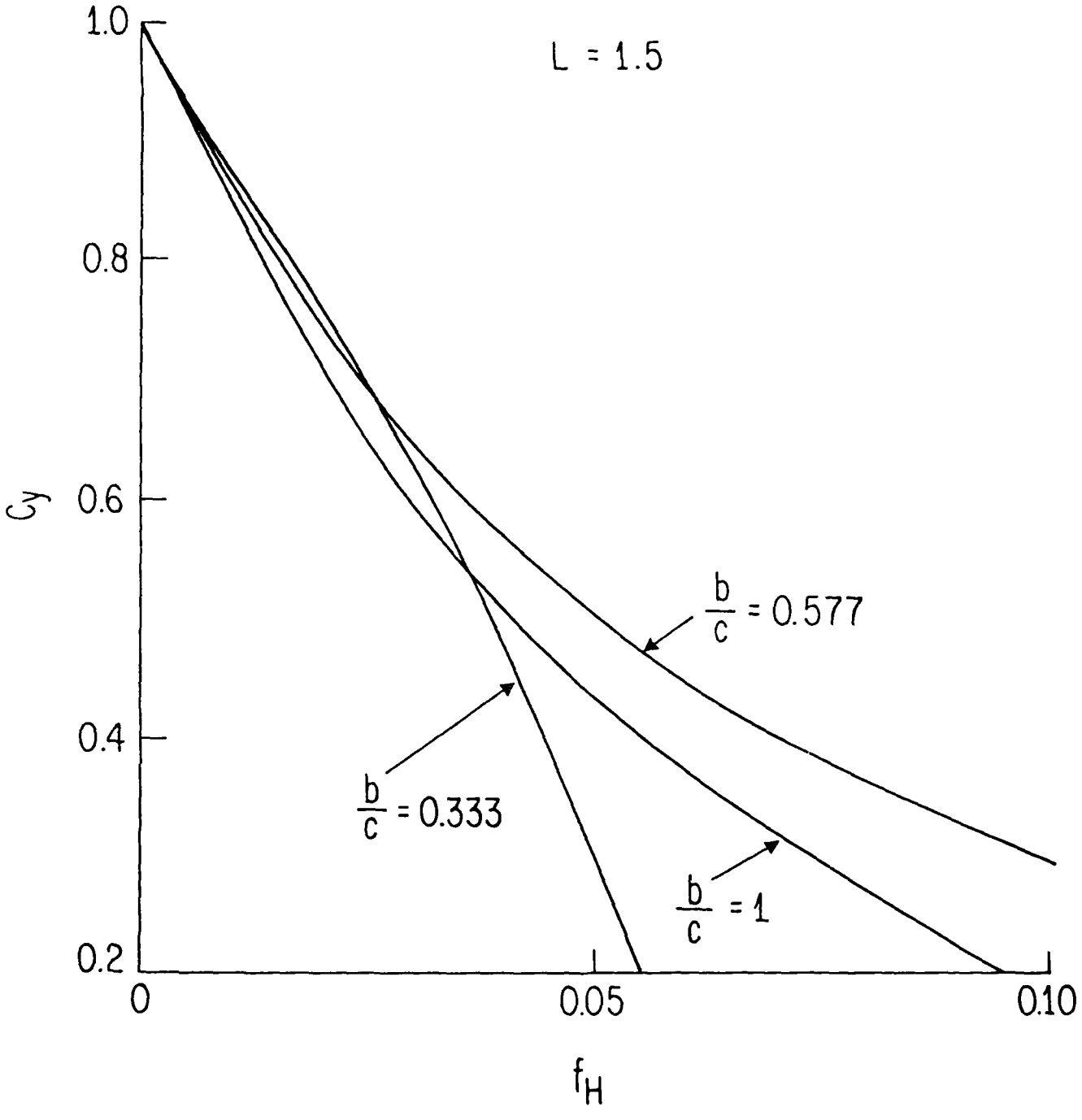
L = 1.5
1.0
0.8
0.6
0.4
0.2
C_y
0
0.05
0.10
f_H
$\frac{b}{c} = 0.577$
$\frac{b}{c} = 0.333$
$\frac{b}{c} = 1$

Figure 13

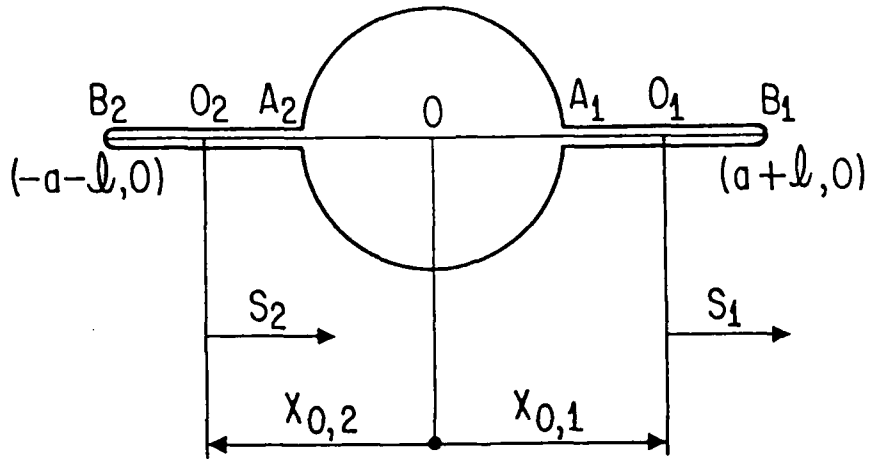

Figure A1-1

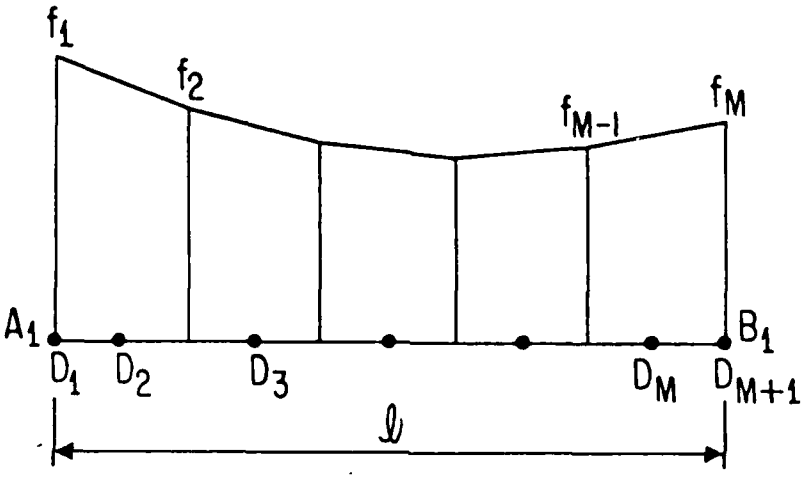

Figure A1-2

CHAPTER IV

A MICROCRACK MODEL OF DILATANCY IN BRITTLE MATERIALS*

by

S. Nemat-Nasser
M. Obata

Table of Contents

*Submitted to: Journal of Applied Mechanics, in press.

CHAPTER IV

A MICROCRACK MODEL OF DILATANCY IN BRITTLE MATERIALS

by

S. Nemat-Nasser* and M. Obata**

ABSTRACT

For a solid containing preexisting flaws, overall nonlinear constitutive relations are developed on the basis of a model which endows a preexisting flaw with frictional and cohesive resistance, and which includes nucleation and growth of tension cracks at the preexisting flaw, as it deforms under the action of an overall compressive load. The preexisting flaws may be randomly distributed or may have an initial preferential distribution. They may be of varying sizes and orientations. Even when the flaws are randomly distributed, their preferential activation, and the nucleation and growth of tension cracks at preferential flaws, render the overall response of the solid highly anisotropic. As a first step toward a more complete constitutive micromechanical modeling, a dilute distribution of preexisting flaws is assumed, rate constitutive relations are developed for loading and unloading, which include hysteresis, dilatancy, and other characteristics observed experimentally in rocks, ceramics, concrete, and similar brittle materials. A number of illustrative examples are worked out, and the results are compared to relevant experimental observations.

---

* Professor of Applied Mechanics and Engineering Sciences, University of California, San Diego, La Jolla, CA 92093

** Postdoctoral Research Fellow, Department of Applied Mechanics and Engineering Sciences, University of California, San Diego, La Jolla, CA 92093

1. INTRODUCTION

Ceramics, rocks, concrete, and similar brittle materials have a highly nonlinear and complex overall response to applied loads. This includes load-induced anisotropy, hysteresis, dilatancy, and strongly path-dependent stress-strain relations. Such complex behavior, to a great extent, stems from the activation of microdefects which are commonly present in these materials. The defects may be preexisting cracks, cavities, soft or hard inclusions, etc. These defects serve as stress concentrators and therefore they locally change the state of stress, leading to the formation of tension cracks, even under overall compressive loads. It has been demonstrated experimentally and supported by theoretical models that tension cracks of this kind nucleate and grow in a highly preferential manner and therefore, even when the microdefects are randomly distributed, so that initially the solid is basically isotropic, the response of the solid becomes highly anisotropic and stress-path-dependent as loading continues; see Horii and Nemat-Nasser (1982). The failure modes in compression of solids of this kind have been extensively studied and modeled analytically, as well as illustrated by model experiments; Brace and Bombolakis (1963), McClintock and Walsh (1963), Hoek and Bieniawski (1965), Scholz (1968), Scholz and Kranz (1974), Zoback and Byerlee (1975), Holcomb (1978), Holzhausen (1978), Paterson (1978), Kachanov (1982), Moss and Gupta (1982), Nemat-Nasser and Horii (1982), Kranz (1983), and Horii and Nemat-Nasser (1985a,1986). In particular, it has been shown by Nemat-Nasser and Horii (1982) and Horii and Nemat-Nasser (1985a,1986) that axial splitting, often observed under uniaxial compression, can be explained in terms of a model which considers an isolated preexisting thin straight flaw endowed with frictional and cohesive resistance, which nucleates tension cracks at its tips under the

action of axial compression. The model of a sliding crack with frictional resistance (but without cohesive resistance) has been criticized by some authors (e.g., Holcomb and Stevens, 1980; Janach and Guex, 1980; Dey and Wang, 1981; Costin, 1983) on the grounds that actual electron microscopic observations do not seem to support the presence of such cracks, but rather show a complex pattern of axial tension cracks emanating from a variety of sources. There are, however, a number of reasons which seem to support the usefulness of the basic model for the micromechanical constitutive formulation of the inelastic response and the failure modes of materials of this kind. These include: (1) The criticism of the sliding crack model has been based on qualitative aspects of microscopic observations. (2) Recent data by Sondergeld and Estey (1982) and Yanagidani et al. (1985), suggest that the focal mechanism for stress induced acoustic emission involves double couples and hence shear motion. (3) Recent quantitative stereologic evaluation of SEM analysis of rocks by Wong (1985) shows that the results obtained from the sliding crack model are not in conflict with SEM observations. Furthermore, recognizing the limitations of the model (e.g., two-dimensionality), Wong comments that the agreement between the theoretical prediction and the quantitative microscopy results is quite remarkable. (4) Recently, Scholz et al. (1986) have reexamined Bridgman's ring experiment by subjecting a fully jacketed ring of pyrex glass tightly fitted over a polished and hardened steel rod, to overall hydrostatic pressure, and observed isolated axial cracks growing in a stable manner from interior tiny flaws of no greater than 20μm. Analysis based on Nemat-Nasser and Horii's (1982) sliding crack formulation showed that under the prevailing all-around compressive stresses in this experiment, microflaws of abount 10μm are sufficient to initiate such axial cracks. Scholz et al.

(1986) conclude that "axial cracks can be initiated by tiny flaws and grow stably for long distances under an overall compressive stress state. Thus shear cracks or other types of stress concentrations would not necessarily be expected to be prominent in SEM studies. In a heterogeneous material such as rock, where stress concentrations like those we observed at the ring-rod interface, can be expected to occur commonly at grain boundaries, it is not surprising that axial cracking predominates." In view of these observations, and considering the resolution limit of the SEM (about 0.02μm), criticism of the sliding crack model based on the qualitative examination of SEM results seems to require reevaluation.

Notwithstanding the above comments, we do not intend to suggest the sliding crack mechanism as the only source, or even the major source, of axial cracking. (Indeed, model studies (Nemat-Nasser, 1985) have shown microcracking under axial compression from inclusions and cavities of various geometric shapes.) What we intend to do is to consider the sliding crack model as a representative of a thin flaw which can deform plastically (and hence has cohesive resistance) and can slide (and hence has frictional resistance), and in a systematic and rigorous manner examine the results. These results then can be used to study the merits or shortcomings of the basic model.

To this end, we shall consider a solid which contains a dilute distribution of such ideal flaws. The flaws may be of varying sizes and orientations which may have either random or preferential distributions. The matrix is assumed to be isotropically elastic. Inelasticity and anisotropy develop because of the frictional and cohesive resistance of the preexisting flaws, and because of the formation and growth of tension cracks

at the tips of the flaws. During unloading, the effects of frictional locking and the cohesive resistance of the flaws, their backsliding upon further unloading, the partial closure of tension cracks, and finally the residual strains are included. All calculations are made for a two-dimensional model. Once the basic parameters of the model are defined, then the problem is analyzed consistently and systematically, without introducing additional assumptions. This allows us to make a judgment on the merits of the model from the obtained results which are then a true reflection of the basic model's assumptions.

2. FORMULATION

We consider a micromechanical modeling of the inelastic response of brittle materials such as ceramics and rocks at relatively low temperatures and under moderate confining pressures so that: (1) rate effects can be ignored; and (2) micro-cracking and inelastic slip at preexisting flaws can be regarded as the basic micromechanisms giving rise to inelasticity; for rather detailed discussions and extensive lists of relevant references, see Paterson (1978), Kranz (1983), and Horii and Nemat-Nasser (1986). The basic building block of the model is the mechanism shown in Fig. 1. It consists of an isolated preexisting flaw PP' and tension cracks PQ and P'Q' embedded in an isotropically elastic unbounded solid. Under the action of farfield compressive stresses, the preexisting flaw PP' undergoes frictional sliding which may be accompanied by cohesive (due to possible plastic deformation of the flaw) resistance as well as, possibly, dilatancy normal to PP', due to the deformation of the flaw and the possible presence of asperities. The relative deformation of the two faces of the flaw results in the creation of high tensile fields at the flaw's tips and leads to the formation of tension cracks which grow toward the direction of maximum compression. The model of

frictional sliding of preexisting cracks (without cohesion or dilatancy) which leads to the formation of tension cracks at its tips was originally suggested by Brace and Bombolakis (1963) and has been studied both by model experiments and analytically by a number of investigators; McClintock and Walsh (1963), Holzhauzen (1978), Moss and Gupta (1982), Kachanov (1982), Nemat-Nasser and Horii (1982), Horii and Nemat-Nasser (1985a,b,1986), and Steif (1984). Although micromechanical observations on actual rocks have not clearly identified preexisting cracks as the basic source of inelasticity in rocks, recent analysis by Wong (1985) seems to suggest that the model is indeed viable and does capture both qualitatively and quantitatively some of the main features of the problem.

In this section we shall calculate the inelastic strain due to: (1) slip along the preexisting flaw, (2) dilatancy normal to the flaw, and (3) the associated out-of-plane tension cracks at the tips of the flaw. (2.1) The dilatancy normal to the flaw will be assumed to be very small, but its effect on creating tension cracks at the tips of the flaw is significant.

The total strain at each state depends on the parameters that define the basic model shown in Fig. 1. The values of these parameters are highly stress-path-dependent. Hence, an incremental solution is necessary. Using the computed strain tensor, we formulate a rate-constitutive relation, using the equilibrium conditions for a representative flaw and the associated tension cracks.

Throughout this paper we shall use a fixed rectangular Cartesian coordinate system, x_1, x_2, as the background frame of reference. To simplify notation, we use the following direct representation:

$$\underset{\sim}{a}:\underset{\sim}{b} = a_{ij}b_{ij},$$

$$\underset{\sim}{L}:\underset{\sim}{b} = L_{ijkl}b_{kl},$$

$$\underset{\sim}{a}\otimes\underset{\sim}{b} = a_{ij}b_{kl}, \quad i,j,k,l = 1,2,$$

where repeated indices are summed.

2.1 Description of Strain

The total strain consists of an elastic strain due to the elastic deformation of the matrix, plus an inelastic strain due to slip and dilatancy of the preexisting flaws, accompanied by inelastic strain due to micro-cracking. In the sequel all physical quantities with the dimension of length are normalized by dividing by half of the preexisting flaw length, c. For example, if $\bar{b}$ is the slip (assumed constant) along flaw PP', we use $b = \bar{b}/c$ to represent the dimensionless slip. Similarly, if $\bar{d}$ is the displacement (assumed constant over the flaw length) of a flaw normal to its face, we use $d = \bar{d}/c$.

Let

$$f = c^2N \tag{2.2}$$

represent the density of the flaws of length 2c and orientation ϕ, where N is the number of such flaws per unit area. The strain due only to slip b of these flaws then is

$$\underset{\sim}{\varepsilon}_b = 2fb\underset{\sim}{p}_0, \tag{2.3a}$$

where

$$\underset{\sim}{p}_0 = \frac{1}{2}\begin{bmatrix} -\sin 2\phi & \cos 2\phi \\ \cos 2\phi & \sin 2\phi \end{bmatrix}. \tag{2.3b}$$

Similarly, the strain due to dilatancy d normal to PP′ is given by

$$\underset{\sim}{\varepsilon}_d = 2fd\underset{\sim}{p}_1 \tag{2.4a}$$

where

$$\underset{\sim}{p}_1 = \begin{bmatrix} \cos^2\phi & \cos\phi\sin\phi \\ \cos\phi\sin\phi & \sin^2\phi \end{bmatrix}; \tag{2.4b}$$

see Appendix A. Since the sliding-induced opening of a preexisting flaw normal to the surface must be bounded, we shall assume that this opening becomes saturated and hence use

$$d = d_0(1 - e^{-\zeta b}). \tag{2.5}$$

Note that b (and hence d) is assumed to be uniform along the flaw. This simplification is reasonable once tension cracks are suitably long.

Slip b and dilatancy d introduce normal and tangential concentrated gaps of values (b sin θ + d cos θ) and (b cos θ - d sin θ), at points P and P′, for cracks PQ and P′Q′, of common length ℓ, and orientation θ with respect to the preexisting flaw PP′. The strain associated with these gaps can be computed and is given by

$$\underset{\sim}{\varepsilon}_c = fb\ell\underset{\sim}{q}_0 + fd\ell\underset{\sim}{q}_1, \tag{2.6a}$$

where

$$\underset{\sim}{q}_0 = \frac{1}{2}\begin{bmatrix} -2\sin\phi\cos(\theta+\phi) & \cos(\theta+2\phi) \\ \cos(\theta+2\phi) & 2\cos\phi\sin(\theta+\phi) \end{bmatrix}, \tag{2.6b}$$

$$\underset{\sim}{q}_1 = \frac{1}{2}\begin{bmatrix} 2\cos\phi\cos(\theta+\phi) & \sin(\theta+2\phi) \\ \sin(\theta+2\phi) & 2\sin\phi\sin(\theta+\phi) \end{bmatrix}; \tag{2.6c}$$

see Appendix B.

The applied stresses change the crack opening displacement. This is not included in expression (2.6a). Under the condition of a positive Mode I stress intensity factor at Q and Q' (crack closure will be considered later on), i.e., for $K_I > 0$, the strain due to the change in crack opening caused by the applied loads can be computed and is given as follows:

$$\underset{\sim}{\varepsilon}_a = f\frac{1 - \nu}{8\mu}\pi\ell^2[4(\underset{\sim}{\sigma}:\underset{\sim}{\alpha})\underset{\sim}{\alpha} + (\underset{\sim}{\sigma}:\underset{\sim}{\beta})\underset{\sim}{\beta}], \tag{2.7a}$$

where

$$\underset{\sim}{\alpha} = \begin{bmatrix} \cos^2(\theta + \phi) & \cos(\theta + \phi)\sin(\theta + \phi) \\ \sin(\theta + \phi)\cos(\theta + \phi) & \sin^2(\theta + \phi) \end{bmatrix}, \tag{2.7b}$$

$$\underset{\sim}{\beta} = \frac{\partial \underset{\sim}{\alpha}}{\partial \theta} = \begin{bmatrix} -\sin 2(\theta + \phi) & \cos 2(\theta + \phi) \\ \cos 2(\theta + \phi) & \sin 2(\theta + \phi) \end{bmatrix}; \tag{2.7c}$$

see Appendix C. In (2.7a), μ is the shear modulus, ν is Poisson's ratio, and $\underset{\sim}{\sigma}$ is the stress tensor.

With $\underset{\sim}{L}$ denoting the elastic modulus tensor of the matrix material, the total strain tensor is now given by

$$\begin{aligned} \underset{\sim}{\varepsilon} = {} & \underset{\sim}{L}^{-1}:\underset{\sim}{\sigma} \\ & + 2fb\underset{\sim}{p}_0 + 2fd\underset{\sim}{p}_1 \\ & + fb\ell\underset{\sim}{q}_0 + fd\ell\underset{\sim}{q}_1 \\ & + f\frac{1 - \nu}{8\mu}\pi\ell^2[4(\underset{\sim}{\sigma}:\underset{\sim}{\alpha})\underset{\sim}{\alpha} + (\underset{\sim}{\sigma}:\underset{\sim}{\beta})\underset{\sim}{\beta}]. \end{aligned} \tag{2.8}$$

2.2 Rate Constitutive Relations

To complete the formulation, we must relate the kinematic parameters b, d, ℓ and θ to the applied stress $\underset{\sim}{\sigma}$. We shall do this by calculating the opening mode stress intensity factor, K_I, at crack tips Q and Q' in two

different ways: (1) by considering the applied loads and the condition of slip across the flaw (see Fig. 2a), as discussed by Horii and Nemat-Nasser (1986), and (2) by calculating the stress intensity factor in the presence of the applied stress and the imposed concentrated gaps at P and P' (see Fig. 2b).

As has been shown and verified by numerical examples by Horii and Nemat-Nasser (1986), the Mode I stress intensity factor at Q and Q' of cracks PQ and P'Q' can be computed with very good accuracy by considering an equivalent crack of length 2ℓ, subjected to a pair of colinear concentrated forces, F, as well as the applied overall stresses, as shown in Fig. 2. In this representation, F denotes the driving force transmitted across the preexisting flaw; it lies along the flaw and equals in magnitude the resultant force transmitted across the flaw. Following the procedure outlined by Horii and Nemat-Nasser (1986), we obtain

$$K_I = \frac{2}{\sqrt{\pi(\ell + \ell^*)}} (\underset{\sim}{\sigma}:\underset{\sim}{p}_2 - \tau_c)\sin\theta + \underset{\sim}{\sigma}:\underset{\sim}{\alpha}\sqrt{\pi\ell}, \tag{2.9a}$$

where

$$\underset{\sim}{p}_2 = \underset{\sim}{p}_0 + \bar{\mu}\,\underset{\sim}{p}_1, \quad \ell^* = 0.27, \quad \tau_c = \tau_c^0 e^{-\eta|b|}, \quad |b| = \int_0^t |\dot{b}|dt. \tag{2.9b-d}$$

Here, $\bar{\mu}$ is the coefficient of friction, τ_c is the value of cohesion at the current value of the total absolute value of slip (we shall assume that cohesion is an exponentially decaying function of the accumulated slip with decaying factor η defined by (2.9d)), and τ_c^0 is the initial cohesion. The parameter ℓ^* is introduced in such a manner that (2.9a) is valid even at crack initiation, i.e., at $\ell = 0^+$. Since the opening mode stress intensity factor for a closed sliding crack is maximum in a direction which makes an angle $\theta_c = 0.39\pi$ with the crack orientation, ℓ^* is obtained by equating the

stress intensity factor given by (2.9a) at $\ell = 0$ and $\theta = \theta_c$ to that maximum value. In the present application the effect of tension cracks is important once they become relatively long. Hence, whether or not ℓ^* is included in Eq. (2.9a) does not affect the results, although its presence renders K_I non-singular at $\ell = 0$.

The Mode I stress intensity factor associated with the gaps and in the presence of applied stresses, on the other hand, is given by

$$K_I' = \frac{\mu}{1 - \nu} \frac{1}{\sqrt{2\pi(\ell + \ell^{**})}} (b \sin \theta + d \cos \theta) + \underset{\sim}{\sigma}:\underset{\sim}{\alpha} \sqrt{\frac{\pi \ell}{2}}, \quad (2.10a)$$

where

$$\ell^{**} = \frac{\pi^2}{32} \ell^*; \quad (2.10b)$$

see Appendix D.

To obtain a relation between b and $\underset{\sim}{\sigma}$, we require

$$K_I = K_I' \quad \text{when} \quad \underset{\sim}{\sigma}:\underset{\sim}{p}_2 - \tau_c \geq 0. \quad (2.11)$$

Furthermore the crack length ℓ is obtained such that

$$K_I = K_c, \quad (2.12)$$

where K_c is the critical value of the stress intensity factor in the opening mode. θ is determined so as to maximize K_I for a given length ℓ.

It should be noted that model experiments (Nemat-Nasser and Horii, 1982) and exact analysis (Horii and Nemat-Nasser, 1983, 1985a) show that tension cracks emanate from the flaw tips at an angle of about 70° with respect to the orientation of the flaw, and curve toward the direction of the maximum compression. The model shown in Fig. 1 substitutes the curved

crack by an equivalent straight one; the equivalence is in the sense that the orientation θ of the equivalent straight crack is computed at each incremental loading by maximizing K_I with respect to θ.

Because of the complex and nonlinear relations that exist among various parameters which defined the basic model shown in Fig. 1, the overall stress-strain relation will be highly nonlinear and stress-path-dependent. It is therefore necessary to formulate the problem incrementally. To this end we will express $\dot{\ell}$, $\dot{\theta}$, and $\dot{b}$, in terms of $\dot{\underset{\sim}{\sigma}}$, for given loading regimes. These quantities can be written symbolically as

$$\dot{\ell} = \underset{\sim}{A}:\dot{\underset{\sim}{\sigma}}, \quad \dot{\theta} = \underset{\sim}{B}:\dot{\underset{\sim}{\sigma}}, \quad \dot{b} = \underset{\sim}{C}:\dot{\underset{\sim}{\sigma}}. \tag{2.13a-c}$$

We will calculate the second-order tensors $\underset{\sim}{A}$, $\underset{\sim}{B}$, and $\underset{\sim}{C}$ for prescribed loading regimes. Note that, in view of assumption (2.5), we have

$$\dot{d} = \zeta(d_0 - d)\dot{b}. \tag{2.14}$$

With Eqs. (2.13) and (2.14), and upon time differentiation of (2.8), we obtain the following rate constitutive equation:

$$\begin{aligned}
\dot{\underset{\sim}{\varepsilon}} &= \underset{\sim}{D}:\dot{\underset{\sim}{\sigma}}, \\
\underset{\sim}{D} &= \underset{\sim}{L}^{-1} \\
&+ f\{b\underset{\sim}{q}_0 + d\underset{\sim}{q}_1 + \frac{1-\nu}{4\mu}\pi\ell[4(\underset{\sim}{\sigma}:\underset{\sim}{\alpha})\underset{\sim}{\alpha} + (\underset{\sim}{\sigma}:\underset{\sim}{\beta})\underset{\sim}{\beta}]\} \otimes \underset{\sim}{A} \\
&+ f\{b\ell\underset{\sim}{r}_0 + d\ell\underset{\sim}{r}_1 + \frac{1-\nu}{8\mu}\pi\ell^2[4(\underset{\sim}{\sigma}:\underset{\sim}{\beta})\underset{\sim}{\alpha} + 4(\underset{\sim}{\sigma}:\underset{\sim}{\alpha})\underset{\sim}{\beta} + (\underset{\sim}{\sigma}:\underset{\sim}{\gamma})\underset{\sim}{\beta} + (\underset{\sim}{\sigma}:\underset{\sim}{\beta})\underset{\sim}{\gamma}]\} \otimes \underset{\sim}{B} \\
&+ f\{2\underset{\sim}{p}_0 + \ell\underset{\sim}{q}_0 + \zeta(d_0 - d)(2\underset{\sim}{p}_1 + \ell\underset{\sim}{q}_1)\} \otimes \underset{\sim}{C} \\
&+ f\frac{1-\nu}{8\mu}\pi\ell^2[4\underset{\sim}{\alpha}\otimes\underset{\sim}{\alpha} + \underset{\sim}{\beta}\otimes\underset{\sim}{\beta}],
\end{aligned} \tag{2.15a}$$

where

$$\underset{\sim}{\gamma} = \frac{\partial \underset{\sim}{\beta}}{\partial \theta}, \quad \underset{\sim}{r}_0 = \frac{\partial \underset{\sim}{q}_0}{\partial \theta}, \quad \underset{\sim}{r}_1 = \frac{\partial \underset{\sim}{q}_1}{\partial \theta}. \tag{2.15b-d}$$

2.3 Specific Cases During Loading

In what follows, we consider various loading cases separately. We shall use a symbolic representation, and give the details of expressions such as $\partial K_I/\partial b$ and $\underset{\sim}{b}_1$ in Appendices E and F.

(i) Sliding occurs without crack growth: This happens when the driving shear stress on the flaw exceeds the frictional and cohesive resistance of the flaw, i.e., when $\underset{\sim}{\sigma}:\underset{\sim}{p}_2 - \tau_c \geq 0$, while $K_I < K_c$. From condition $K_I = K_I'$, we obtain, by time differentiation,

$$\left[\frac{\partial K_I}{\partial b} - \frac{\partial K_I'}{\partial b}\right] \dot{b} = (\underset{\sim}{b}_1 - \underset{\sim}{b}_2):\dot{\underset{\sim}{\sigma}}, \tag{2.16}$$

where $\underset{\sim}{b}_1$ and $\underset{\sim}{b}_2$ are the matrix coefficients of $\dot{\underset{\sim}{\sigma}}$, obtained from (2.9a) and from (2.10a), respectively. Thus we have

$$\dot{b} = \frac{1}{\dfrac{\partial K_I}{\partial b} - \dfrac{\partial K_I'}{\partial b}} (\underset{\sim}{b}_1 - \underset{\sim}{b}_2):\dot{\underset{\sim}{\sigma}}, \tag{2.17}$$

and, hence,

$$\underset{\sim}{C} = \frac{1}{\dfrac{\partial K_I}{\partial b} - \dfrac{\partial K_I'}{\partial b}} (\underset{\sim}{b}_1 - \underset{\sim}{b}_2), \qquad \underset{\sim}{A} = \underset{\sim}{0}, \qquad \underset{\sim}{B} = \underset{\sim}{0}. \tag{2.18a-c}$$

(ii) Sliding occurs with crack growth: This happens when $K_I = K_c$ and $\underset{\sim}{\sigma}:\underset{\sim}{p}_2 - \tau_c \geq 0$. The problem can be stated as follows: Maximize K_I with respect to θ and b under the condition that $K_I = K_I'$. With the aid of a Lagrangian multiplier, we arrive at the following conditions:

$$K_I = K_I' = K_c,$$

$$\frac{\partial K_I}{\partial \theta}\frac{\partial K_I'}{\partial b} - \frac{\partial K_I}{\partial b}\frac{\partial K_I'}{\partial \theta} = J = 0. \qquad (2.19a,b)$$

Time differentiation yields,

$$\frac{\partial K_I}{\partial \ell}\dot{\ell} + \frac{\partial K_I}{\partial \theta}\dot{\theta} + \frac{\partial K_I}{\partial b}\dot{b} = \underset{\sim}{b}_1 : \dot{\underset{\sim}{\sigma}},$$

$$\frac{\partial K_I'}{\partial \ell}\dot{\ell} + \frac{\partial K_I'}{\partial \theta}\dot{\theta} + \frac{\partial K_I'}{\partial b}\dot{b} = \underset{\sim}{b}_2 : \dot{\underset{\sim}{\sigma}}, \qquad (2.20a\text{-}c)$$

$$\frac{\partial J}{\partial \ell}\dot{\ell} + \frac{\partial J}{\partial \theta}\dot{\theta} + \frac{\partial J}{\partial b}\dot{b} = \underset{\sim}{b}_3 : \dot{\underset{\sim}{\sigma}}.$$

These linear equations yield $\dot{\ell}$, $\dot{\theta}$, and $\dot{b}$. The solution is in the form (2.13).

2.4 Specific Cases During Unloading

After a continued loading regime, we consider unloading by reducing the applied stresses. Unloading at specific flaws may also take place when, for example, we change the load path. Our analysis of unloading includes all cases when the net shear traction, $\underset{\sim}{\sigma} : \underset{\sim}{p}_2 - \tau_c$, transmitted across a preexisting flaw decreases for whatever reason.

(i) Crack grows without sliding: Upon unloading, cracks may continue to grow as the lateral compression is reduced but, because of an initial locking of the flaw, the maximum gaps at P and P′ remain fixed. The conditions for crack growth then are

$$K_I' = K_c, \qquad \frac{\partial K_I'}{\partial \theta} = 0. \qquad (2.21a,b)$$

Equation (2.21b) ensures that cracks grow in a direction which maximizes K_I'. Time differentiation now yields

$$\frac{\partial K_I'}{\partial \ell}\dot{\ell} + \frac{\partial K_I'}{\partial b}\dot{\theta} = \underset{\sim}{b}_2 : \dot{\underset{\sim}{\sigma}},$$

$$\frac{\partial}{\partial \ell}\left(\frac{\partial K_I'}{\partial \theta}\right)\dot{\ell} + \frac{\partial}{\partial \theta}\left(\frac{\partial K_I'}{\partial \theta}\right)\dot{\theta} = \frac{\partial}{\partial \theta}\underset{\sim}{b}_2 : \dot{\underset{\sim}{\sigma}}. \qquad (2.23a\text{-}b)$$

From these we have $\dot{\ell}$ and $\dot{\theta}$ in the form (2.13). Since b remains fixed, in this case $\dot{b} = 0$, and hence $\underset{\sim}{C} = \underset{\sim}{0}$.

(ii) Backsliding occurs without crack closure: When the residual shear stress on the preexisting flaw overcomes the cohesive and frictional resistance, backsliding of the flaw may take place. Since the frictional and cohesive resistance on the preexisting flaw acts against the direction of the relative displacement, K_I in (2.9a) must be redefined for the unloading case by

$$K_I = \frac{2}{\sqrt{\pi(\ell + \ell^*)}}(\underset{\sim}{\sigma} : \underset{\sim}{p}_2' + \tau_c)\sin\theta + \underset{\sim}{\sigma} : \underset{\sim}{\alpha}\sqrt{\pi\ell}, \qquad (2.24a)$$

$$\underset{\sim}{p}_2' = \underset{\sim}{p}_0 - \bar{\mu}\underset{\sim}{p}_1. \qquad (2.24b)$$

Before backsliding takes place, K_I of (2.24a) may formally be larger than the actual stress intensity factor K_I' obtained on the basis of the applied overall loads and the existing gaps at P and P'. This is similar to the loading case with $\underset{\sim}{\sigma} : \underset{\sim}{p}_2 - \tau_c \le 0$, so that no slip occurs. The quantity K_I, defined by (2.24a), attains its usual physical meaning only when backsliding occurs, or is just about to occur. Therefore, the condition for the initiation of backsliding is given by

$$K_I \le K_I'; \qquad (2.25)$$

see Appendix G. During backsliding, however, we require that

$$K_I = K_I'. \qquad (2.26)$$

Upon time differentiation at fixed ℓ and θ we obtain an equation similar to (2.17) for $\dot{b}$.

(iii) Crack closure without backsliding: When crack closure occurs, the strain tensor is given by

$$\begin{aligned}\underset{\sim}{\varepsilon} &= \underset{\sim}{L}^{-1}:\underset{\sim}{\sigma} \\ &+ 2fbp_0 + 2fdp_1 \\ &- f\frac{1}{2\pi}\frac{\mu}{1-\nu}\frac{1}{(\underset{\sim}{\sigma}:\underset{\sim}{\alpha})}(b\sin\theta + d\cos\theta)^2\underset{\sim}{\alpha} \\ &+ f\frac{\ell_m}{2}(b\cos\theta - d\sin\theta)\underset{\sim}{\beta} \\ &+ f\frac{1-\nu}{8\mu}\pi\ell_m^2(\underset{\sim}{\sigma}:\underset{\sim}{\beta})\underset{\sim}{\beta},\end{aligned} \tag{2.27}$$

where ℓ_m denotes the maximum crack length; see Appendix H. From the time differentiation of (2.27) and Eqs. (2.13), we obtain the rate constitutive equation for this special case in the following explicit form: (2.29)

$$\begin{aligned}\dot{\underset{\sim}{\varepsilon}} &= \underset{\sim}{D}:\dot{\underset{\sim}{\sigma}}, \\ \underset{\sim}{D} &= \underset{\sim}{L}^{-1} \\ &+ f\,[2\underset{\sim}{p}_0 + 2\zeta(d_0 - d)\underset{\sim}{p}_1 \\ &\quad - \frac{1}{\pi}\frac{\mu}{1-\nu}\frac{1}{\underset{\sim}{\sigma}:\underset{\sim}{\alpha}}(\sin\theta + \zeta(d_0 - d)\cos\theta)(b\sin\theta + d\cos\theta)\underset{\sim}{\alpha} \\ &\quad + \frac{\ell_m}{2}(\cos\theta - \zeta(d_0 - d)\sin\theta)\underset{\sim}{\beta}]\otimes\underset{\sim}{C} \\ &+ f\left(\frac{1}{2\pi}\frac{\mu}{1-\nu}\frac{1}{(\underset{\sim}{\sigma}:\underset{\sim}{\alpha})^2}(b\sin\theta + d\cos\theta)^2\underset{\sim}{\alpha}\otimes\underset{\sim}{\alpha} + \frac{1-\nu}{8\mu}\pi\ell_m^2\underset{\sim}{\beta}\otimes\underset{\sim}{\beta}\right).\end{aligned} \tag{2.28}$$

Note that θ is fixed in this case.

The condition for crack closure without backsliding of the flaw is

$$K_I' = 0,$$

whose time differentiation at constant θ and b yields

$$\dot{\ell} = (\underset{\sim}{b}_2 : \dot{\underset{\sim}{\sigma}}) / \left(\frac{\partial K_I'}{\partial \ell}\right) = \underset{\sim}{A} : \dot{\underset{\sim}{\sigma}}, \quad \underset{\sim}{B} = \underset{\sim}{C} = \underset{\sim}{0}. \tag{2.30a-c}$$

(iv) Crack closure with backsliding: The conditions are

$$K_I = K_I' = 0. \tag{2.32a,b}$$

Since θ remains constant during crack closure, only $\dot{\ell}$ and $\dot{b}$ must be expressed in terms of $\dot{\underset{\sim}{\sigma}}$. This is done by time differentiation of $K_I = 0$ and $K_I' = 0$ at constant θ and by solving the resulting linear equations for $\dot{\ell}$ and $\dot{b}$. $\underset{\sim}{B} = \underset{\sim}{0}$ because θ remains constant.

2.4 Comments on the Model

The model presented above includes a number of features which have been suggested by several researchers in the past, e.g. Brace and Bombolakis (1963), Zoback and Byerlee (1975), Kachanov (1982), and Moss and Gupta (1982). In particular, Moss and Gupta have obtained nonlinear stress-strain and dilatancy relations based on a sliding preexisting crack with tension cracks (wing cracks) emanating from its tips. These authors include frictional and cohesive effects, and calculate the inelastic strain associated with the slip of the preexisting crack as well as of the tension cracks. In their model, however, the orientation of the tension cracks (wings) relative to the preexisting crack is fixed throughout the entire loading history and must be prescribed. Moreover, in their model it is necessary to prescribe an initial length and crack opening displacement for the wings. In the model presented here, the flaws at which tension cracks nucleate, the orientation and the length of the tension cracks, their

opening displacement, and whether they continue to grow, become dormant, or actually close, are all obtained as part of the solution to the problem and, indeed, change during the course of loading and unloading, in a rather complex manner. Indeed, in our model the tension cracks may continue to grow at a state of unloading, because of the locking of the preexisting flaw, as illustrated in the examples given in Sec. 4. Furthermore, we have attempted to render the model self-consistent in the sense that the stress intensity factors at the tips of the tension cracks are obtained on the basis of the existing gap (created due to the sliding of the preexisting flaw) and in the presence of farfield loads, and these are then made to correspond to the stress intensity factors calculated on the basis of the applied loads and the effective total force transmitted across the preexisting flaw. In the model of Moss and Gupta, the stress intensity factors are calculated only on the basis of the applied loads and the effective force across the preexisting crack. We note that if the preexisting flaw is locked, then the stress intensity factors must be computed on the basis of the existing gaps and the applied loads, and these stress intensity factors may not be equal to the ones calculated on the basis of the applied loads and the effective force across the preexisting flaw, when the flaw remains dormant.

3. AVERAGE QUANTITIES

So far, the problem has been formulated for flaws of fixed orientation ϕ and size 2c. When a dilute distribution of preexisting flaws is involved, the interaction effects may be neglected, and the overall strains and strain rates may be estimated by a simple average of the individual contributions. To this end let $N = N(\phi)$ be the number of flaws of orientation ϕ and size 2c per unit area. Hence, $f = c^2N$ is given as a function of ϕ. The average

strain, $\bar{\underset{\sim}{\varepsilon}}$, then may be computed from

$$\bar{\underset{\sim}{\varepsilon}} = \frac{1}{2\pi}\int_0^{2\pi} \underset{\sim}{\varepsilon}(\phi, f(\phi))d\phi, \tag{3.1}$$

where $\underset{\sim}{\varepsilon}(\phi, f(\phi))$ is given, in our analysis, by (2.8) or by (2.27). A similar expression can be written for the average strain rate. When a finite number of specific orientations of preexisting flaws is involved, the integral in (3.1) reduces to a finite sum,

$$\bar{\underset{\sim}{\varepsilon}} = \frac{1}{M}\sum_{\alpha=1}^{M} \underset{\sim}{\varepsilon}(\phi_\alpha, f(\phi_\alpha)), \tag{3.2}$$

where M is the total number of involved orientations.

In the formulation presented above and in the preceding section, no attempt is made to include interaction among neighboring flaws and their associated cracks. There are a number of possible ways that this interaction may be included. Perhaps the most effective way would be to estimate the stress intensity factors at the crack tips by considering several interacting flaws or an infinite row of such flaws, in the manner discussed by Horii and Nemat-Nasser (1983, 1985a,b, 1986). This poses an extremely complex mathematical problem where, although solvable as shown by Horii and Nemat-Nasser (1985b), the resulting equations are so involved that they do not lend themselves to simple analytic calculations of the kind given in the present paper.

An alternative approach is to consider an averaging technique similar to the self-consistent scheme; see Budiansky (1965) and Hill (1965). This would require the solution of the problem of out-of-plane crack growth from a preexisting flaw embedded in a linearly elastic but anisotropic material, which currently is not available. Therefore, any improvement on the simple

averaging procedure given by (3.1) seems to require either extensive and complicated computations beyond the scope of the present work or it must be based on additional simplifying assumptions, which is not our intention at this time.

In the following section we shall assume a dilute distribution of preexisting flaws, use the simple averaging given by (3.2), and present a number of illustrative examples.

4. RESULTS AND DISCUSSIONS

In this section, we shall illustrate the predictive capability of the model presented in the preceding section, in terms of several numerical examples, and discuss the results.

The basic parameters of the model are:

1) $f = c^2N$ which represents the density and the size of the flaws. It can be given any suitable distribution in terms of the flaw orientation ϕ. In our examples we shall assume it to be constant.
2) M_0 which is the number of flaw orientations between 0° and 90°. In our examples we shall assume an isotropic initial flaw distribution, and therefore use finite, equally spaced orientations between 0° and 90°.
3) $K_c = \bar{K}_c/(\tau_c^0\sqrt{c})$ which is the dimensionless critical value of the stress intensity factor. Since typical values of fracture toughness, $\bar{K}_c$, for rocks are of the order of $10^5 \sim 10^6$ $Nm^{-3/2}$, taking a typical flaw length to be of the order of 10^{-4}m, and the cohesive stress to be of the order of 10^7 Nm^{-2}, we estimate K_c to be of the order of 1.
4) d_0 which represents the limiting maximum flaw expansion (dilatancy) normal to its face; see Eq. (2.5). It is nondimensionalized using half the flaw length c. It is also <u>normalized</u> by dividing by τ_c^0/μ. Hence,

$d_0 = 1$, for example, represents an actual maximum possible flaw expansion of 0.5% of half the flaw length c when $\tau_c^0/\mu = 5.0 \times 10^{-3}$.

5) ζ which is the coefficient of the exponential saturation of the flaw dilatancy with respect to the flaw slip. Since we normalize the slip b (and the dilatancy d) by measuring it in units of τ_c^0/μ, ζ (and η in item 6 below) is measured in units of μ/τ_c^0 which is of the order of $10^2 \sim 10^3$, a rather large dimensionless number. For all examples, we use $\zeta = 1$; hence, full flaw expansion is attained at flaw slips of less than 1% of the flaw length.

6) η which is the coefficient of the exponential decay of the rate of cohesive resistance of the preexisting flaw.

7) $\bar{\mu}$ which is the coefficient of internal friction possibly having a value between 0 and 1.

8) ν which is the Poisson ratio of the elastic matrix. In actual cases, ν should be interpreted as the average overall Poisson ratio of a solid with microdefects.

For the examples displayed in Figs. 3-6, we have used $f = 0.3$, $M_0 = 10$, $\nu = 0.25$, $\zeta = 1.0$, and, unless otherwise indicated explicitly, $K_c = 1.0$, $d_0 = 0.05$, $\eta = 0.05$, and $\bar{\mu} = 0.30$. In these figures, stresses are normalized by τ_c^0 and strains by (τ_c^0/μ).

Figures 3a and b show typical responses in uniaxial compression. In Fig. 3a the normalized overall volumetric strain and in Fig. 3b the normalized overall axial compressive strain are plotted on the horizontal axis in terms of the normalized compression as ordinate. As is common in the rock mechanics literature, compression and contraction are viewed as positive. Up to point A, the overall response is linearly elastic, because the local stresses acting on the preexisting flaws are not as yet large

enough to activate these flaws. At point A, frictional sliding initiates on some flaws, and at point B, cracks nucleate at some suitably oriented flaws. Upon further loading, tension cracks begin to grow, leading to substantial dilatancy which quickly offsets the elastic volumetric contraction, leading to overall volumetric expansion as the axial compressive load is further increased; see Fig. 3a.

The stress-strain relation shown in Fig. 3b remains monotonic in uniaxial loading, and closely resembles the experimentally observed behavior of rocks; see, e.g., Brace and Bombolakis (1963). In the presence of lateral tension, however, the curve would terminate at a point when a most critical tension crack begins to grow in the axial direction in an unstable manner, leading to axial splitting; see Nemat-Nasser and Horii (1982). In the presence of lateral compression, the stress-strain curve remains monotonic and no failure is predicted by this model because the interaction effects among neighboring flaws are not incorporated in the present model. As has been shown by Horii and Nemat-Nasser (1985a,1986), the interaction among a row of suitably oriented preexisting flaws can lead to the formation of a fault, as tension cracks nucleate at these flaws and grow in an unstable manner. The analytical computations associated with such a model of faulting are rather complex and therefore considerable simplification is necessary before such a failure model can be incorporated into a micromechanically based constitutive relation of the kind developed in the preceding section. The present constitutive model, therefore, is not suitable for such loading regimes.

At point C in Figs. 3a and b, unloading has been initiated. The response from C to D is linearly elastic. However, the material is slightly

more compliant, since microcracking has led to certain stiffness degradation. The difference between the elastic moduli at initial loading and at unloading from point C is rather small in the axial direction, but it is considerable for lateral tension (but not for lateral compression). This is because during axial compression, cracks grow essentially in the axial direction, and such cracks do not influence much the axial stiffness of the material, but they do have considerable weakening effect for lateral tension.

The instantaneous compliances at several states during the course of a monotonic axial compression and of unloading are given in Table 1. As is seen, strong anisotropy develops due to slip and microcracking.

From point C to point D in Figs. 3a and b, all the flaws are locked and all the tension cracks remain open. Backsliding of some preexisting flaws initiates at point D. In addition, some tension cracks grow before being dormant. Considerable volumetric contraction begins to occur after this state. In this example, no crack closure occurs during the entire unloading process which leads to point E corresponding to some permanent total volumetric expansion. This type of response has been inferred by Scholz and Kranz (1974) on the basis of experimental observations.

In Figs. 4, we show examples of loading-path-dependency. Fig. 4a shows the stress-strain curves for two different loading paths defined in Fig. 4b. On path I, uniaxial compression is applied until point A, producing slip and microcracks at some preexisting flaws. Then, with axial compression held fixed, the lateral compressive stress is applied up to point C. During this regime, no further slip occurs on any flaws because the driving shear stresses on the flaws actually decrease, but not enough to initiate

backsliding. At point B, closure of some tension cracks begins.

Path II, on the other hand, defines a proportional loading directly to point C'. Unlike for the path I loading, for path II no slip is activated. The response, therefore, is linearly elastic. The microstructures of the material for points C and C' are quite different.

Our model includes a number of important parameters, and we now proceed to examine their effects on the model's predictions. These parameters are listed at the beginning of this section. Except for ζ, η, and d_0, they all have rather clear physical significance, and therefore their values may be estimated on the basis of experimental observations. The parameter d_0 represents maximum expansion (due to asperities or other effects) that the flaw itself can undergo because of sliding. The parameters ζ and η represent the rate at which flaw expansion saturates and the rate at which the cohesive resistance of the flaw decays, both measured per unit rate of sliding. These parameters have a rather significant influence on the overall volumetric response predicted by the model.

Figures 5 and 6 show the effect of η and of d_0 in uniaxial compression, followed by unloading. As pointed out before, when $(\tau_c^0/\mu) = 5.0 \times 10^{-3}$, $d_0 = 1$ represents an actual maximum limiting flaw expansion normal to its surface of only 0.5% of half the total flaw length, and hence it is small. Nevertheless, it has a rather significant influence on the response predicted by the model.

The influence of internal friction $\bar{\mu}$ and the normalized fracture toughness K_c on the dilatancy in uniaxial compression followed by unloading is depicted in Figs. 7 and 8, respectively. As one would expect, a greater

dilatancy results at lower frictional resistance of the flaws and lower fracture toughness of the matrix material. It should be noted that there is a considerable difference between the effects of the frictional parameter $\bar{\mu}$ and the normalized fracture toughness K_c on the overall response: whereas the friction coefficient $\bar{\mu}$ affects the flaw response during the entire loading and unloading regime, K_c's influence emerges only with tension crack initiation. Note also that normalized K_c involves the flaw size 2c and the cohesive stress τ_c^0, as well as the actual fracture toughness of the surrounding material. Therefore, while the order of magnitude of K_c can be estimated on the basis of experimental observations, its actual value involves quantities that are difficult to measure. For example, the fracture toughness should actually reflect the behavior of aggregates of crystals involving a variety of preexisting defects in a rock or ceramic sample.

As a final illustration, we seek to fit the model to experimental results reported by Zoback and Byerlee (1975). Since actual rocks contain preexisting open cracks and pores which tend to close upon application of loads, the initial stress-strain relations often reported are considerably softer than the subsequent response. We have not included this in our calculations, although it can easily be done, as detailed by Horii and Nemat-Nasser (1982). Therefore, we do not seek to match the initial portion of the stress-strain curves, but only compare their overall shapes. To offset the initial soft response, we simply shift the model's prediction, as shown in Figs. 9a and b.

Since the model is a two-dimensional one, whereas the experimental results are for uniaxial compression of a cylindrical sample, a certain

amount of adjustment in the model parameters is required. The reported flaw size 2c is of the order $4 \sim 8 \times 10^{-4}$, and taking $f = N(c/V)^3 \sim 0.2$, for the two-dimensional case we choose $f = (0.2)^{2/3} \sim 0.34$. The Poisson ratio and the shear modulus are estimated to be $\nu = 0.35$ and $\mu = 2.1 \times 10^4$ MNm^{-2}, based on the data reported by Zoback and Byerlee (1975). In addition, we take $\bar{K}_c = 0.7$ MNm$^{-3/2}$, $\tau_c^0 = 21$ MNm^{-2}, and set $2c = 5.0 \times 10^{-4}$m (therefore, $K_c = 2.1$). The coefficient of friction is taken as $\bar{\mu} = 0.1$, which is rather small, but may be justified on the grounds that many of the flaws seem to have been initially open and therefore their frictional resistance ought to be small. Considering the simplicity of the model, the fit shown in Figs. 9a and b is rather good. Nevertheless, in view of the number of free parameters involved, the comparison should be regarded as an illustration and not necessarily a direct support of the viablity of the model.

In summary, it may be concluded that the micromechanical model consisting of preexisting flaws, with frictional and cohesive resistance to sliding, and capable of nucleating tension cracks, seems to capture a number of important features observed in the response of brittle materials with microdefects. The model presented here does not include the important interaction effects among neighboring flaws. Judging from results reported by Horii and Nemat-Nasser (1986) on the failure in compression of materials of this kind under moderate and large confining pressures, we feel that constitutive modeling based on the mechanisms considered by these authors should prove to be effective.

Figure Captions

Figure 1: An isolated preexisting flaw PP' with tension cracks P'Q' and PQ.

Figure 2: (a) An equivalent isolated crack with a pair of colinear concentrated forces applied at its center. (b) An equivalent isolated crack with concentrated gap at its end.

Figure 3: (a) Volumetric strain versus differential stress curve for a loading and unloading loop. (b) Axial strain versus stress curve for a loading and unloading loop; $f = 0.3$, $M_0 = 10$, $\nu = 0.25$, $\bar{\mu} = 0.3$, $K_c = 1.0$, $d_0 = 0.05$, and $\eta = 0.05$.

Figure 4: (a) Axial strain versus differential stress for different loading paths; $f = 0.3$, $M_0 = 10$, $\nu = 0.25$, $\bar{\mu} = 0.3$, $d_0 = 0$, $K_c = 1.0$, and $\eta = 0.05$. (b) Loading paths.

Figure 5: Volumetric strain versus differential stress curves for various η; $f = 0.3$, $M_0 = 10$, $\nu = 0.25$, $\bar{\mu} = 0.3$, $d_0 = 0$, and $K_c = 1.0$.

Figure 6: Volumetric strain versus differential stress curves for various d_0; $f = 0.3$, $M_0 = 10$, $\nu = 0.25$, $\bar{\mu} = 0.3$, $K_c = 1.0$, and $\eta = 0.05$.

Figure 7: Volumetric strain versus differential stress curves for various $\bar{\mu}$; $f = 0.3$, $M_0 = 10$, $\nu = 0.25$, $K_c = 1.0$, $d_0 = 0.05$, and $\eta = 0.05$.

Figure 8: Volumetric strain versus differential stress curves for various K_c; $f = 0.3$, $M_0 = 10$, $\nu = 0.25$, $\bar{\mu} = 0.3$, $d_0 = 0.05$, and $\eta = 0.05$.

Figure 9: Comparison with experimental data reported by Zoback and Byerlee (1975): (a) Volumetric strain versus differential stress curve. (b) Axial strain versus differential stress curve; $f = 0.35$, $M_0 = 10$, $\nu = 0.35$, $\bar{\mu} = 0.1$, $K_c = 2.1$, $d_0 = 0$, $\eta = 0$. $\mu = 2.1 \times 10^{10}$ Nm^{-2}, and $\tau_c^0 = 2.1 \times 10^7$ Nm^{-2}.

REFERENCES

Brace, W.F. and Bombolakis, E.G., A note on brittle crack growth in compression, J. Geophys. Res., 68, (1963), 3709-3713.

Budiansky, B., On the elastic moduli of some heterogeneous materials, J. Mech. Phys. Solids, 13, (1965), 223-227.

Costin, L., A microcrack model for deformation of brittle rock, J. Geophys. Res., 88, (1983), 9485-9492.

Dey, T. and Wang, C.Y., Some mechanisms of microcrack growth and interaction in compressive rock failure, Int. J. Rock Mech. Min. Sci., 18, (1981), 199-209.

Hill, R., A self-consistent mechanics of composite materials, J. Mech. Phys. Solids, 13, (1965), 213-222.

Hoek, E. and Bieniawski, Z.T., Brittle fracture propagation in rock under compression, Int. J. Fract. Mech., 1, (1965), 137-155.

Holcomb, D.J., A quantitative model of dilatancy in dry rock and its application to Westerly granite, J. Geophys. Res., 83, (1978), 4941-4950.

Holcomb, D.J. and Stevens, J.L., The reversible Griffith crack: a viable model for dilatancy, J. Geophys. Res., 85, (1980), 7101-7107.

Holzhausen, G.R. Sheet structure in rock and some related problems in rock mechanics, Ph. D. thesis, Stanford Univ., Stanford, CA. (1978).

Horii, H. and Nemat-Nasser, S., Overall moduli of solids with microcracks: load-induced anisotropy, J. Mech. Phys. Solids, 31, (1982), 155-171.

Horii, H. and Nemat-Nasser, S., Estimate of stress intensity factors for interacting cracks, Advances in Aerospace Structures, Materials and Dynamics, AD-06, (1983), eds. U. Yuceoglu, R.L. Sierakowski and D.A. Glasgow, ASME, New York, 111-117.

Horii, H. and Nemat-Nasser, S., Compression-induced microcrack growth in brittle solids: axial splitting and shear failure, J. Geophys. Res., 90, (1985a), 3105-3125.

Horii, H. and Nemat-Nasser, S., Elastic fields of interacting inhomogeneities, Int. J. Solids Struct., 21, (1985b), 731-745.

Horii, H. and Nemat-Nasser, S., Brittle failure in compression: splitting, faulting, and brittle-ductile transition, Philosophical Transactions, Royal Society London, 319, (1986), 337-374.

Janach, W. and Guex, L.H., In-plane propagation of shear microcracks in brittle rocks under triaxial compression, J. Geophys. Res., 85, (1980), 2543-2553.

Kachanov, M.L., A microcrack model of rock inelasticity, part II: propagation of microcracks, Mech. Mater. 1, (1982), 29-41.

Kranz, R.L. Microcracks in rocks: a review, Tectonophysics, 100, (1983), 449-480.

McClintock, F.A. and Walsh, J.B., Friction on Griffith cracks in rocks under pressure, Proc. the 4th U.S. Nat. Congr. Appl. Mech., (1962), ASME, New York, 1015-1021.

Moss, W.C. and Gupta, Y.M., A constitutive model describing dilatancy and failure in brittle rock, J. Geophys. Res., 87, (1982), 2985-2998

Muskhelishvili, N.I., Singular Integral Equations, (1953), Noordhoff, Groningen, Holland.

Nemat-Nasser, S., Discussion of "Geometric probability approach to the characterization and analysis of microcracking in rocks", Mech. of Mater., 4, (1985), 277-281.

Nemat-Nasser, S. and Horii, H., Compression-induced nonplanar crack extension with application to splitting, exfoliation, and rockburst, J. Geophys. Ref., 87, (1982), 6805-6821.

Paterson, M.S., Experimental rock deformation - the brittle field, Springer-Verlag, Berlin-Heidelberg-New York, (1978).

Scholz, C. H., Experimental study of the fracturing process in brittle rock, J. Geophys. Res., 73, (1968), 1447-1454.

Scholz, C.H., Boitnott, G., and Nemat-Nasser, S., The Bridgman ring paradox revisited, Pure and Applied Geophysics, 124, (1986), 587-599.

Scholz, C.H. and Kranz, R., Notes on dilatancy recovery, J. Geophys. Res., 79, (1974), 2132-2135.

Sondergeld, C.H. and Estey, L.H., Source mechanism and microfracturing during uniaxial cycling of rock, Pure and Applied Geophysics, 120, (1982), 151.

Steif, P.S., Crack extension under compressive loading, Engineering Fracture Mechanics, 20, (1984), 463-473.

Wong, T.F., Geometric probability approach to the characterization and analysis of microcracking in rocks, Mech. Mater., 4, (1985). 261-276.

Yanagidani, T. and Ehara, S., Nishizawa, O., Kusunose, K, and Terada, M., Localization of dilatancy in Westerly granite under constant uniaxial stress, J. Geophys. Res., 90, (1985), 6840-6858.

Zoback, M.D. and Byerlee, J.D., The effect of cyclic differential stress on dilatancy in Westerly granite under uniaxial and triaxial conditions, J. Geophys. Res., 80, (1975), 1526-1530.

APPENDIX A: Strains Due to Crack Opening

The strain due to the crack opening displacement is given by

$$\varepsilon_{ij} = \frac{1}{2}\frac{N}{V}\int_{-c}^{c}(n_i[u_j] + n_j[u_i])ds, \tag{A.1}$$

where V is the volume, N is the number of cracks in this volume, $\underset{\sim}{n}$ is a unit vector normal to a crack surface, and $[u_i]$ is the i-th component of the crack opening displacement. From this, the inelastic strain due to crack slip is computed as follows. In a local coordinate system with the crack on the x_1-axis,

$$\begin{aligned} &\varepsilon_{12} = \varepsilon_{21} = \frac{N}{V}\int_0^c [u_2]dx = \frac{N}{V}\bar{b}c = fb, \\ &\varepsilon_{11} = \varepsilon_{22} = 0, \; b = \bar{b}/c. \end{aligned} \tag{A.2}$$

Transformation to the global coordinate system is made with the following matrix:

$$\underset{\sim}{T} = \begin{bmatrix} \cos\phi & \sin\phi \\ -\sin\phi & \cos\phi \end{bmatrix}, \tag{A.3}$$

where ϕ is the angle between the local and global x_1-axis. By use of this matrix, we have

$$\underset{\sim}{\varepsilon}_b = 2fb\frac{1}{2}\begin{bmatrix} -\sin 2\phi & \cos 2\phi \\ \cos 2\phi & \sin 2\phi \end{bmatrix}, \tag{A.4}$$

in the global coordinate system.

For the Mode I crack displacement, we have

$$\varepsilon_{11} = 2 \times \frac{N}{V}\int_0^c [u_1]dx = 2fd, \tag{A.5}$$

in the local coordinates, and

$$\underset{\sim}{\varepsilon}_d = 2fd\begin{bmatrix} \cos^2\phi & \cos\phi\sin\phi \\ \cos\phi\sin\phi & \sin^2\phi \end{bmatrix}, \qquad (A.6)$$

in the global coordinates.

APPENDIX B: Strains Due to a Dislocated Crack

First, we examine the Mode I crack displacement. Consider an array of edge dislocations continuously distributed along $-a < x_2 < a$, $x_1 = 0$; see Fig. B.1. The corresponding normal stress is (see, e.g., Muskhelishvili, 1953).

$$\sigma_{11}(x_2,0) = -\frac{1}{2\pi}\frac{\mu}{1-\nu}\int_{-a}^{a}\frac{B_1(\xi)}{\xi - x_2}d\xi, \tag{B.1}$$

and the displacement in the x_1-direction on the x_2-axis is given by

$$u_1(0,x_2) = g(x_2) = -\int_{-\infty}^{x_2} B_1(\xi)d\xi, \tag{B.2}$$

where $B_1(x_2)$ is the dislocation density. Since crack surfaces are traction-free, with the farfield stresses applied, the following integral equation defines the dislocation density:

$$-\frac{1}{2\pi}\frac{\mu}{1-\nu}\int_{-a}^{a}\frac{B_1(\xi)}{\xi - x_2}d\xi + p(x_2) = 0, \quad -a < x_2 < a, \tag{B.3}$$

where $p(x_2)$ is the traction on the x_2-axis due to farfield stress.

A solution of (B.3) singular at $x_2 = \pm a$ is given by (e.g., Muskhelishvili, 1953)

$$B_1(x_2) = -\frac{1}{\pi^2}\frac{1}{\sqrt{a^2 - x_2^2}}\left\{2\pi\frac{1-\nu}{\mu}\int_{-a}^{a}\frac{\sqrt{a^2-\xi^2}}{\xi - x_2}p(\xi)d\xi + C\right\}, \tag{B.4}$$

where C is a constant yet to be determined by another boundary condition. In this case, the farfield stress is zero, but the crack is dislocated at $x_2 = a$,

$$p(x_2) = 0, \quad [u_1](a) = g_1. \tag{B.5}$$

From (B.2), (B.4), and (B.5), we have

$$B_1(x_2) = -\frac{g_1}{\pi}\frac{1}{\sqrt{a^2 - x_2^2}}. \tag{B.6}$$

Note that the condition $[u_1] = 0$ for $-a > x_2$ is automatically satisfied by this array of dislocations. Substituting (B.6) into (B.1), we obtain the normal stresses on $x_1 = 0$,

$$\sigma_{11}(x_2,0) = -\frac{g_1}{2\pi}\frac{\mu}{1-\nu}\frac{\mathrm{sgn}(x_2)}{\sqrt{x_2^2 - a^2}}\, H(|x_2| - a), \tag{B.7}$$

where $H(x)$ is the Heaviside step function. The stress intensity factor at $x_2 = -a$ now is

$$K_I = \frac{g_1}{2}\frac{\mu}{1-\nu}\frac{1}{\sqrt{\pi a}}. \tag{B.8}$$

From (B.2),(B.5), and (A.1), we compute the strain components in the local coordinate system as follows:

$$\begin{aligned} \varepsilon_{11} &= g_1 a, \\ \varepsilon_{12} &= \varepsilon_{21} = \varepsilon_{22} = 0. \end{aligned} \tag{B.9}$$

Note that both g_1 and a are dimensionless; see Appendix A.

Now consider the Mode II crack displacement. If the concentrated gap at $x_2 = a$ is denoted by g_2, we obtain

$$\varepsilon_{12} = \varepsilon_{21} = \frac{1}{2} g_2 a. \tag{B.10}$$

In our particular problem,

$$\begin{aligned} g_1 &= b \sin\theta + d\cos\theta, \\ g_2 &= b\cos\theta - d\sin\theta, \\ a &= \frac{\ell}{2}. \end{aligned} \tag{B.11}$$

Thus, considering that we have a pair of dislocated cracks, the strain components in the local coordinate system are given by

$$\underset{\sim}{\varepsilon}_c = f\frac{b\ell}{2}\begin{bmatrix} 2\sin\theta & \cos\theta \\ \cos\theta & 0 \end{bmatrix} + f\frac{d\ell}{2}\begin{bmatrix} 2\cos\theta & -\sin\theta \\ -\sin\theta & 0 \end{bmatrix}. \qquad (B.12)$$

The transformation to the global coordinate system is made with

$$\underset{\sim}{T} = \begin{bmatrix} \cos(\theta+\phi) & \sin(\theta+\phi) \\ -\sin(\theta+\phi) & \cos(\theta+\phi) \end{bmatrix}, \qquad (B.13)$$

and we obtain

$$\underset{\sim}{\varepsilon}_c = fb\ell\frac{1}{2}\begin{bmatrix} -2\sin\phi\cos(\theta+\phi) & \cos(\theta+2\phi) \\ \cos(\theta+2\phi) & 2\cos\phi\sin(\theta+\phi) \end{bmatrix} + fd\ell\frac{1}{2}\begin{bmatrix} 2\cos\phi\cos(\theta+\phi) & \sin(\theta+2\phi) \\ \sin(\theta+2\phi) & 2\sin\phi\sin(\theta+\phi) \end{bmatrix}, \qquad (B.14)$$

in the global coordinate system.

APPENDIX C: Strains Due to Crack Displacement Caused by Applied Stresses

Under the farfield stresses T and S, the crack opening displacements are given by

$$[u_1] = 2T\frac{1-\nu}{\mu}\sqrt{(\ell/2)^2-x_2^2},$$
$$[u_2] = 2S\frac{1-\nu}{\mu}\sqrt{(\ell/2)^2-x_2^2}. \tag{C.1}$$

In our particular problem, $T = \underset{\sim}{\sigma}:\underset{\sim}{\alpha}$ and $S = \underset{\sim}{\sigma}:\underset{\sim}{\beta}/2$. Therefore, after integrating, the strains in the local coordinate system are expressed as

$$\underset{\sim}{\varepsilon}_a = f\frac{1-\nu}{8\mu}\pi\ell^2\begin{bmatrix} 4\underset{\sim}{\sigma}:\underset{\sim}{\alpha} & \underset{\sim}{\sigma}:\underset{\sim}{\beta} \\ \underset{\sim}{\sigma}:\underset{\sim}{\beta} & 0 \end{bmatrix}. \tag{C.2}$$

Using (B.11), we have the expression in the global coordinate system,

$$\underset{\sim}{\varepsilon}_a = f\frac{1-\nu}{8\mu}\pi\ell^2[4(\underset{\sim}{\sigma}:\underset{\sim}{\alpha})\underset{\sim}{\alpha} + (\underset{\sim}{\sigma}:\underset{\sim}{\beta})\underset{\sim}{\beta}]. \tag{C.3}$$

APPENDIX D: Stress Intensity Factor of a Dislocated Crack

Consider the case where the crack opening displacement normal to the flaw is zero. By use of (B.8), the Mode I stress intensity factor of a dislocated crack of length ℓ is obtained to be

$$K_I' = \frac{\mu}{1-\nu}\frac{b}{\sqrt{2\pi\ell}} + \underset{\sim}{\sigma}:\underset{\sim}{\alpha}\sqrt{\frac{\pi\ell}{2}}. \tag{D.1}$$

Since this expression is singular when $\ell = 0$, we replace it by the following non-singular form

$$K_I' = \frac{\mu}{1-\nu}\frac{1}{\sqrt{2\pi(\ell+\ell^{**})}}\, b + \underset{\sim}{\sigma}:\underset{\sim}{\alpha}\sqrt{\frac{\pi\ell}{2}}, \tag{D.2}$$

and seek to estimate ℓ^{**} such that at $\ell = 0^+$, $K_I' = K_I$. When $\ell = 0$, the average slip of the preexisting flaw equals the average Mode II crack displacement, and is given by

$$\bar{b} = \frac{1}{2c}\int_{-c}^{c} 2(\underset{\sim}{\sigma}:\underset{\sim}{p}_2 - \tau_c)\frac{1-\nu}{\mu}\sqrt{c^2-x^2}\,dx = \frac{1}{2}\frac{1-\nu}{\mu}\pi c(\underset{\sim}{\sigma}:\underset{\sim}{p}_2 - \tau_c) \tag{D.3}$$

On the other hand, when $\ell = 0$, (2.9a) reduces to

$$K_I = \frac{2}{\sqrt{\pi\ell^*}}(\underset{\sim}{\sigma}:\underset{\sim}{p}_2 - \tau_c)\sin\theta, \tag{D.4}$$

which is maximum at $\theta = \pi/2$. From (D.2), (D.3), and (D.4) with $\theta = \pi/2$, ℓ^{**} is determined to be

$$\ell^{**} = \frac{\pi^2}{32}\ell^*. \tag{D.5}$$

We simply generalize this result when dilatancy d is included. The final form of K_I' then is

$$K_I' = \frac{\mu}{1-\nu}\frac{1}{\sqrt{2\pi(\ell+\ell^{**})}}(b\sin\theta + d\cos\theta) + \underset{\sim}{\sigma}:\underset{\sim}{\alpha}\sqrt{\frac{\pi\ell}{2}}. \tag{D.6}$$

APPENDIX E: Some Basic Equations in Loading

$$\frac{\partial K_I}{\partial \ell} = -\frac{\pi}{2}\left[\frac{2}{\{\pi(\ell+\ell^*)\}^{3/2}}(\underset{\sim}{\sigma}:\underset{\sim}{p}_2 - \tau_c)\sin\theta - \underset{\sim}{\sigma}:\underset{\sim}{\alpha}\frac{1}{\sqrt{\pi\ell}}\right],$$

$$\frac{\partial K_I}{\partial \theta} = \frac{2}{\sqrt{\pi(\ell+\ell^*)}}(\underset{\sim}{\sigma}:\underset{\sim}{p}_2 - \tau_c)\cos\theta + \underset{\sim}{\sigma}:\underset{\sim}{\beta}\sqrt{\pi\ell},$$

$$\frac{\partial K_I}{\partial b} = \frac{2\eta}{\sqrt{\pi(\ell+\ell^*)}}\tau_c \sin\theta,$$

$$\frac{\partial K_I'}{\partial \ell} = -\frac{\pi}{2}\left[\frac{\mu}{1-\nu}\frac{2}{\{2\pi(\ell+\ell^{**})\}^{3/2}}(b\sin\theta + d\cos\theta) - \underset{\sim}{\sigma}:\underset{\sim}{\alpha}\frac{1}{\sqrt{2\pi\ell}}\right],$$

$$\frac{\partial K_I'}{\partial \theta} = \frac{\mu}{1-\nu}\frac{1}{\sqrt{2\pi(\ell+\ell^{**})}}(b\cos\theta - d\sin\theta) + \underset{\sim}{\sigma}:\underset{\sim}{\beta}\sqrt{\frac{\pi\ell}{2}},$$

$$\frac{\partial K_I'}{\partial b} = \frac{\mu}{1-\nu}\frac{1}{\sqrt{2\pi(\ell+\ell^{**})}}\{\sin\theta + \zeta(d_0 - d)\cos\theta\},$$

$$\frac{\partial J}{\partial \ell} = \frac{\partial}{\partial \ell}\left(\frac{\partial K_I}{\partial \theta}\right)\frac{\partial K_I'}{\partial b} + \frac{\partial K_I}{\partial \theta}\frac{\partial}{\partial \ell}\left(\frac{\partial K_I'}{\partial b}\right) - \frac{\partial}{\partial \ell}\left(\frac{\partial K_I}{\partial b}\right)\frac{\partial K_I'}{\partial \theta} - \frac{\partial K_I}{\partial b}\frac{\partial}{\partial \ell}\left(\frac{\partial K_I'}{\partial \theta}\right),$$

$$\frac{\partial J}{\partial \theta} = \frac{\partial}{\partial \theta}\left(\frac{\partial K_I}{\partial \theta}\right)\frac{\partial K_I'}{\partial b} + \frac{\partial K_I}{\partial \theta}\frac{\partial}{\partial \theta}\left(\frac{\partial K_I'}{\partial b}\right) - \frac{\partial}{\partial \theta}\left(\frac{\partial K_I}{\partial b}\right)\frac{\partial K_I'}{\partial \theta} - \frac{\partial K_I}{\partial b}\frac{\partial}{\partial \theta}\left(\frac{\partial K_I'}{\partial \theta}\right),$$

$$\frac{\partial J}{\partial b} = \frac{\partial}{\partial b}\left(\frac{\partial K_I}{\partial \theta}\right)\frac{\partial K_I'}{\partial b} + \frac{\partial K_I}{\partial \theta}\frac{\partial}{\partial b}\left(\frac{\partial K_I'}{\partial b}\right) - \frac{\partial}{\partial b}\left(\frac{\partial K_I}{\partial b}\right)\frac{\partial K_I'}{\partial \theta} - \frac{\partial K_I}{\partial b}\frac{\partial}{\partial b}\left(\frac{\partial K_I'}{\partial \theta}\right),$$

$$\frac{\partial}{\partial \ell}\left(\frac{\partial K_I}{\partial \theta}\right) = -\frac{\pi}{2}\left[\frac{2}{\{\pi(\ell + \ell^*)\}^{3/2}}\,(\underset{\sim}{\sigma}:\underset{\sim}{p}_2 - \tau_c)\cos\theta - \underset{\sim}{\sigma}:\underset{\sim}{\beta}\,\frac{1}{\sqrt{\pi\ell}}\right],$$

$$\frac{\partial}{\partial \ell}\left(\frac{\partial K_I}{\partial b}\right) = -\pi\,\frac{\eta}{\{\pi(\ell + \ell^*)\}^{3/2}}\,\tau_c \sin\theta,$$

$$\frac{\partial}{\partial \ell}\left(\frac{\partial K_I'}{\partial \theta}\right) = -\frac{\pi}{2}\left[\frac{\mu}{1-\nu}\,\frac{2}{\{2\pi(\ell + \ell^{**})\}^{3/2}}(b\cos\theta - d\sin\theta) - \underset{\sim}{\sigma}:\underset{\sim}{\beta}\,\frac{1}{\sqrt{2\pi\ell}}\right],$$

$$\frac{\partial}{\partial \ell}\left(\frac{\partial K_I'}{\partial b}\right) = -\frac{\pi}{2}\,\frac{\mu}{1-\nu}\,\frac{2}{\{2\pi(\ell + \ell^{**})\}^{3/2}}\{\sin\theta + \zeta(d_0 - d)\cos\theta\},$$

$$\frac{\partial}{\partial \theta}\left(\frac{\partial K_I}{\partial \theta}\right) = -\frac{2}{\sqrt{\pi(\ell + \ell^*)}}\,(\underset{\sim}{\sigma}:\underset{\sim}{p}_2 - \tau_c)\sin\theta + \underset{\sim}{\sigma}:\underset{\sim}{\gamma}\sqrt{\pi\ell},$$

$$\frac{\partial}{\partial \theta}\left(\frac{\partial K_I}{\partial b}\right) = \frac{2\eta}{\sqrt{\pi(\ell + \ell^*)}}\,\tau_c\cos\theta,$$

$$\frac{\partial}{\partial \theta}\left(\frac{\partial K_I'}{\partial \theta}\right) = -\frac{\mu}{1-\nu}\,\frac{1}{\sqrt{2\pi(\ell + \ell^{**})}}(b\sin\theta + d\cos\theta) + \underset{\sim}{\sigma}:\underset{\sim}{\gamma}\sqrt{\frac{\pi\ell}{2}},$$

$$\frac{\partial}{\partial \theta}\left(\frac{\partial K_I'}{\partial b}\right) = \frac{\mu}{1-\nu}\,\frac{1}{\sqrt{2\pi(\ell + \ell^{**})}}\{\cos\theta - \zeta(d_0 - d)\sin\theta\},$$

$$\frac{\partial}{\partial b}\left(\frac{\partial K_I}{\partial b}\right) = -\frac{2\eta^2}{\sqrt{\pi(\ell + \ell^*)}}\,\tau_c\sin\theta,$$

$$\frac{\partial}{\partial b}\left(\frac{\partial K_I'}{\partial b}\right) = -\frac{\mu}{1-\nu}\,\frac{\zeta^2}{\sqrt{2\pi(\ell+\ell^{**})}}\,(d_0-d)\cos\theta,$$

$$\underset{\sim}{b}_1 = -\frac{2\underset{\sim}{p}_2}{\sqrt{\pi(\ell+\ell^{*})}}\sin\theta - \underset{\sim}{\alpha}\sqrt{\pi\ell},$$

$$\underset{\sim}{b}_2 = -\underset{\sim}{\alpha}\sqrt{\frac{\pi\ell}{2}},$$

$$\underset{\sim}{b}_3 = -\frac{\mu}{1-\nu}\,\frac{1}{\sqrt{2\pi(\ell+\ell^{**})}}\{\sin\theta + \zeta(d_0-d)\cos\theta\}$$

$$\times\left\{\frac{\underset{\sim}{p}_2}{\sqrt{\pi(\ell+\ell^{*})}}\cos\theta + \underset{\sim}{\beta}\sqrt{\pi\ell}\right\}$$

$$+\frac{2\eta}{\sqrt{\pi(\ell+\ell^{*})}}\,\tau_c\sin\theta\sqrt{\frac{\pi\ell}{2}}\,\underset{\sim}{\beta}.$$

APPENDIX F: Some Basic Equations in Unloading

In the case of unloading,

the following quantities are different from those of the loading case:

$$\frac{\partial K_I}{\partial \ell} = -\frac{\pi}{2}\left[\frac{2}{(\pi(\ell+\ell^*))^{3/2}}(\underset{\sim}{\sigma}:\underset{\sim}{p}_2' + \tau_c)\sin\theta - \underset{\sim}{\sigma}:\underset{\sim}{\alpha}\frac{1}{\sqrt{\pi\ell}}\right],$$

$$\frac{\partial K_I}{\partial \theta} = \frac{2}{\sqrt{\pi(\ell+\ell^*)}}(\underset{\sim}{\sigma}:\underset{\sim}{p}_2' + \tau_c)\cos\theta + \underset{\sim}{\sigma}:\underset{\sim}{\beta}\sqrt{\pi\ell},$$

$$\frac{\partial K_I}{\partial b} = \frac{2\eta}{\sqrt{\pi(\ell+\ell^*)}}\tau_c \sin\theta.$$

APPENDIX G: Stress Intensity Factor in Unloading

Equation (2.25) with K_I defined by (2.24a), may be explained in the following way. At the end of a loading regime when the applied farfield stresses are $\underset{\sim}{\sigma}_{max}$, the residual stress on the preexisting flaw is given by

$$\tau_m = \underset{\sim}{\sigma}_{max} : \underset{\sim}{p}_2 - \tau_c . \tag{G.1}$$

Here, τ_m is the maximum shear stress experienced by the flaw during this loading regime. Backsliding is considered to occur when this residual stress overcomes the frictional and cohesive resistance of the flaw, i.e., when

$$\tau_m - \underset{\sim}{\sigma} : \underset{\sim}{p}_0 \geq \tau_c - \bar{\mu}\, \underset{\sim}{\sigma} : \underset{\sim}{p}_1 . \tag{G.2}$$

At the end of a loading regime, we have

$$K_I = K_I' = \frac{2}{\sqrt{\pi(\ell + \ell^*)}} \tau_m \sin\theta + \underset{\sim}{\sigma}_{max} : \underset{\sim}{\alpha} \sqrt{\pi \ell} . \tag{G.3}$$

Therefore, at the onset of backsliding, the equality in (G.2) yields

$$K_I' \simeq K_I . \tag{G.4}$$

The essential difference between (2.24a) and (2.10a) is due to the terms associated with the farfield applied stress, i.e., $\underset{\sim}{\sigma} : \underset{\sim}{\alpha} \sqrt{(\pi \ell / 2)}$ and $\underset{\sim}{\sigma} : \underset{\sim}{\alpha} \sqrt{(\pi \ell)}$. This difference stems from the fact that the computation of the stress intensity factor in the presence of a gap is for a crack of length ℓ, whereas that associated with the force F is for a crack of length 2ℓ.

Because tension cracks grow in the the maximum compressive stress direction, this difference is quite small. Even for extreme cases, e.g., just after crack nucleation, ℓ is small and hence this term is very small. We may therefore use the expression (2.25) and (2.26) with K_I defined by (2.24a), in order to ensure a consistent formulation without loss of accuracy.

APPENDIX H: Partially Closed Dislocated Crack

We consider the case shown in Fig. B.1. In this case, the integral equation corresponding to Eq. (B.3) becomes

$$\int_{-a}^{a} \frac{B_1(\xi)}{\xi - x_2} d\xi = 2\pi \frac{1 - \nu}{\mu} T. \tag{H.1}$$

If we solve this equation under the condition that σ_{11} is bounded at $x_2 = -a$ and unbounded at $x_2 = a$, we obtain (e.g., Muskhelishvili, 1953)

$$B_1(x) = 2T \frac{1 - \nu}{\mu} \frac{\sqrt{a + x_2}}{\sqrt{a - x_2}}. \tag{H.2}$$

After integration of (B.2), the crack opening displacement is given by

$$[u_1](x_2) = -\frac{1 - \nu}{\mu} 2T \left[a \sin^{-1} \frac{x_2}{a} + a \frac{\pi}{2} - \sqrt{a^2 - x_2^2} \right]. \tag{H.3}$$

The condition at $x_2 = a$ yields

$$a = -\frac{1}{2\pi} \frac{\mu}{1 - \nu} \frac{g_1}{T}. \tag{H.4}$$

Apparently, this result is reasonable only when $T < 0$. In our particular problem,

$$g_1 = b \sin \theta + d \cos \theta, \quad T = \underset{\sim}{\sigma} : \underset{\sim}{\alpha}. \tag{H.5}$$

Thus, integration of the crack opening displacement leads to the following expression for the strain component ε_{11} in the local coordinate system:

$$\varepsilon_{11} = -f \frac{1}{2\pi} \frac{\mu}{1 - \nu} \frac{1}{(\underset{\sim}{\sigma} : \underset{\sim}{\alpha})} (b \sin \theta + d \cos \theta)^2. \tag{H.6}$$

The strain component ε_{12} requires no modification when we assume no friction on tension cracks. Considering the contribution by the farfield stresses as well as the dislocation array, we obtain

$$\varepsilon_{12} = f\frac{\ell_m}{2}(b\cos\theta - d\sin\theta) + f\frac{1-\nu}{8\mu}\pi\ell_m^2(\underset{\sim}{\sigma}:\underset{\sim}{\beta}) \tag{H.7}$$

in the local coordinate system. The transformation to the global coordinate system is done by Eq. (B.13). In the global coordinate system, we hence have

$$\begin{aligned}\underset{\sim}{\varepsilon}_c = &- f\frac{1}{2\pi}\frac{\mu}{1-\nu}\frac{1}{(\underset{\sim}{\sigma}:\underset{\sim}{\alpha})}(b\sin\theta + d\cos\theta)^2\underset{\sim}{\alpha} \\ &+ f\frac{\ell_m}{2}(b\cos\theta - d\sin\theta)\underset{\sim}{\beta} \\ &+ f\frac{1-\nu}{8\mu}\pi\ell_m^2(\underset{\sim}{\sigma}:\underset{\sim}{\beta})\underset{\sim}{\beta}.\end{aligned} \tag{H.8}$$

Table 1: Instantaneous compliance, at various loading and unloading states.

σ_{11}/τ_c^0	$\epsilon_{11}/(\tau_c^0/\mu)$	μD_{1111}	μD_{1122}	μD_{2222}	μD_{2211}	μD_{1212}
0*	0	0.375	-0.125	0.375	-0.125	0.25
3.68	1.42	0.421	-0.212	0.462	-0.171	0.257
7.46	3.21	0.483	-0.652	3.775	-0.510	0.331
13.1**	5.99	0.391	-0.391	27.6	-1.18	2.368
5.28†	2.95	0.472	-1.03	14.2	-0.648	2.657

* Initial elastic loading
** Upon unloading
† Unloading with backsliding

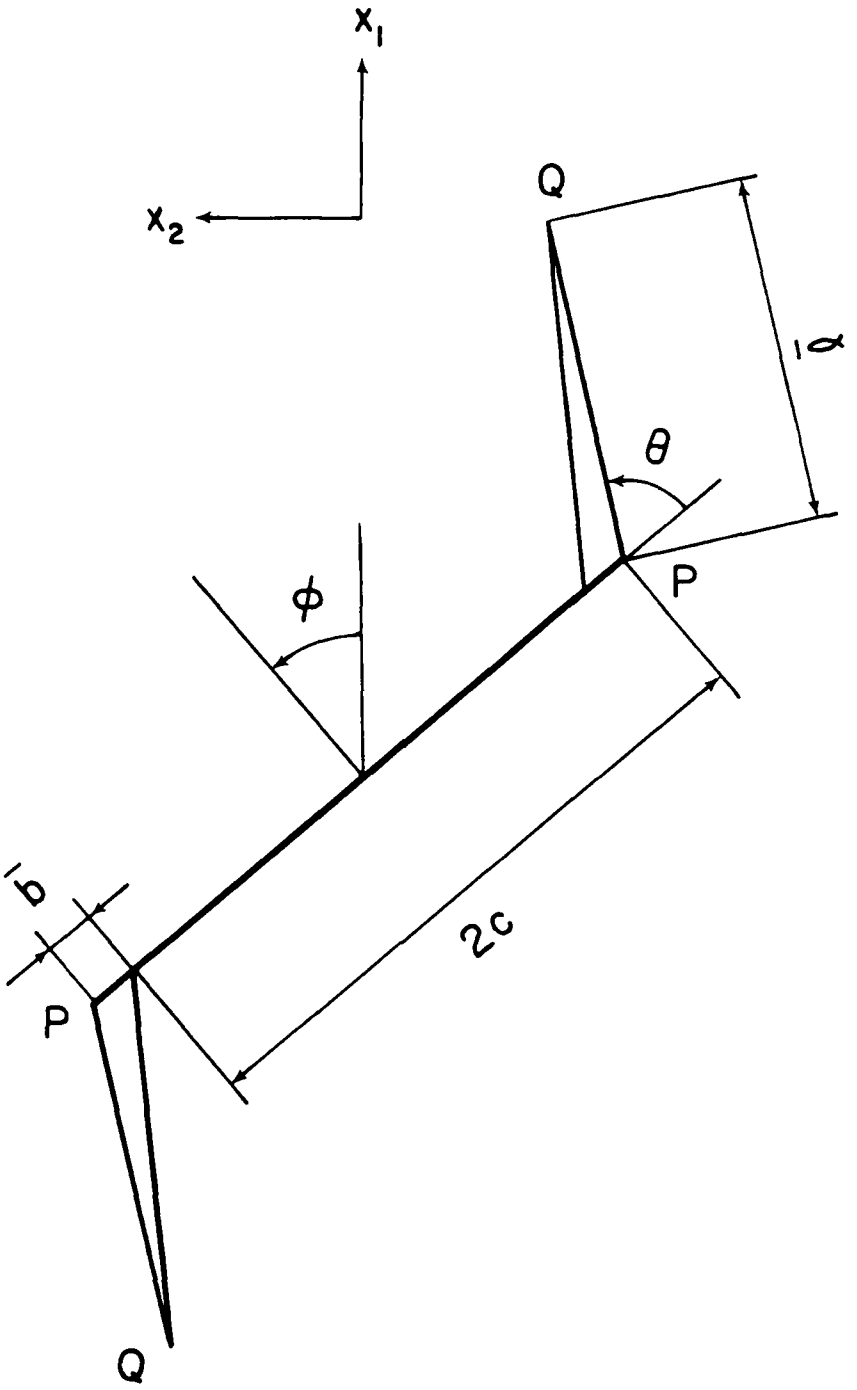

Figure 1

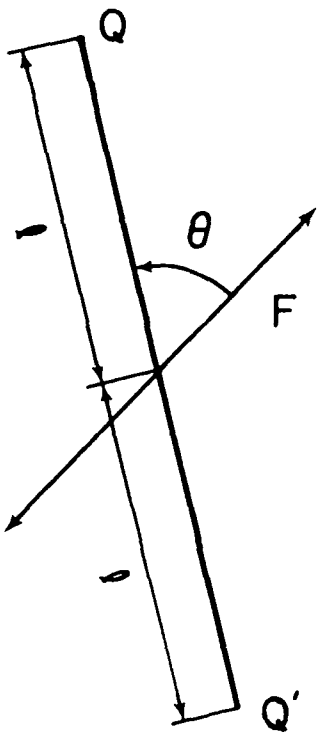

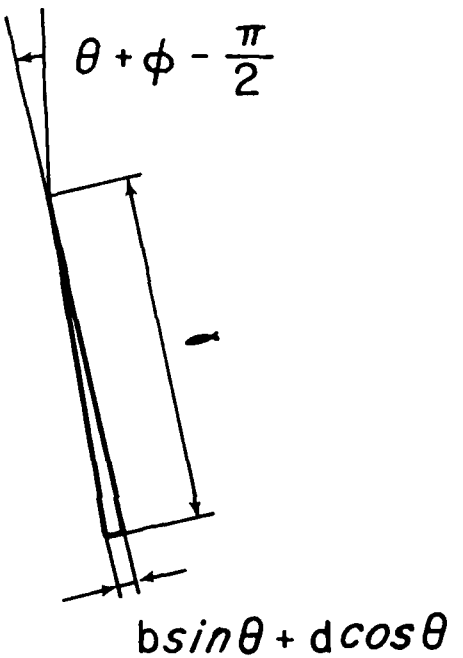

Figure 2

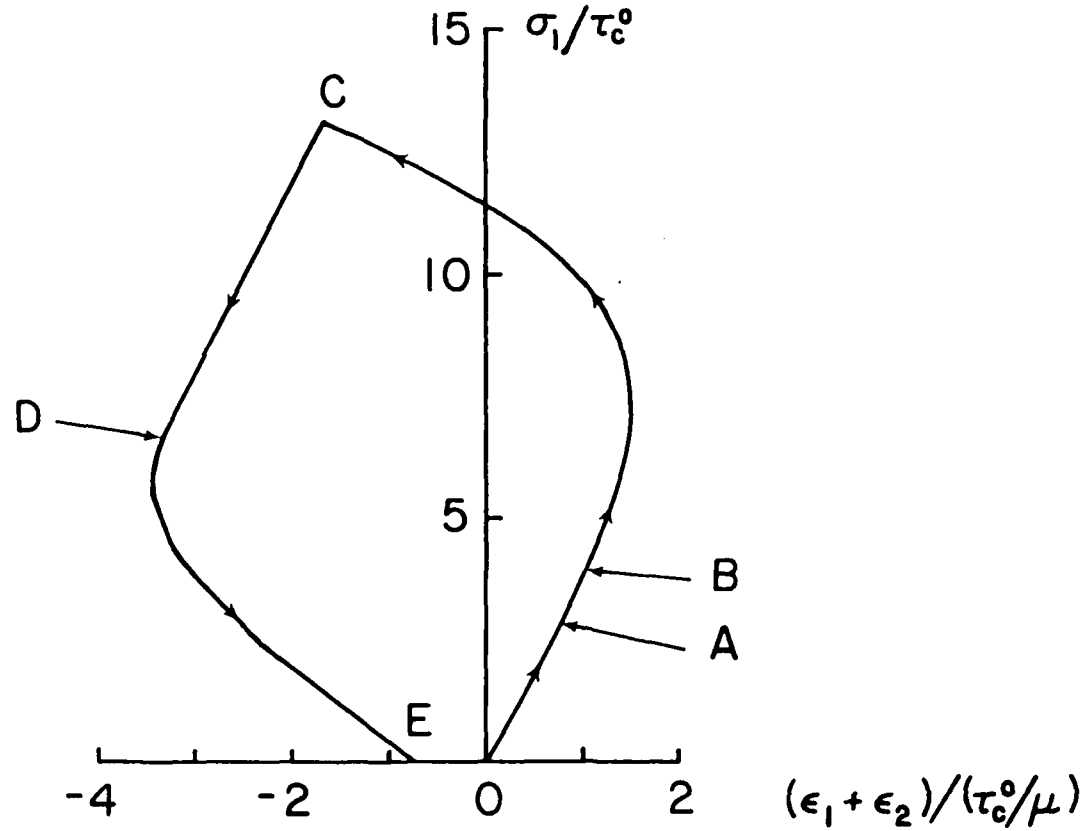

Figure 3 (a)

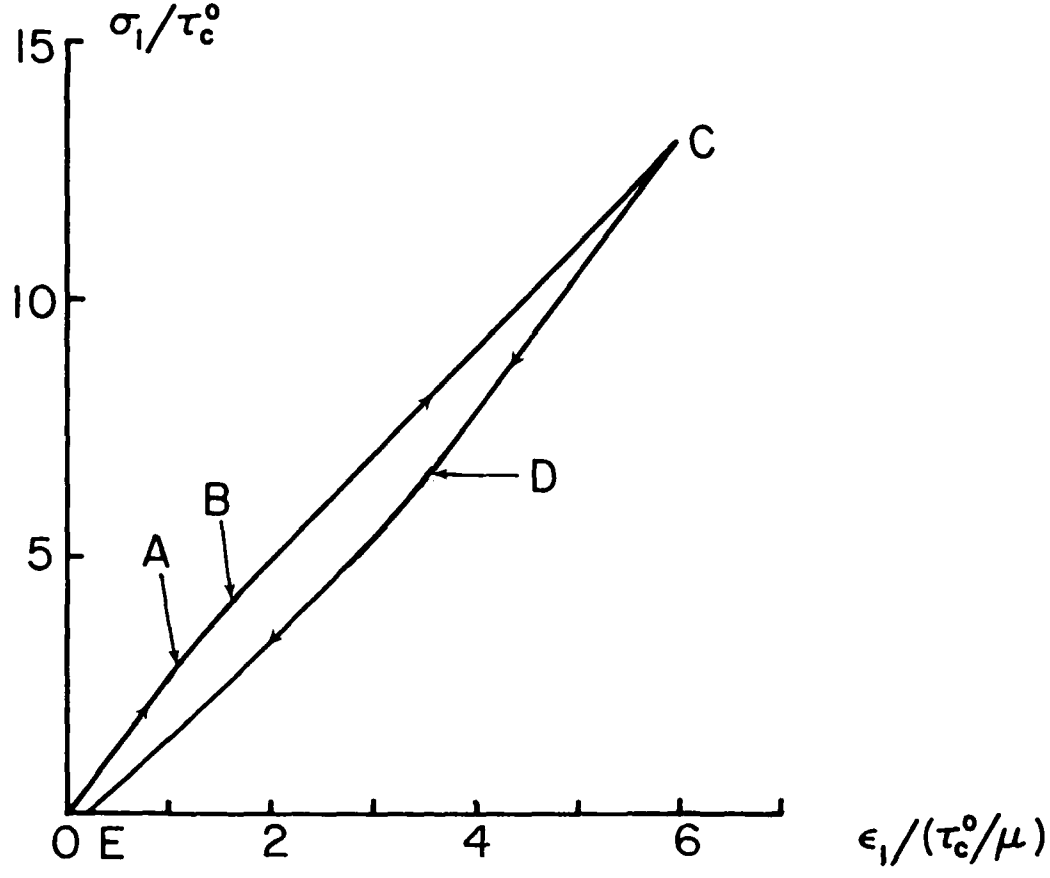

Figure 3 (b)

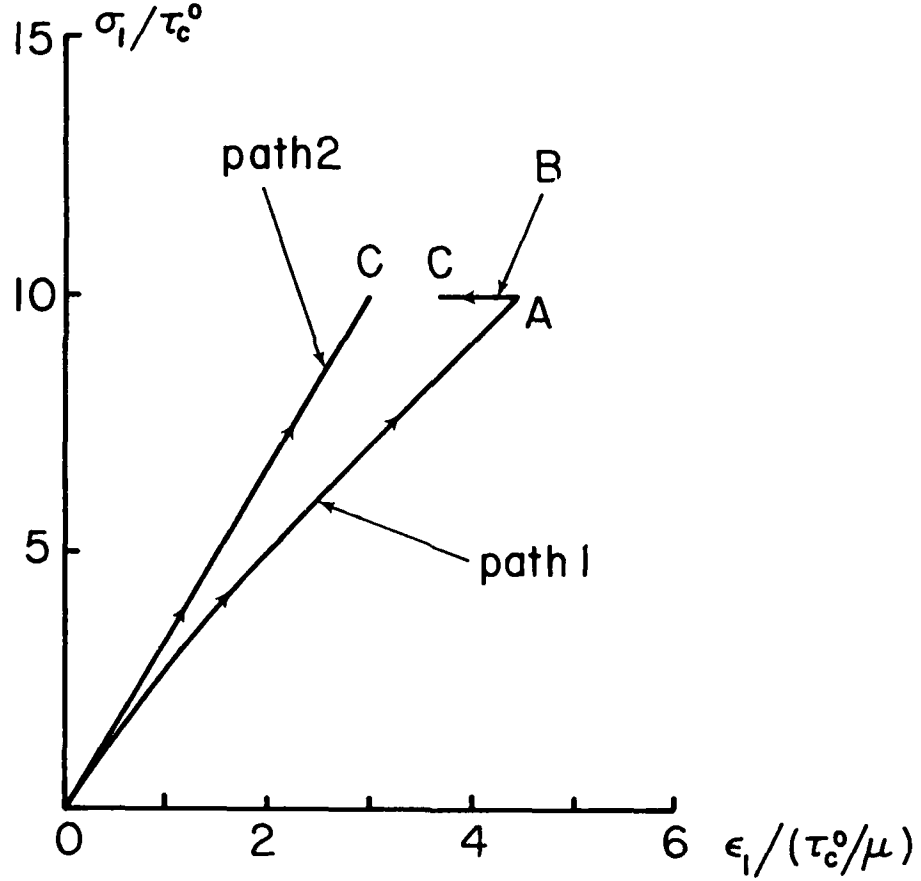

Figure 4 (a)

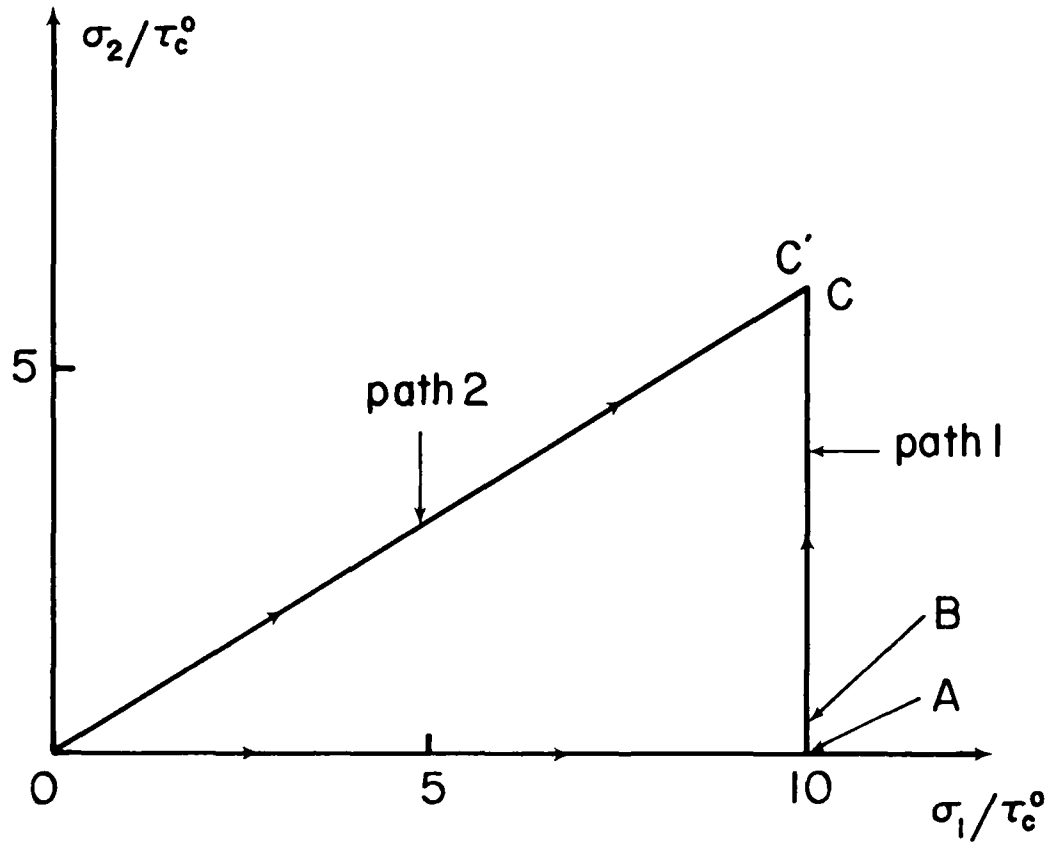

Figure 4 (b)

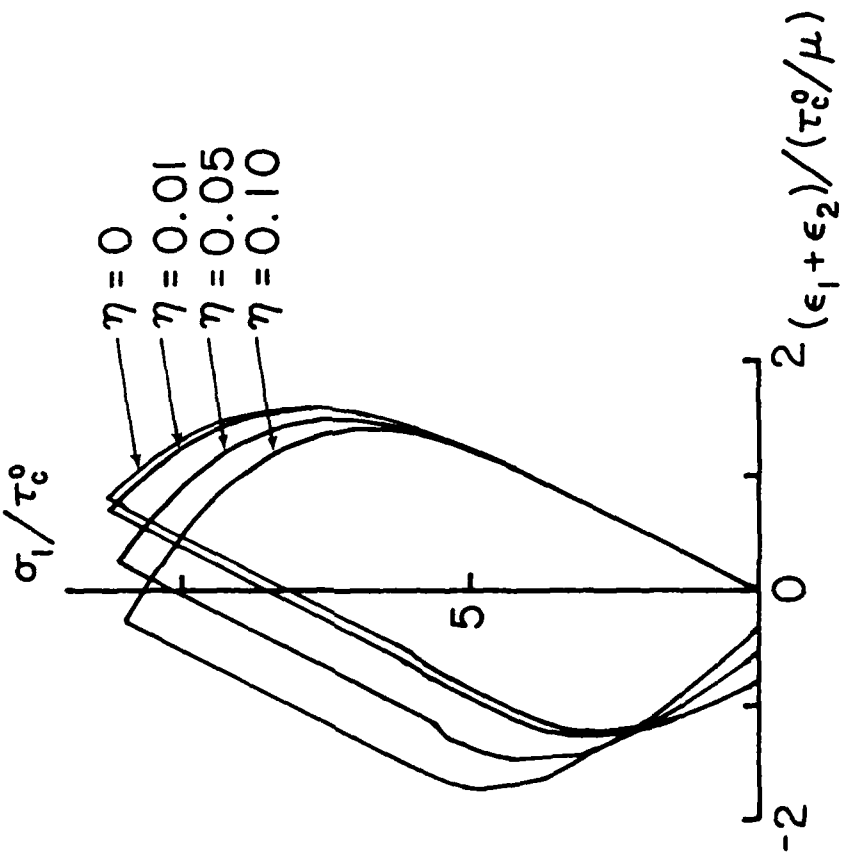
$\eta = 0$
$\eta = 0.01$
$\eta = 0.05$
$\eta = 0.10$
σ_1/τ_c^o
5
0
-2
$2(\epsilon_1+\epsilon_2)/(\tau_c^o/\mu)$

Figure 5

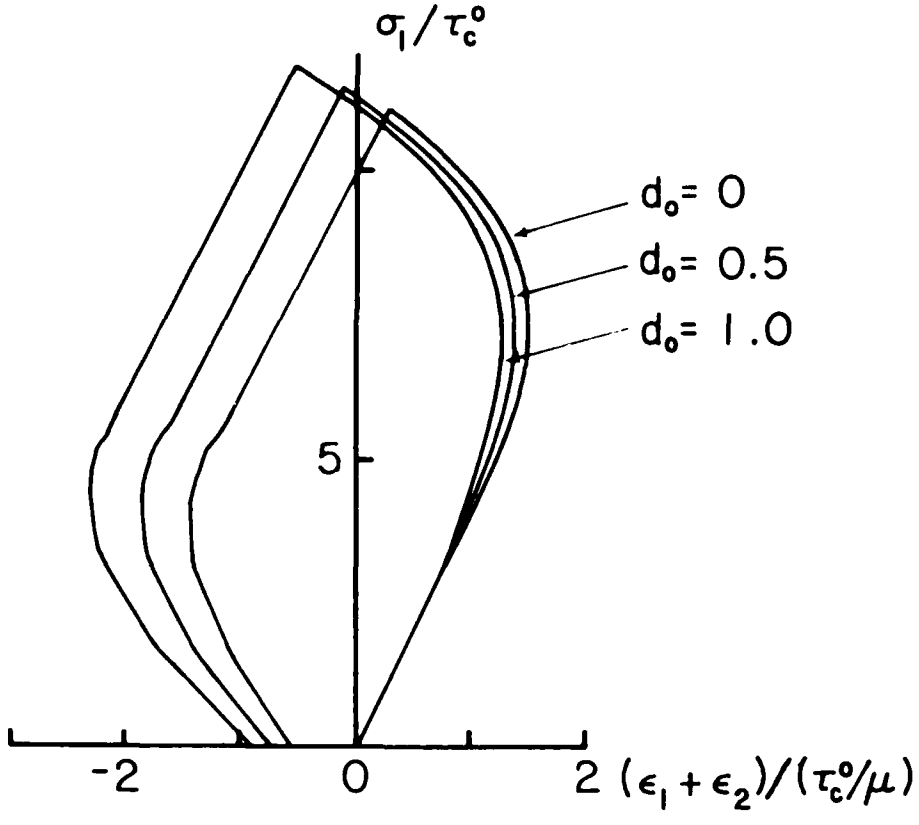

Figure 6

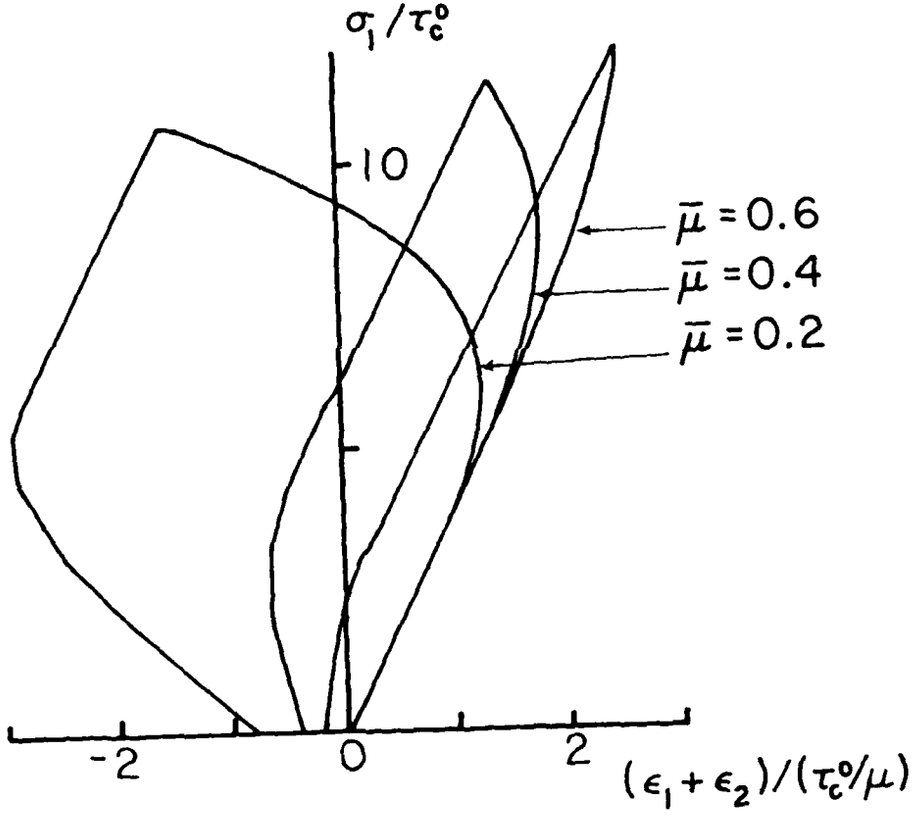
σ_1/τ_c^o
10
$\bar{\mu}$ = 0.6
$\bar{\mu}$ = 0.4
$\bar{\mu}$ = 0.2
-2
0
2
$(\epsilon_1+\epsilon_2)/(\tau_c^o/\mu)$

Figure 7

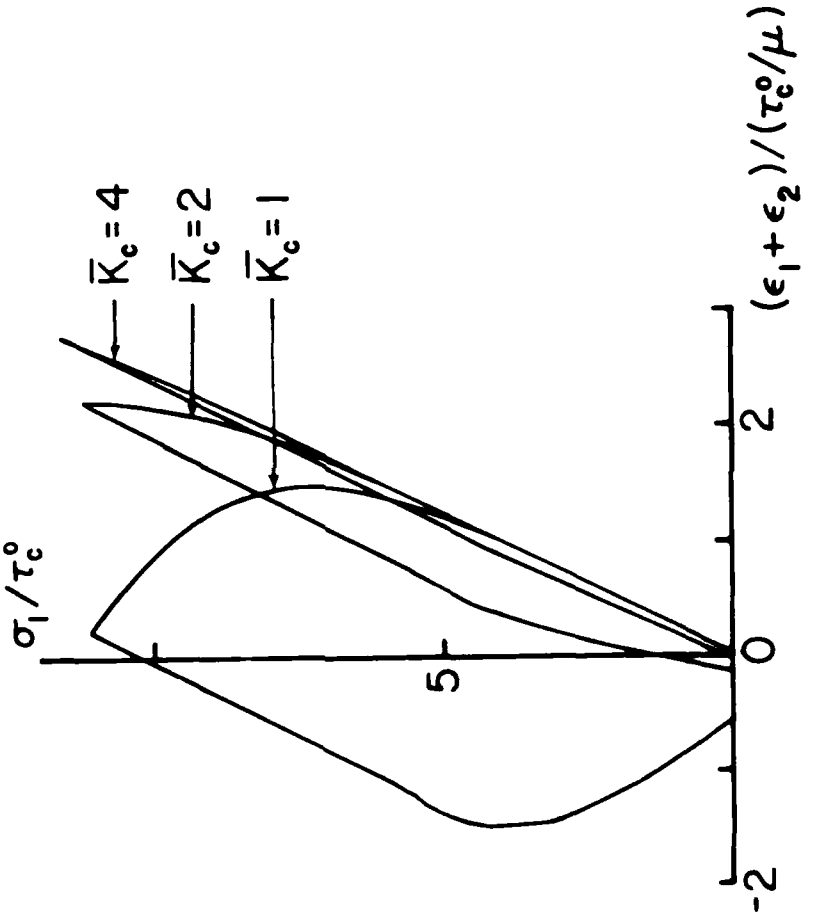
$\bar{K}_c=4$
$\bar{K}_c=2$
$\bar{K}_c=1$
σ_1/τ_c^o
5
0
2
-2
$(\epsilon_1+\epsilon_2)/(\tau_c^o/\mu)$

Figure 8

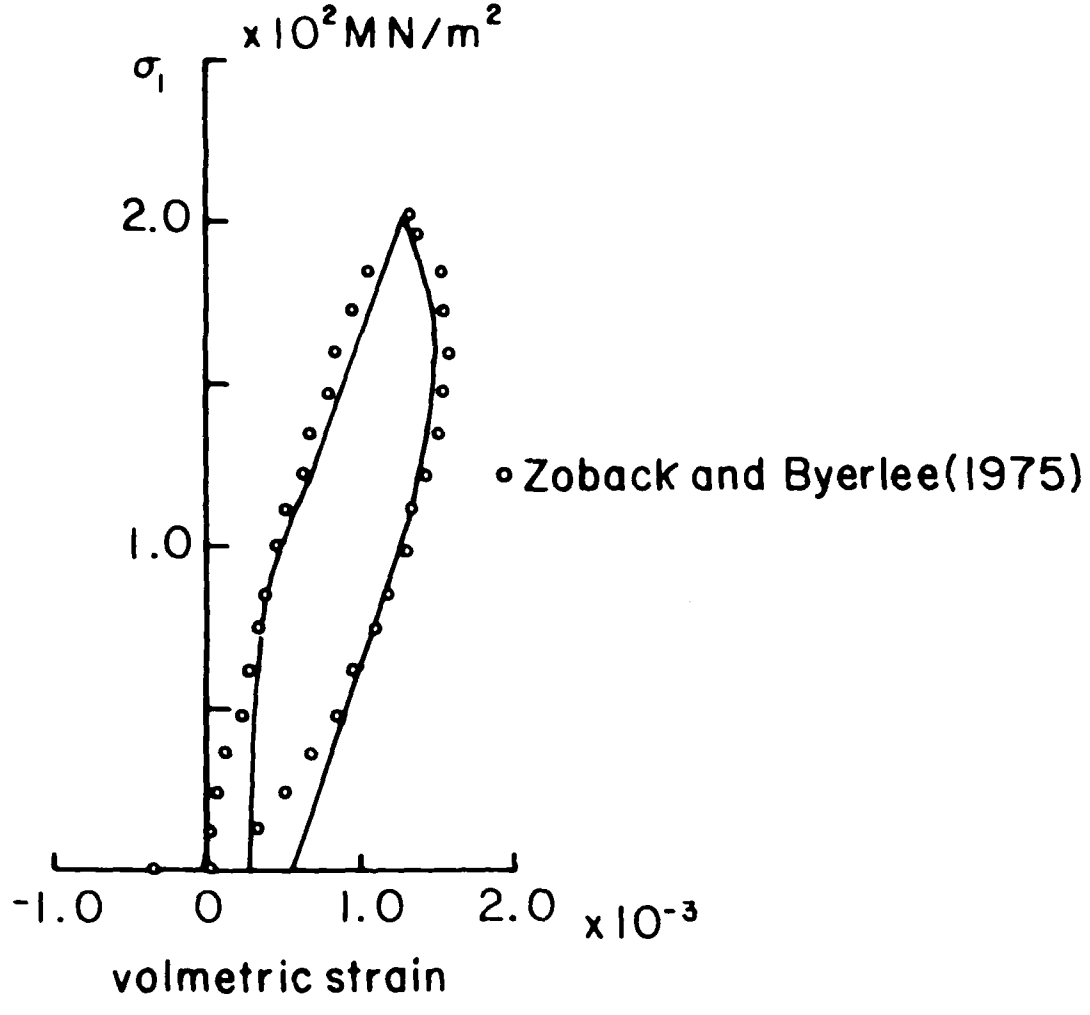
x10²MN/m²
σ1
2.0
1.0
-1.0
0
1.0
2.0
x10⁻³
volmetric strain
o Zoback and Byerlee(1975)

Figure 9 (a)

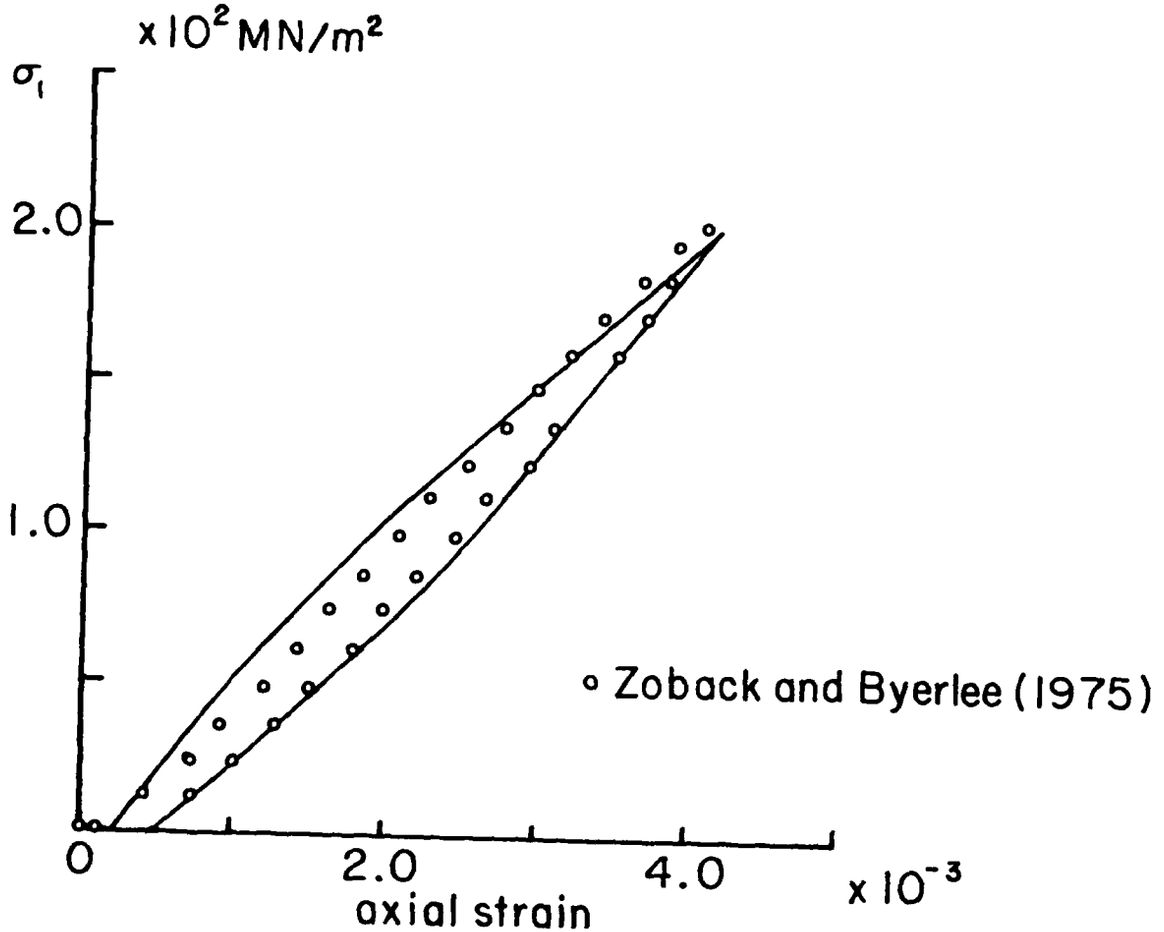
x 10² MN/m²
σ1
2.0
1.0
0
2.0
4.0
x 10⁻³
axial strain
o Zoback and Byerlee (1975)

Figure 9 (b)

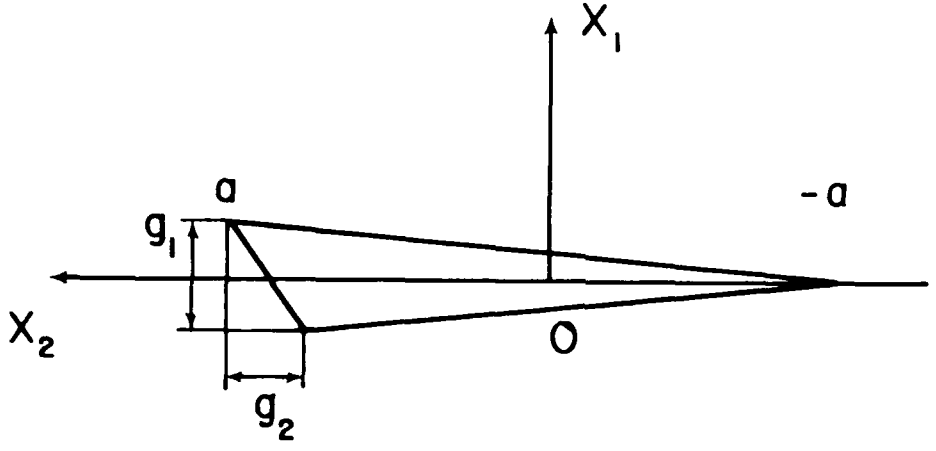

Figure B.1

END

8-87

DTIC